DEC 20 1957

UNIVERSITY OF MICHIGAN

DEC 17 1957

PHYSICS LIBRARY

Journal of Research

of the

National Bureau of Standards

DECEMBER 1957

VOLUME 59 NUMBER 6

U. S. DEPARTMENT OF COMMERCE
Sinclair Weeks, Secretary
NATIONAL BUREAU OF STANDARDS
A. V. Astin, Director

DECEMBER • 19
VOLUME • 5
NUMBER •

JOURNAL OF RESEARCH
of the
NATIONAL BUREAU OF STANDARDS

The National Bureau of Standards

Functions and Activities

The functions of the National Bureau of Standards are set forth in the Act of Congress, March 3, 1901, as amended by Congress in Public Law 619, 1950. These include the development and maintenance of the national standards of measurement and the provision of means and methods for making measurements consistent with these standards; the determination of physical constants and properties of materials; the development of methods and instruments for testing materials, devices, and structures; advisory services to Government Agencies on scientific and technical problems; invention and development of devices to serve special needs of the Government; and the development of standard practices, codes, and specifications. The work includes basic and applied research, development, engineering, instrumentation, testing, evaluation, calibration services, and various consultation and information services. A major portion of the Bureau's work is performed for other Government Agencies, particularly the Department of Defense and the Atomic Energy Commission. The scope of activities is suggested by the listing of divisions and sections on the inside of the back cover.

Publications

The results of the Bureau's work take the form of either actual equipment and devices or published papers. These papers appear either in the Bureau's own series of publications or in the journals of professional and scientific societies. The Bureau itself publishes three monthly periodicals, available from the Government Printing Office: The Journal of Research, which presents complete papers reporting technical investigations; the Technical News Bulletin, which presents summary and preliminary reports on work in progress; and Basic Radio Propagation Predictions, which provides data for determining the best frequencies to use for radio communications throughout the world. There are also five series of nonperiodical publications: The Applied Mathematics Series, Circulars, Handbooks, Building Materials and Structures Reports, and Miscellaneous Publications.

Information on the Bureau's publications can be found in NBS Circular 460, Publications of the National Bureau of Standards ($1.25) and its Supplement ($0.75), available from the Superintendent of Documents, Government Printing Office, Washington 25, D. C.

Order all publications from the Superintendent of Documents.
U. S. Government Printing Office, Washington 25, D. C.

Use of funds for printing this publication approved by the Director of the Bureau of the Budget (May 14, 1956)

Journal of Research of the National Bureau of Standards Vol. 59, No. 6, December 1957 Research Paper 2806

Some Factors Affecting the Surface Area of Hydrated Portland Cement as Determined by Water-Vapor and Nitrogen Adsorption

L. A. Tomes,[1] C. M. Hunt, and R. L. Blaine

Brunauer-Emmett-Teller (BET) surface areas of hydrated portland cement have been calculated from water-vapor and nitrogen-adsorption data. The adsorption and desorption of water vapor caused measurable decreases in specific surface areas by both water-vapor and nitrogen adsorption. Changes were also produced by wetting and drying. The adsorption and desorption of nitrogen at the boiling point of liquid nitrogen did not produce similar effects.

The specific surface and nonevaporable-water content of a hydrated cement are also somewhat dependent on the initial drying treatment. The effect of measuring water-vapor surface and nonevaporable water with specimens dried for different periods of time is also considered.

1. Introduction

Measurements of water vapor [1, 2, 3a, 3b, 4] [2] and nitrogen sorption [4, 5], as well as other evidence [6, 7], have demonstrated that the hydration products of portland cement are largely colloidal in nature. Powers and Brownyard [3a, 3b] have carried out water-vapor adsorption measurements on a number of hydrated cements and found that v_m, the parameter in the Brunauer-Emmett-Teller (BET) equation [8], from which a value for specific surface is calculated, was proportional to w_n, the nonevaporable-water content of the hydrated cement. They found the ratio of v_m/w_n to be relatively constant and not greatly affected by the age or water-cement ratio of the specimen. The constant proportionality between v_m and w_n indicates that surface computed from water-vapor adsorption data is proportional to the amount of hydration products present. This evidence suggests that some kind of structural similarity exists between the hydration products formed during the first few days of hydration, and those formed during the later stages of hydration [3a].

Although the constant v_m/w_n ratio for specimens made from a given cement provides an important clue in determining the submicroscopic morphology of hydrated portland cement, both v_m [9] and w_n [3a, 9, 10] are somewhat dependent upon the arbitrary conditions under which they are determined. For example, it was noted by Powers and Brownyard [3a] that successive sorption isotherms by the same specimen of hardened cement paste were not reproducible, a fact that suggests strong interaction between water vapor and one or more of the hydration products of cement. Thus, whereas specific surface is a function of the amount of hydration products present, nonreversible sorption behavior suggests that it also depends on the history of a specimen after hydration has stopped. The present paper considers the nonreversible sorption behavior of hydrated cement and gives further examples that illustrate the effect of wetting or exposure to water vapor upon subsequent adsorption of water vapor by hardened cement paste. Nitrogen-adsorption measurements have also been made as an independent method of detecting small changes in the colloidal structure of hydrated cement.

Another factor to be considered in the determination of v_m and w_n is the difficulty of determining how much of the water in a hardened cement is chemically combined [3a, 9, 10, 11]. However, by carefully controlling the conditions of drying, it is possible to obtain a reproducible but arbitrary dry weight, which affords a baseline from which to determine v_m and w_n. Powers and Brownyard [3a, 3b] have determined these quantities after drying hardened cement paste in a vacuum system containing magnesium perchlorate dihydrate and tetrahydrate, whereas Copeland and Hayes [9] have described a procedure for vacuum-drying cement pastes, which uses a dry-ice trap in the system to establish the water-vapor concentration. According to Copeland and Bragg [12], nonevaporable water in specimens dried by this latter procedure probably corresponds rather closely to chemically combined water. However, hardened cement pastes and hydrated calcium silicates reach constant weight almost asymptotically when dried in vacuum at room temperature. It is common practice to discontinue drying while the specimens are still losing weight at a very small but detectable rate [9, 13]. Therefore, this paper also considers the manner in which v_m and w_n vary when they are determined on specimens of the same paste that have been dried for different periods of time.

2. Methods and Materials

2.1. Water-Vapor and Nitrogen Adsorption Measurements

Two types of water-vapor sorption apparatus were used in these experiments, a vacuum apparatus

[1] Research Associate representing the Calcium Chloride Institute at the National Bureau of Standards.
[2] Figures in brackets indicate the literature references at the end of this paper.

similar to the McBain-Bakr Balance [14], and a gas-stream apparatus. The essential features of the vacuum apparatus, including one of its six quartz springs, is illustrated in figure 1. The apparatus could accommodate specimens weighing 0.4 to 0.8 g. Spring extensions were measured with an external cathetometer. The gas-stream apparatus, illustrated in figure 2, was similar to the one described by Powers and Brownyard [3a]; however, it used nitrogen instead of air to transport the water vapor. Five-gram specimens were used with this apparatus, although it could handle much larger specimens. Five to seven days were allowed for sorption equilibrium with the gas-stream apparatus, whereas 24 hr were allowed with the vacuum apparatus. Exposure of hardened cement pastes for longer periods of time at these relative humidities has indicated that very little additional water was taken up, and a few specimens actually lost weight, a behavior previously noted by Powers and Brownyard [3a]. Both the vacuum and gas-stream apparatus were operated in a cabinet maintained at 25.0° ±0.1° C.

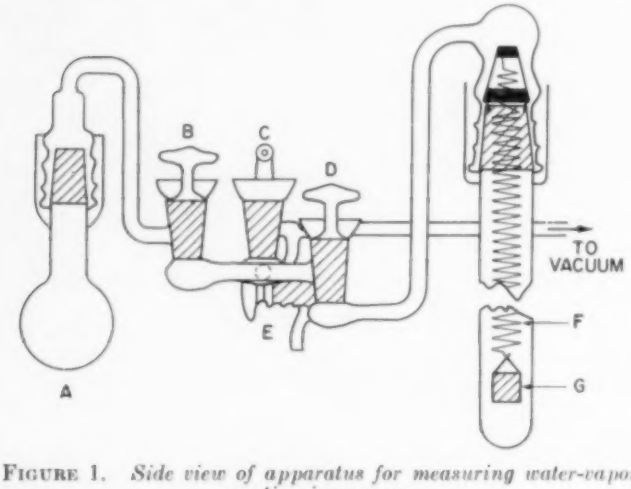

FIGURE 1. *Side view of apparatus for measuring water-vapor sorption in vacuum.*

Solutions used and relative vapor pressures [15] are: Sodium hydroxide, 0.0703; lithium chloride, 0.1105; potassium acetate, 0.2245; magnesium chloride, 0.3300. A, Flask containing saturated solution for establishing water-vapor pressure; B, stopcock for isolating solution flask; C, stopcock to vacuum pump; D, stopcock for isolating specimen tubes; E, stopcock for admitting air to apparatus; F, quartz spring; G, specimen bucket.

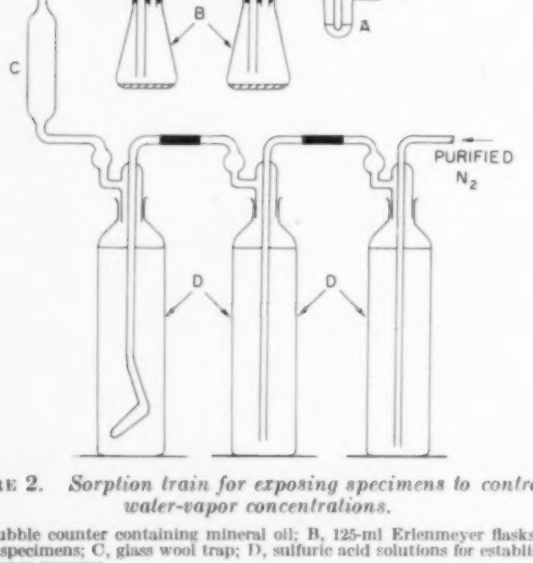

FIGURE 2. *Sorption train for exposing specimens to controlled water-vapor concentrations.*

A, Bubble counter containing mineral oil; B, 125-ml Erlenmeyer flasks containing specimens; C, glass wool trap; D, sulfuric acid solutions for establishing water vapor pressure.

Specimens were vacuum dried in an apparatus similar to the one described by Copeland and Hayes [9], in which a trap maintained at the temperature of dry ice was placed between the specimens and the pump. The system maintained a vacuum of about 2 μ of mercury in the final stages of drying, and it was operated in a room maintained at 21° C. The vapor pressure of water at −78° C is 0.56 μ. When the vacuum apparatus illustrated in figure 1 was used, final drying and water-vapor adsorption measurements were carried out in the same apparatus.

Values of v_m were calculated by the BET equation [8],

$$\frac{p}{v(p_0-p)}=\frac{1}{v_mC}+\frac{C-1}{v_mC}\,p/p_0,$$

where p is the pressure of water vapor in equilibrium with the specimen, p_0 is the vapor pressure of pure water, C is a constant related to the heat of adsorption, and v is the amount of water adsorbed per gram of specimen. Because the adsorption of water was measured gravimetrically, v and v_m have been expressed in grams of water per gram of specimen. To compute surface areas, an area coverage of 10.6 A^2 was assumed for the water molecule.

Nitrogen adsorption measurements were made with an apparatus similar to that described by Emmett [16]. Specimens were outgassed overnight at 100° to 110° C before measuring their nitrogen adsorption. Surface areas were calculated, assuming each molecule to cover an area of 16.2 A^2.

2.2. Nonevaporable Water Determination

The values for nonevaporable water appearing in figure 6 were determined by igniting the specimens to constant weight at 1,050° C after they were vacuum dried in a system containing a trap at the temperature of dry ice. This is essentially the procedure of Copeland and Hayes [9], except that drying time has been purposely made variable. The nonevaporable water differs from the loss on ignition by an amount equal to the ignition loss of the original cement. As Powers and Brownyard have pointed out [3a], there is some uncertainty in this correction, which means that the absolute values of nonevaporable water are known with less certainty than the relative values.

2.3. Preparation of Specimens

Neat cement pastes, having a water-cement ratio of 0.5, were prepared in a mechanical mixer and cast in the form of square wafers 1 cm thick and 5 cm on

each side. The specimens were removed from the molds after 24 hr and cured in closed quart jars in the presence of high concentrations of water vapor for periods indicated in the experiments. To stop hydration, the specimens were vacuum dried for 2 days. They were broken into smaller pieces and stored several months in sealed glass tubes before sampling. In this way, storage changes were not taking place at a significant rate at the start of the experiments.

The chemical composition of the clinker and the cement from which the pastes were prepared is given in table 1.

TABLE 1. *Composition of cement clinker* [a]

Oxide	Percentage by weight	Calculated composition, percentage by weight [b]	
		Composition	Percentage
CaO	65.13	3 $CaO \cdot SiO_2$	56
SiO_2	22.62	3 $CaO \cdot Al_2O_3$	3
Al_2O_3	4.41	4 $CaO \cdot Al_2O_3 \cdot Fe_2O_3$	16
Fe_2O_3	5.33	2 $CaO \cdot SiO_2$	23
SO_3	0.10		
MgO	1.71		
Na_2O	0.04		
K_2O	.28		
Loss on ignition [a]	.37		
Insoluble residue	.14		

[a] This clinker was interground with gypsum and blended to a 1.8-percent SO_3 content. The ignition loss of the blended cement at 1,050° C was 1.69 percent.
[b] Composition calculated from equations found in Bogue, The Chemistry of Portland Cement, p. 548 (Reinhold Publishing Co., Inc., New York, N. Y., 1947). The values represent potential composition at equilibrium crystallization.

3. Results

3.1. Sorption and Desorption of Water Vapor

Table 2 gives the amounts of water adsorbed by two specimens of paste which were subjected to several cycles of drying and exposure to water vapor. The experiment was carried out in the apparatus illustrated in figure 1. The specimens were dried 6 days from the stored state before initial exposure to water vapor. In cycles 2 through 7 the specimens were redried as nearly as possible to their cycle 1 dry weight before exposure to water vapor. When dried in this way, permanent loss of chemically combined water would appear in table 2 as a decrease in the amount of water adsorbed, because all of the sorption sites initially available would not be uncovered by redrying specimens to their initial dry weight. In cycle 8, however, the specimens were dried 41 days, so that any initially available sites would be uncovered, unless the specimens had undergone change during the experiment.

It may be seen from table 2 that the specimens adsorbed less water with each repeated exposure to water vapor for the first 4 or 5 cycles. Thereafter, the effects were less marked. This is illustrated in another way in figure 3, where calculated surface areas have been plotted for each cycle of drying and humidification. In the eighth cycle, after the 41-day drying treatment, slightly more water was adsorbed than in the preceding cycle, but the original sorptive capacity of the specimens was never regained. The

TABLE 2. *Amounts of water adsorbed by cement paste during several cycles of drying and adsorption*

Specimen [a]	Cycle	[b] Grams of water adsorbed per gram of dry paste at relative vapor pressure (p/p_0)—			
		0.0703	0.1105	0.2245	0.3300
1. Lumps of paste 5 to 8 mm in diameter.	1	0.0214	0.0249	0.0314	0.0355
	2	.0190	.0215	.0271	.0308
	3	.0178	.0201	.0248	.0283
	4	.0169	.0190	.0236	.0266
	5	.0154	.0183	.0225	.0256
	6	.0159	.0182	.0218	.0248
	7	.0155	.0174	.0211	.0242
	8	.0165	.0192	.0228	.0257
2. Pulverized paste less than 1 mm in diameter	1	.0229	.0262	.0325	.0364
	2	.0196	.0231	.0273	.0308
	3	.0173	.0198	.0241	.0271
	4	.0169	.0193	.0229	.0260
	5	.0146	.0172	.0210	.0238
	6	.0157	.0176	.0210	.0233
	7	.0140	.0158	.0193	.0220
	8	.0152	.0175	.0209	.0230

[a] The specimens were obtained from paste that was cured in moist air for 1 week. Specimen 1 weighed 0.6636 g and specimen 2 weighed 0.7181 g in their dryest state (cycle 8).
[b] $(w - w_d)/w_{d8}$; w = weight of conditioned specimen, w_d = dry weight of specimen for respective cycle, and w_{d8} = dry weight of specimen for cycle 8.

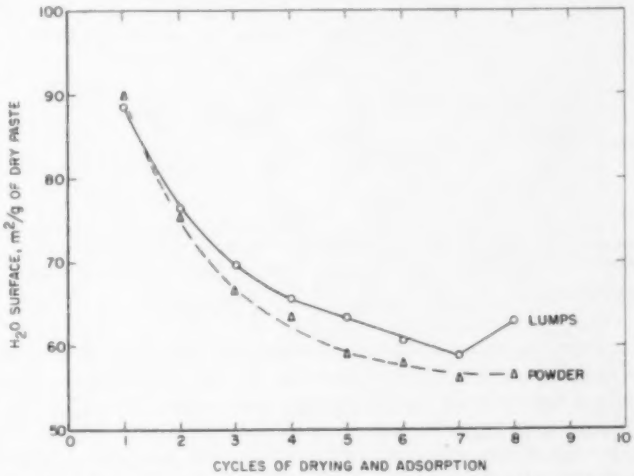

FIGURE 3. *Specific surface by water-vapor adsorption obtained by repeated measurement of the same specimens of hardened cement paste.*

dry weight of the specimens did not decrease by more than 2 to 3 mg per gram of paste between the seventh and eighth cycles. There may be uncertainties in this estimate, due to gain of small amounts of carbon dioxide or other atmospheric contaminants during the course of the experiment, but the change in dry weight could be much larger than 2 to 3 mg and still be too small to account for change in nonevaporable water proportional to the change in computed surface. Therefore, the loss in sorptive capacity probably involves small changes in the colloidal structure of the paste.

The first specimen in table 2 consisted of lumps of hardened paste 5 to 8 mm in diameter, whereas the second specimen was crushed in an atmosphere of nitrogen until most of it was reduced to a powder much finer than the 1-mm upper limit given in the table. Comparison of the results obtained with

these two specimens shows them to be slightly different. However, it is evident that the amount of water adsorbed and the change in sorptive capacity during the course of the experiment was not extremely dependent on the state of subdivision of the specimens.

Surface areas determined by nitrogen adsorption also showed the effect of exposure to water vapor. In table 3, surface values are given for specimens that were measured after initial drying, and specimens that were exposed to water vapor at relative humidities up to 24 percent and redried. The redried specimens had smaller surfaces, affording independent evidence of change in the colloidal structure of the paste. There is no evidence that the adsorption and desorption of nitrogen at low temperatures brought about changes similar to those produced with water vapor.

TABLE 3. *Effect of adsorption and desorption of water vapor on the nitrogen surfaces of cement pastes*

Curing time	Measured after initial drying		Measured after adsorption and desorption of water vapor	
	Specimen [a]	Surface	Specimen [a]	Surface
		m^2/g		m^2/g
1 day	3A	19.6	3C	11.4
1 day	3B	18.0	3D	
1 week	4A	19.9	4C	15.9
1 week	4B	18.5	4D	16.1
1 month	5A	21.8	5C	17.5
1 month	5B	21.8	5D	18.0

[a] The A, B, C, and D specimens were taken from the same sample of hardened paste, which was not blended to produce uniformity as were samples in the ensuing experiments.

3.2. Wetting and Drying

Because the adsorption and desorption of water vapor resulted in changes in hydrated cement, the effect of wetting and drying was also investigated. Table 4 gives the amount of water vapor adsorbed by three specimens of paste, one of which was measured after the initial drying, and the others after rewetting and redrying. The experiment was performed with 5-g specimens, and adsorption measurements were made with the apparatus illustrated in figure 2. Rewetting and redrying were accomplished by covering the specimens with water for 1 hr at 21° ±2°C and carefully reevaporating the water in vacuum. The entire operation was performed in the adsorption flasks, so that any extracted material would be redeposited with the specimens. The results in table 4 have been expressed in grams of water adsorbed per gram of ignited paste, to permit closer comparison of different specimens. The paste from which these specimens were obtained was crushed and carefully blended before sampling. Analysis of data from 35 hardened pastes has shown that the amount of water adsorbed by different specimens from the same blended paste can be determined with a standard deviation of 0.3 mg per gram of ignited paste. This reproducibility indicates that the results in table 4 are highly significant.

TABLE 4. *Effect of wetting and drying on the subsequent adsorption of water vapor by a dried cement paste*

Specimen [a]	Number of times wet and dried	Grams of water adsorbed per gram of ignited paste at relative vapor pressure (p/p_0)—			
		0.0980	0.1462	0.1946	0.2380
6A	0	0.0275	0.0304	0.0327	0.0348
6B	1	.0265	.0293	.0316	.0336
6C	3	.0255	.0276	.0297	.0314

[a] These specimens were obtained from paste that was cured in moist air for 1 week.

Comparison of table 4 with table 2 shows that wetting and drying produced less change in water-sorptive capacity than was produced by adsorption and desorption of water vapor. This difference suggests that the adsorption and desorption process may have occurred in a relative humidity range where shrinkage effects predominated, whereas wetting and drying produced strong swelling and shrinking during each cycle.

The nitrogen surface was larger after a single rewetting, but smaller after the process was repeated two more times. The results are given in table 5. It is believed that these changes do not represent a spurious effect, because they could be produced with other pastes. The change in water-vapor surface after a single rewetting was quite small, as shown in table 5. This suggests that a small shrinkage of the

TABLE 5. *Comparison of water vapor and nitrogen surface areas of cement pastes, showing the effects of wetting and drying*

Number of times wet and dried	Water vapor		Nitrogen	
	Specimen [a]	Surface [b]	Specimen [a]	Surface [b]
		m^2/g		m^2/g
0	6A	97.7	6D	12.7
1	6B	94.5	6E	23.2
3	6C	87.3	6F	10.5

[a] These specimens were obtained from paste that was cured in moist air for 1 week.
[b] Specific surface based on ignited weight of paste.

regions accessible to water may increase the size or number of channels accessible to nitrogen, whereas further shrinkage reduces accessibility to both water vapor and nitrogen. Another possible explanation of the changes in nitrogen surface is that most of the water-soluble materials would probably be dissolved from the pores of the paste during the first rewetting, whereas in subsequent wetting and drying the water-soluble materials have already been removed and the shrinkage effect would predominate. It seems reasonable that water-vapor sorption would be relatively unaffected by the presence or absence of water-soluble materials in the pores of the paste.

It was anticipated that wetting the specimens would lead to further hydration, because they were covered with water for 1 hr before drying was started. However, they redried to weights that were 2 parts per thousand less than the original dry weight, and

the effect was very reproducible from specimen to specimen. It was doubtful if additional hydration took place during wetting, but if it did, it was completely obscured by structural changes which facilitated drying.

3.3. v_m and w_n as Functions of Drying Time

v_m and w_n were determined on specimens that were dried for different periods of time. Due to interaction between water vapor and hydrated cement as indicated in the preceding experiments, it was necessary to take a separate specimen for each drying time. The specimens were prepared from a single carefully blended sample of pulverized hydrated cement paste, and each specimen weighed about 5 g. The results, which include drying time, dry weight, and amount of water adsorbed, are given in table 6. All weights are expressed in grams per gram of ignited cement in order to compare data from different specimens. It may be seen from table 6 that the specimens which received longer drying treatments adsorbed more water. Values of v_m and w_n were determined for each specimen and plotted as functions of drying time in figure 4. It is evident that after a week of drying, the rates of change of v_m and w_n were small.

TABLE 6. *Dry weights and amounts of water adsorbed by specimens dried for different periods of time*

Specimen [a]	Cumulative drying time [b]	Dry weight, grams per gram of ignited paste	Grams of water adsorbed per gram of ignited paste at relative vapor pressure (p/p_0)—			
			0.0999	0.1478	0.1954	0.2400
	Days					
7A	2.6	1.1373	0.0147	0.0172	0.0192	0.0214
7B	3.5	1.1234	.0233	.0259	.0284	.0305
7C	4.4	1.1186	.0254	.0285	.0304	.0329
7D	5.4	1.1171	.0259	.0289	.0314	.0336
7E	6.4	1.1155	.0264	.0294	.0320	.0341
7F	8.2	1.1145	.0273	.0303	.0329	.0349
7G	12.1	1.1126	.0283	.0312	.0336	.0359

[a] These specimens were obtained from paste that was cured in moist air for 1 week.
[b] Includes 2 days of predrying the unground paste to stop hydration.

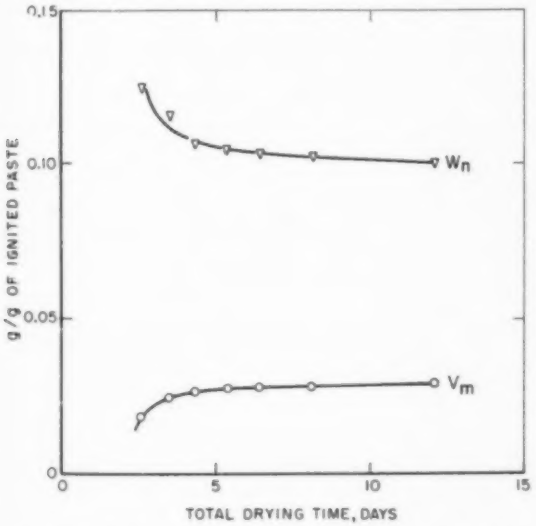

FIGURE 4. *v_m and w_n as functions of drying time.*

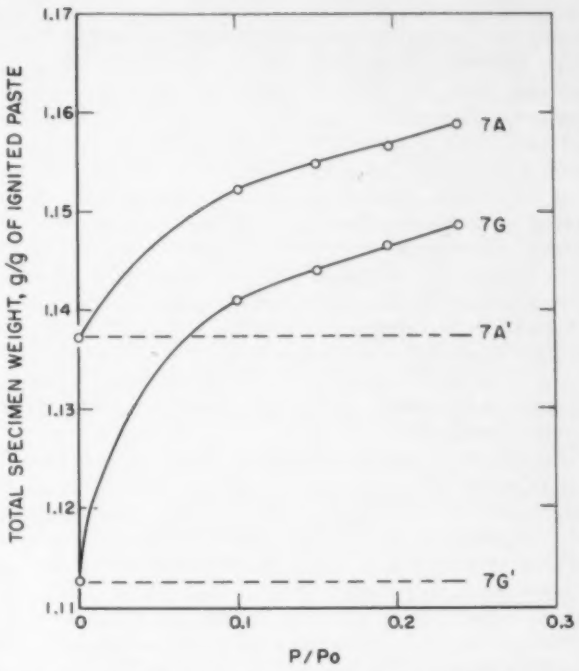

FIGURE 5. *Adsorption isotherms up to 24-percent relative humidity of two specimens of the same cement paste dried to different levels of dryness.*

The dotted lines represent the dry weights of the specimens and the curves represent the specimen weights after exposure to water vapor.

What is not immediately evident from the values in table 6, however, is the fact that the specimens did not resorb all of the water that was removed in the latter stages of drying. It can be readily shown that differences in the amount of water adsorbed by any two specimens at the same relative humidity are smaller than the differences in their respective dry weights. Failure to regain all of this weight may be illustrated in another way. Using data from table 6, the adsorption isotherms for specimens 7A and 7G up to 24 percent relative humidity are plotted in figure 5. The amount of water adsorbed has been added to the dry weight, and the values so obtained are plotted as a function of relative vapor pressure. The horizontal dotted lines 7A′ and 7G′ represent the dry weights per gram of ignited paste. It is evident that the isotherm for specimen 7G, which was dried much longer than specimen 7A, did not retrace the 7A isotherm. The isotherms were completed in about 40 days, and there is no evidence from the rates at which they gained weight that the two specimens would have reached the same weight in a much longer period.

4. Discussion

The water molecule, by virtue of its small molecular size and polar nature, is able to penetrate into colloidal domains of many adsorbents to which nitrogen cannot penetrate. This is true of hydrated cement, as shown by the results of Gleysteen and Kalousek [4], as well as the values given in table 5.

The polar and reactive nature of the water molecule raises some question as to the mechanism of sorption where certain adsorbents are involved [17,18,19,20]. This may also be true of hydrated portland cement. However, Bogue [6] has briefly reviewed evidence that the surface area of hydrated cement, by water-vapor adsorption, is of the magnitude to be expected from electron microscope and low-angle X-ray scattering measurements. For the purposes of the present discussion, it is not essential that either the water vapor or nitrogen surface represent absolute surface values, to bring out the structurally significant fact that water vapor has access to sorption sites in hydrated portland cement that are inaccessible to nitrogen, or to investigate a few of the factors affecting the magnitude and reproducibility of surface values obtained.

The present paper considers some characteristics of hydrated cement which are important in the design and interpretation of gas and vapor adsorption experiments. They illustrate some of the problems involved in the determination of specific surface and nonevaporable water, and they also suggest that exposure to water or water vapor should not be one of the unintentional or uncontrolled variables in an experiment.

The isotherms of Powers and Brownyard [3a], mentioned in the early part of this paper, were measured at relative vapor pressures extending from dryness to slightly less than saturation pressure, and the specimens showed permanent gain in weight when redried. They attributed differences in successive isotherms to irreversible shrinkage at low relative humidity and additional hydration at relative humidities greater than 80 percent. In the present experiments, the specimens were not exposed to relative humidities greater than 33 percent, except those that were rewet and redried. Furthermore, it was possible to redry all specimens to weights close to their original dry weights. In this connection, Powers [21] has presented data showing that the hydration of an unhydrated cement was virtually unmeasureable when the cements were stored at relative humidities below 30 percent. He also found that hydration was slight unless the cement was exposed to relative humidities greater than 70 percent. Thus, in the present experiments, changes in specific surface of the order of 10 to 30 percent of the initial value were produced with little if any change in the degree of hydration.

The changes in surface and v_m obtained here might be predicted from Powers and Brownyard's results, or from the changes in structure that are believed to take place in other inorganic gels during aging [22, 23], wetting and drying [23], or adsorption and desorption of vapors [23]. However, this would not be predicted from the earlier isotherms of Jesser, which indicated that once initial drying shrinkage had taken place, adsorption and desorption of water vapor were reversible [1, 2, 24]. However, some differences between Jesser's experiments and the present ones might be pointed out. He measured comparatively large specimens of low water-cement ratio that were never subjected to vacuum drying, whereas the specimens in the present experiments were broken into small pieces, or even pulverized, and dried in vacuum. Jesser's experiments resemble, to some extent, conditions to which a concrete might be exposed in service, whereas the present experiments and those of Powers and Brownyard employ rather conventional gas sorption techniques [14].

There are a number of mechanisms by which the accessibility of an adsorbent to nitrogen or water vapor might be reduced, and a few examples might be cited. Rao found "drift" in the water-sorption isotherms of titania [25] and ferric oxide [26] gels. He attributed it to coalescence of smaller particles into larger particles, accompanied by a decrease in total capillary volume. An example that may be more closely related to the colloid chemistry of hydrated portland cement is Taylor's evidence [27] that calcium silicate hydrate I, sometimes referred to as tobermorite [28, 29], possesses an expanding layer structure similar to that found in some clay minerals. He also found that water-vapor isobars of this compound did not return to their starting point [30], and suggested that this was due to failure of the lattice to reexpand to its original dimensions when brought back to the original conditions of temperature and humidity. Another process by which the surface of an adsorbent might change is polymorphic transformation. Kalousek [31] noted changes in the X-ray pattern of one of his calcium silicate hydrate preparations. Also Brunauer, Copeland, and Bragg [32] reported indications that removal of lime from their tobermorite preparation resulted in formation of small amounts of afwillite. Whatever the mechanism by which the sorptive capacity of hydrated portland cement changes, the present experiments suggest changes in sorptive capacity, and the factors producing these changes are fully as interesting as the surface values themselves.

Another point should be mentioned in connection with the initial drying of hydrated cement paste. If one takes the data shown in figure 4 and plots v_m

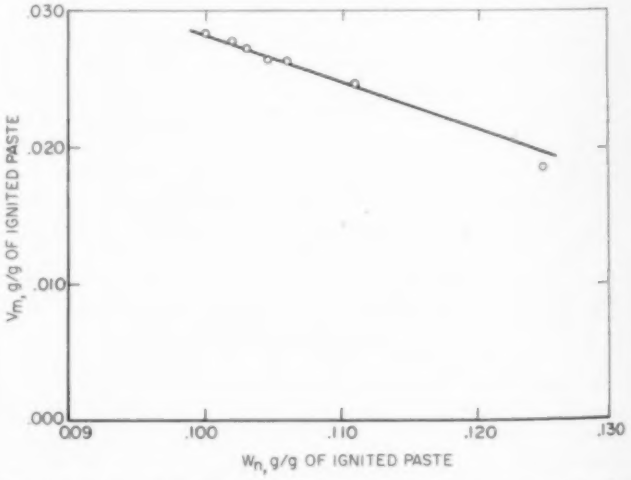

FIGURE 6. *v_m as a function of nonevaporable water content of a cement paste dried to different levels of dryness.*

as a function of w_n as has been done in figure 6, a linear relationship is obtained. This line differs from the v_m/w_n plots of Powers and Brownyard [3b], because all of the points have been obtained by drying the same paste for different periods of time, while the plots of Powers and Brownyard were obtained with pastes of different ages which were all dried the same way. The slope of the line in figure 6 is -0.35, which means that v_m increased by 0.35 mg for every milligram of water removed during the latter stages of drying. Expressed as specific surface, 0.35 mg corresponds to 1.2 m^2/g. Copeland and Hayes [9] have pointed out that there is no simple way of calculating a change in v_m corresponding to a change in w_n produced by a different drying treatment. The linear relationship in figure 6 suggests a possible empirical approach to the problem.

5. Summary

Adsorption and desorption of water vapor and repeated wetting and drying resulted in decrease in the water-vapor sorptive capacity of a hardened cement paste. Changes were also produced in the nitrogen sorptive capacity. These results do not preclude the possibility of very small losses of chemically combined water or gains of small amounts of atmospheric contaminants; however, they probably represent shrinkage or other modification of the colloidal structure of cement paste. If surface areas calculated from sorption data are to be treated as functions of the amount of hydration products present, it is important to consider the history of a specimen after hydration has stopped.

The effect of varying the drying time before measuring the nonevaporable water content and surface area by water-vapor adsorption was also considered. When a hardened paste received successively longer drying treatments, a linear relationship between v_m and w_n was obtained as the paste approached dryness.

The authors are indebted to T. C. Powers and L. E. Copeland of the Portland Cement Association for many useful suggestions, particularly those relating to the design of equipment for drying cement pastes and measuring water-vapor adsorption. The authors also gratefully acknowledge the assistance of Vernon Dantzler in performing the nitrogen-adsorption measurements reported here.

6. References

[1] L. Jesser, Kolloidchemische Reaktionen des Tonerdezementmortels, Zement **16,** 741 (1927).

[2] S. Giertz-Hedstrom, The physical structure of hydrated cements, Symposium on the Chemistry of Cements (Stockholm, 1938).

[3] T. C. Powers and T. L. Brownyard, Studies in the physical properties of hardened portland cement paste: (a) Part 2, Studies of water fixation, Proc. Am. Concrete Inst. **43,** 249 (1946); (b) Part 3, Theoretical interpretation of adsorption data, Proc. Am. Concrete Inst. **43,** 469 (1946); also Portland Cement Assoc. Bul. 22.

[4] L. F. Gleysteen and G. L. Kalousek, A simplified method for the determination of apparent surface area of concrete blocks, Proc. Am. Concrete Inst. **51,** 437 (1955).

[5] R. L. Blaine and H. J. Valis, Surface available to nitrogen in hydrated portland cements, J. Research NBS **42,** 257 (1949) RP1967.

[6] J. D. Bernal, The structures of cement hydration compounds, Third International Symposium on the Chemistry of Cement, p. 222 (London, 1952). See also, appended discussions by Grudemo, p. 247, R. H. Bogue, p. 254, and author's closure, p. 257.

[7] M. Swerdlow, H. F. McMurdie, and F. A. Heckman, Hydration of tricalcium silicate, Proc. Intern. Conf. Electron Microscopy, p. 500 (London, July 1954). Roy. Microscopical Soc. paper No. 119; also Portland Cement Assoc. Fellowship Paper 71.

[8] S. Brunauer, P. H. Emmett, and E. Teller, Adsorption of gases in multimolecular layers, J. Am. Chem. Soc. **60,** 309 (1938).

[9] L. E. Copeland and J. C. Hayes, Determination of nonevaporable water in hardened portland cement paste, Am. Soc. Testing Materials Bul. 194, p. 70 (1953); also Portland Cement Assoc. Bul. 47.

[10] T. C. Powers, Nonevaporable water content of hardened portland cement paste—its significance for concrete research and its method of determination, Am. Soc. Testing Materials Bul. 158 (May 1949); also Portland Cement Assoc. Bul. 29.

[11] F. M. Lea, Water in set cement, Cement and Cement Manuf. **5,** 395 (1932).

[12] L. E. Copeland and R. H. Bragg, Self desiccation in portland cement pastes, Am. Soc. Testing Materials Bul. 204, p. 34 (1955).

[13] S. Brunauer, L. E. Copeland, and R. H. Bragg, The stoichiometry of the hydration of tricalcium silicate at room temperature. I. Hydration in a ball mill, J. Phys. Chem. **60,** 112 (1956).

[14] J. W. McBain, The sorption of gases and vapors by solids, p. 23 (G. Routledge & Sons, Ltd., London, 1932).

[15] R. H. Stokes and R. A. Robinson, Standard solutions for humidity control at 25° C, Ind. Eng. Chem. **41,** 2013 (1949).

[16] P. H. Emmett, A new method for measuring the surface areas of finely divided materials and for determining the size of particles, Symposium on new methods for particle size determination in the subsieve range, Am. Soc. Testing Materials (March 1941).

[17] P. H. Emmett, Gas adsorption methods for measuring surface area of adsorbents, Ind. Eng. Chem. **37,** 642 (1945).

[18] H. S. Frey and W. J. Moore, Adsorption of water vapor on glycine, leucine, diketopiperizene, and diglycylglycine, J. Am. Chem. Soc. **70,** 3644 (1948).

[19] M. Dole, Statistical thermodynamics of the sorption of vapors by solids, J. Chem. Phys. **16,** 25 (1948).

[20] J. P. Quirk, Significance of surface areas calculated from water vapor sorption isotherms by use of the BET equation, Soil Sci. **80,** 423 (1955).

[21] T. C. Powers, A discussion of cement hydration in relation to the curing of concrete, Proc. Highway Res. Bd. **27,** 178 (1947); also published as Portland Cement Assoc. Bul. 25.

[22] H. B. Weiser, A textbook of colloid chemistry, p. 316 (John Wiley and Sons, New York, N. Y., 1949).

[23] S. Brunauer, The adsorption of gases and vapors, p. 408 (Princeton Univ. Press, Princeton, N. J., 1945).

[24] F. M. Lea, The chemistry of cement and concrete, p. 223 (St. Martin's Press, Inc., New York, N. Y., 1956).

[25] K. S. Rao, Hysteresis in sorption. I. Permanence of the hysteresis loop, titania gel-water system, J. Phys. Chem. **45,** 500 (1941).

[26] K. S. Rao, Hysteresis in sorption. V. Permanence, scanning, and drift of the hysteresis loop, ferric oxide gel-carbon tetrachloride and ferric oxide gel-water systems, J. Phys. Chem. **45,** 522 (1941).

[27] H. F. W. Taylor, Hydrated calcium silicates. I. Compound formation at ordinary temperatures, J. Chem. Soc. (London) p. 3682 (1950).

[28] R. H. Bogue, A note on the nomenclature of the calcium silicate hydrates, Mag. of Concrete Research No. 14, p. 87 (1953); also issued as Portland Cement Assoc. Fellowship Paper 66.
[29] G. P. Claringbull and M. H. Hey, A re-examination of tobermorite, Min. Mag. and J. Min. Soc. **29,** 960 (1952).
[30] H. F. W. Taylor, Hydrated calcium silicates. V. The water content of calcium silicate hydrate I, J. Chem. Soc. (London) p. 163 (1953).
[31] George L. Kalousek, Tobermorite and related phases in the system CaO–SiO_2–H_2O, Proc. Am. Concrete Inst. **51,** 989 (1955).
[32] S. Brunauer, L. E. Copeland, and R. H. Bragg, The stoichiometry of the hydration of tricalcium silicate at room temperature. II. Hydration in paste form. J. Phys. Chem. **60,** 117 (1956).

WASHINGTON, January 14, 1957.

Journal of Research of the National Bureau of Standards Vol. 59, No. 6, December 1957 Research Paper 2807

Excitation of Surface Waves on Conducting, Stratified, Dielectric-Clad, and Corrugated Surfaces

James R. Wait

An expression for the field of an electric dipole located over a flat surface with a specified surface impedance Z is derived from the formal integral solution by a modified saddle-point method. Using the value of Z appropriate for a homogeneous conducting ground, the general expressions reduce to those given by Norton. In this case the phase of Z lies between 0 and 45°. When the phase exceeds 45°, as it may for a stratified ground, the radiated wave of the dipole becomes partially trapped to the interface. This effect is most pronounced for an inductive surface where the phase of Z is 90°, in which case the energy of the wave is confined within a small distance from the surface. Such inductive surfaces are a metallic plane with a thin dielectric film or a corrugated surface.

This unifying treatment provides a link between the surface waves of Zenneck, Sommerfeld, Norton, and Goubau, and indicates that the phase angle of Z controls the extent to which these waves may exist for a dipole excitation.

1. Introduction

The propagation of radio waves along the surface of the ground has been discussed from a theoretical standpoint for many years. As long ago as 1907, Zenneck [1] [1] showed that a wave, which was a solution of Maxwell's equations, traveled without change of pattern over a flat surface bounding two homogeneous media of different conductivity and dielectric constants. When the upper medium is air and the lower medium is a homogeneous dissipative ground, the wave is characterized by a phase velocity greater than that of light and a small attenuation in the direction along the interface. Furthermore, this Zenneck surface wave, as it has been called, is highly attenuated with height above the surface. In 1909 Sommerfeld [2] solved the problem of a vertical dipole over a homogeneous ground (half-space). In an attempt to explain the physical nature of his solution, he divided the expression for the field into a "space wave" and a "surface wave." Both parts, according to Sommerfeld, are necessary in order to satisfy Maxwell's equations and the appropriate boundary conditions. The surface-wave part varied inversely as the square root of the range, and it was identified as the radial counterpart of the plane Zenneck surface wave.

For many years it was believed that this Sommerfeld surface wave was the predominant component of the field radiated from a vertical antenna over a finitely conducting ground. It was not until 1935 that an error in sign in Sommerfeld's 1909 paper [2] was pointed out by Norton [3], which also partly accounted for the unusual calculated field-strength curves of Rolf [4]. At about this time there was a series of papers by Weyl, Van der Pol, Niessen, Wise, and Norton, deriving more accurate representations for the field of the dipole. A discussion of this later work has been given by Bouwkamp [5]. Norton [6, 7], in particular, has developed his formula for the field components to a stage where numerical results can readily be obtained. It is now generally accepted that the Sommerfeld surface wave (or the radial Zenneck wave) does not bear any similarity to the total field of a vertical dipole over a homogeneous conducting earth. In fact, the field excited by a dipole varies as $1/d$, where d is the distance for low frequencies, and it varies as $1/d^2$ for high frequencies. Norton has suggested that the field in air of a dipole over a homogeneous ground be expressed as a sum of three components: A direct ray (or primary influence), a reflected ray which is to be modified by an appropriate Fresnel reflection coefficient, and a correction term. Norton has described the first and second components as the space wave; the third or correction term, the surface wave. This seems to be a logical step,

[1] Figures in brackets indicate the literature references at the end of this paper.

[2] It has been suggested by B. M. Fannin (Final Report, Pt. III, Investigations of air to air and air to ground experimental data, Elec. Eng. Dept., Cornell University, 1951) that Summerfeld did not actually make an "error in sign" in his 1909 paper. Fannin's contention is that Rolf and other workers simply misinterpreted Sommerfeld's formula for the attenuation factor. This can hardly be so, as Sommerfeld himself in 1910 (The propagation in wireless telegraphy, Jahrb. d. Drahtl. Tel. 4, 157, 1910) used the incorrect formula and its resulting series expansion.

although, taken separately, the space and surface waves of Norton are not solutions of Maxwell's equations. On the other hand, his "space wave" is the contribution that would be derived on the basis of geometrical optics, and his "surface wave" is the correction from wave theory. This latter term will be called the "Norton surface wave" as distinct from the Zenneck and Sommerfeld surface waves, and the trapped surface waves discussed below.

It was pointed out by Sommerfeld [8] nearly 60 years ago that a straight cylindrical conductor of finite conductivity can act as a guide for electromagnetic waves. Some 50 years later Goubau [9, 10] demonstrated that such a cylindrical surface can be launched with reasonable efficiency from a coaxial line whose outer surface is terminated in a conical horn. The improvement in the transmission properties by coating the wire with a thin dielectric film has been discussed in detail by Goubau [10]. The plane counterpart of the Goubau-Sommerfeld cylindrical surface wave is obtained when a flat metallic surface is coated with a dielectric film. Atwood [11] has discussed the nature of the surface waves that can exist in a structure of this type. When the film thickness is small compared to the wavelength, the single propagating mode has a phase velocity slower than that of light and is attenuated rapidly above the surface in the air. Such surfaces have been called inductive because the normal surface impedance, looking into the surface, is almost purely imaginary for a low-loss dielectric on a well-conducting base. A similar type of surface wave can exist over a corrugated surface [12, 13, 14] which is inductive if the periodicity and depth of the corrugation are small compared to the wavelength.

The excitation of surface waves on dielectric-clad plane conducting surfaces has been discussed by Tai [15] for a line current source, and Brick [16] for a dipole source. Corresponding treatments for corrugated surfaces have been given by Cullen [17] for a line magnetic or infinite slot source, and Barlow and Fernando [18] for a vertical electric dipole source. In the case of dipole excitation, the field varies predominantly as the inverse square root of the distance along both the dielectric-clad and the corrugated surfaces. Surface waves of this type, which have a phase velocity less than that of light, can be called "trapped surface waves" because they carry most of their energy within a small distance from the interface [19, 20].

It is the purpose of the present paper to study the general problem of a vertical dipole over a flat surface with a specified surface impedance, Z. A solution is obtained for the field in terms of the error function of complex argument. It is shown that, using an appropriate value for Z, the expressions for the Norton space and surface wave for a homogeneous conducting ground are obtained as a special case [7]. By allowing Z to be purely imaginary and using asymptotic expansions for the error function, the field is shown to be of a trapped-surface-wave type [14, 19]. Another special case is for a two-layer conducting ground [21, 22] which can exhibit some of the features of trapped surface waves. Thus, a general connection between these various forms of seemingly unrelated surface waves is developed.

2. Basic Formulation

A vertical electric dipole of length ds and current I is located at a height h over a flat ground plane which exhibits the property of surface impedance. Here the ratio of the tangential electric and magnetic fields is specified on the surface of the ground plane and is denoted by Z. Choosing cylindrical coordinates, the dipole is located at $(0,0,h)$ and the ground plane at $z=0$. As will be seen, the Hertz vector at (ρ,ϕ,z) need have only a z component, Π, to satisfy the boundary condition; consequently, the fields are given by [3]

$$E_\rho=\frac{\partial^2\Pi}{\partial\rho\partial z}, \qquad E_\phi=0, \qquad E_z=\left(\beta^2+\frac{\partial^2}{\partial z^2}\right)\Pi \tag{1}$$

$$H_\rho=0, \qquad H_\phi=\frac{\beta^2}{i\mu\omega}\frac{\partial\Pi}{\partial\rho}, \qquad H_z=0,$$

where $\mu=4\pi\times10^{-7}$ and $\beta=2\pi/$free space wavelength. The resultant Hertz vector, Π, can now

[3] A time factor exp $(i\omega t)$ is suppressed throughout.

be represented as a sum of a primary and secondary part in the manner

$$\Pi=\Pi_p+\Pi_r, \tag{2}$$

where

$$\Pi_p=\bar{c}e^{-i\beta r_1}/r_1 \quad \text{with } \bar{c}=\frac{Ids}{4\pi i\omega\epsilon} \quad \text{and} \quad r_1=[(z-h)^2+\rho^2]^{1/2} \tag{3}$$

and Π_r is to be regarded as the influence of the ground plane. In the most elementary case of a perfectly conducting ground plane (i. e., $Z=0$), Π_r would be given by the simple relation

$$\Pi_r=\bar{c}e^{-i\beta r_2}/r_2 \quad \text{with} \quad r_2=[(z+h)^2+\rho^2]^{1/2}. \tag{4}$$

To find Π_r (or Π) for the more general case, it is necessary to express the primary field in terms of an integral representation [2] (sometimes called Sommerfeld's integral), as follows:

$$\frac{e^{-i\beta r_1}}{r_1}=\int_0^\infty \frac{J_0(\lambda\rho)e^{-u|z-h|}\lambda d\lambda}{u}, \tag{5}$$

where $u=(\lambda^2-\beta^2)^{1/2}$ and $J_0(\lambda\rho)$ is a Bessel function of order zero and argument $\lambda\rho$. Due to the presence of the branch point of u, the contour of the integral is indented *upward* slightly at $\lambda=\beta$. Physically, this integral can be regarded as a means of representing the primary field as a spectrum of plane waves whose angles of incidence, θ, on the ground plane are related to the integration variable by $\lambda=\beta\sin\theta$. Consequently, the angles include both real and complex values, ranging from 0 to $\pi/2$ along the real axis and from $\pi/2$ to $\pi/2+i\infty$ along a line parallel to the imaginary axis.

The form of eq (5) suggests writing Π_r in the following form:

$$\Pi_r=\bar{c}\int_0^\infty \frac{J_0(\lambda\rho)e^{-u(z+h)}R(\lambda)\lambda d\lambda}{u}, \tag{6}$$

where $R(\lambda)$ is now a reflection coefficient for plane wave incident on the ground plane at angle of incidence $\theta=\sin^{-1}\lambda/\beta$. Consequently,

$$R(\lambda)=\frac{u-i\beta\Delta}{u+i\beta\Delta}, \tag{7}$$

where

$$\Delta=\frac{Z\beta}{\mu\omega}=\frac{Z}{120\pi}.$$

In the limiting case of a perfect conductor ($Z=0$) it can be seen that $R(\lambda)=1$, and the integral is of the form of a Sommerfeld integral and Π_r is again given by eq (4).

The Hertzian potential Π can then be written in the form

$$\Pi=\bar{c}\left[\frac{e^{-i\beta r_1}}{r_1}+\frac{e^{-i\beta r_2}}{r_2}-2P\right] \tag{8}$$

where $2P$ is the effect of the imperfection of the ground plane which results from a finite value of the surface impedance Z.

3. Evaluation of the Integral P

The integral

$$P=\int_0^\infty \frac{(i\beta\lambda\Delta)e^{-u(z+h)}}{(u+i\beta\Delta)u}J_0(\lambda\rho)d\lambda \tag{9}$$

must now be evaluated. Before proceeding, certain conditions and restrictions must be clearly stated. At a later stage, these may be relaxed somewhat. For the moment

$$|\Delta|<1, \qquad 0<\arg \Delta<\frac{\pi}{4}, \qquad \text{and } \beta\rho>>1.$$

Since

$$J_0(x)=\frac{1}{2}\left[H_0^{(1)}(x)+H_0^{(2)}(x)\right]$$

and

$$H_0^{(2)}(x)=-H_0^{(1)}(-x)$$

where $H_0^{(1)}$ and $H_0^{(2)}$ are Hankel functions of the first and second kind, respectively, it follows that

$$P=\frac{i\beta\Delta}{2}\int_{-\infty}^{\infty}\frac{\lambda e^{-u(z+h)}}{(u+i\beta\Delta)u}H_0^{(1)}(\lambda\rho)d\lambda \tag{10}$$

Introducing the substitutions $\lambda=\beta\cos\alpha$ and $\Delta=\sin\alpha$, it is seen that

$$P=\frac{i\beta\Delta}{4}\int_{-i\infty}^{\pi+i\infty}\frac{\cos\alpha e^{-i\beta(z+h)\sin\alpha}H_0^{(1)}(\beta\rho\cos\alpha)}{\sin\frac{\alpha+\alpha_0}{2}\cos\frac{\alpha-\alpha_0}{2}}d\alpha. \tag{11}$$

Essentially P is now a spectrum of plane waves traveling away from the ground plane so that the vertical component of the propagation constant is $\beta\sin\alpha$. Again, complex angles are included in the spectrum. When $|\beta\rho\cos\alpha|>>1$, the first term of the asymptotic expansion of the Hankel function can be employed. That is,

$$H_0^{(1)}(\beta\rho\cos\alpha)\cong\left[\frac{2}{\pi\beta\rho\cos\alpha}\right]^{1/2}e^{i\beta\rho\cos\alpha}e^{-i\pi/4}. \tag{12}$$

When this is inserted into eq (11), the equation for P becomes

$$P=-e^{-i\pi/4}\frac{\Delta}{2}\left(\frac{\beta}{2\pi\rho}\right)^{1/2}\int_{-i\infty}^{\pi+i\infty}\frac{(\cos\alpha)^{1/2}e^{-i\beta R\cos(\theta-\alpha)}}{\sin\frac{\alpha+\alpha_0}{2}\cos\frac{\alpha-\alpha_0}{2}}d\alpha. \tag{13}$$

where R and θ are defined by $z+h=R\sin\theta$ and $\rho=-R\cos\theta$. In the usual case, the separation ρ between transmitter and receiver is large compared to their respective heights, h and z, and consequently, θ is slightly less than π. It can be seen that the exponential factor in the integrand of P is rapidly varying except for a region near $\alpha=\theta\cong\pi$. This is, of course, the saddle point of the integrand or the point of stationary phase. The important part of the integrand is in the region near the saddle point. In fact, this is the justification for employing the asymptotic expansion for the Hankel functions $H_0^{(1)}$; the argument $\beta\rho\cos\alpha$ is always large in the region near the saddle point if $\beta\rho$ itself is large and $z+h$ is less than ρ.

The integral for P is now in a form where the saddle-point method of integration can be applied. The usual technique [23] is to deform the contour (which in the present case is along the negative imaginary axis, the real axis from 0 to π, and then along a line parallel to the positive imaginary axis) to a path of steepest descent. For example, if we let

$$\cos(\alpha-\theta)=1-i\tau^2$$

and let τ range from $-\infty$ to $+\infty$ through real values, an integral of the type

$$\int_{-i\infty}^{\pi+i\infty} G(\cos\alpha)e^{-i\beta R\cos(\alpha-\theta)}\,d\alpha \tag{14}$$

where $G(\cos\alpha)$ is slowly varying at $\alpha=\theta$, is transformed to

$$(2i)^{1/2}e^{-i\beta R}\int_{-\infty}^{+\infty}\frac{G(\cos\alpha)}{\sqrt{1-i\tau^2/2}}\,e^{-i\beta R\tau^2}d\tau. \tag{15}$$

In this deformation of the contour, account must be made for the singularities of the integrand that are crossed. In the case of poles, $2\pi i$ times the sum of the residues is added to the new integral. The final step in this classical procedure is to expand $G(\cos\alpha)/\sqrt{1-i\tau^2/2}$ in a power series in τ enabling the integration to be carried out term by term. The leading term of this resulting asymptotic expansion is

$$(2\pi i)^{1/2}G(\cos\theta)e^{-i\beta R}(\beta R)^{-1/2} \tag{16}$$

and succeeding terms contain $(\beta R)^{-3/2}$, $(\beta R)^{-5/2}$, and so on.

As is often the case, the contribution from the saddle point (which is the branch point in the original λ plane) cannot be separated from the pole(s) of the integrand. For example, in the present problem,

$$G(\cos\alpha)=\frac{(\cos\alpha)^{1/2}e^{-i\beta R\cos(\theta-\alpha)}}{\sin\dfrac{\alpha+\alpha_0}{2}\cos\dfrac{\alpha-\alpha_0}{2}} \tag{17}$$

has a pole at $\alpha=\pi+\alpha_0$ which is near the saddle point $\alpha=\theta$ since α_0 is small and θ is near π. In other words, the integrand is not slowly varying near the saddle point on account of the factor $\cos(\alpha-\alpha_0)/2$. The integral is then of the form

$$I=\int_{-i\infty}^{\pi+i\infty}\frac{e^{-i\beta R\cos(\theta-\alpha)}}{\cos\dfrac{\alpha-\alpha_0}{2}}\,d\alpha \tag{18}$$

after the slowly varying factors have been separated out. The necessary modification of the saddle-point method to treat integrals of this type was devised by Van der Waerden [24] and Clemmow [25]. On making the usual deformation of the contour via the substitution $\cos(\theta-\alpha)=1-i\tau^2$, the integral now becomes

$$I=-2e^{-i\pi/4}e^{-i\beta R}\sqrt{2}\cos\left(\frac{\theta-\alpha_0}{2}\right)\int_{-\infty}^{+\infty}\frac{e^{-\beta R\tau_2}d\tau}{\tau^2+i2\left[\cos\left(\dfrac{\theta-\alpha_0}{2}\right)\right]^2}. \tag{19}$$

It can readily be verified that no poles of the integrand are crossed in this deformation for the argument of α_0 (or Δ) less than 45°. The integral to consider is now of the type

$$A=\int_{-\infty}^{+\infty}\frac{e^{-x\tau^2}}{\tau^2+c}\,d\tau \tag{20}$$

where, for real τ, $x=\beta R$ and

$$c=i2\left[\cos\left(\frac{\theta-\alpha_0}{2}\right)\right]^2.$$

Since $\int_{-\infty}^{+\infty}e^{-x\tau^2}d\tau=\left(\dfrac{\pi}{x}\right)^{1/2}$, it follows that

$$A=\frac{1}{c}\left(\frac{\pi}{x}\right)^{1/2}-\frac{2}{c}\int_0^{\infty}\frac{\tau^2}{\tau^2+c}\,e^{-x\tau^2}d\tau. \tag{21}$$

Now it can be seen readily that

$$\frac{d}{dx}\,e^{-xc}A=-\left(\frac{\pi}{x}\right)^{1/2}e^{-xc} \tag{22}$$

and an integration with respect to x from x to ∞ leads to

$$e^{-xc}A=\int_x^\infty\left(\frac{\pi}{x}\right)^{1/2}e^{-xc}\,dx, \tag{23}$$

or, after a change of variable,

$$A=2(\pi/c)^{1/2}e^{xc}\int_{\sqrt{xc}}^\infty e^{-z^2}dz, \tag{24}$$

which holds for *all* c in the c plane with a cut along the negative real axis. This can be written

$$A=\frac{\pi}{\sqrt{c}}\,e^{xc}erfc\sqrt{xc}, \tag{25}$$

where *erfc* is the complement of the error integral given by

$$erfcz_0=\frac{2}{\sqrt{\pi}}\int_{z_0}^\infty e^{-z^2}dz, \tag{26}$$

where the integration in the z plane is directed from z_0 towards the right to $+\infty$. Therefore

$$I=-i2\pi e^{-i\beta R}e^{-w}erfc(iw^{1/2}), \tag{27}$$

where

$$w=-\beta Rc=-2i\beta R\left[\cos\left(\frac{\theta-\alpha_0}{2}\right)\right]^2,$$

and finally, since $R=r_2$,

$$P=\int_0^\infty\frac{(i\beta\lambda\Delta)}{(u_0+i\beta\Delta)}\,e^{-u(z+h)}J_0(\lambda\rho)d\lambda \tag{28}$$

$$\cong i(\pi p)^{1/2}e^{-w}erfc(iw^{1/2})e^{-i\beta r_2}/r_2,$$

where

$$w\cong p\left(1+\frac{(z+h)}{\Delta r_2}\right)^2 \tag{29}$$

and

$$p=-\frac{i\beta r_2}{2}\,\Delta^2=|p|e^{ib}.$$

While the derivation was carried out for the argument of Δ lying in the range 0 to $\pi/4$ or b in the range 0 to $-\pi/2$, the formula is actually valid for all values of b if the above definition of the error function complement is used. The justification for this step is based on the principle of analytical continuation. If, in the initial derivation, the argument of Δ was allowed to exceed $\pi/4$, we would find that a pole would be crossed in the deformation of the contour in the α plane. There would be a corresponding change in the integral A but, after a change of the sign of the variable τ, the expression yielded for I would be unchanged in form if we are consistent in the definition of the complex error function.

4. General Properties of the Solution

The general behavior of the result will be considered now. For the moment the heights of the transmitter and receiver are assumed to be very small. That is $(z+h)<<<\rho$ and, consequently, $w\cong p$ and $r_1\cong r_2\cong\rho$. The Hertz potential then has the form

$$\Pi=2\bar{c}e^{-i\beta\rho}F(p), \tag{30}$$

where

$$F(p)=1-i(\pi p)^{1/2}e^{-p}erfc(ip^{1/2}). \tag{31}$$

The vertical electric field is then given by

$$E_z=\frac{1}{\rho}\frac{\partial}{\partial\rho}\rho\frac{\partial\Pi}{\partial\rho} \tag{32}$$

and, since $\beta\rho>>1$ and $F(p)$ is a slowly varying function, it follows that

$$E_z=+2\bar{c}\beta^2e^{-i\beta\rho}\rho^{-1}F(p). \tag{33}$$

For a highly conducting flat ground plane, $[|p|<<1]$, the electric field denoted by E_z^∞ is given by

$$E_z^\infty=2\bar{c}\beta^2e^{-i\beta\rho}\rho^{-1}. \tag{34}$$

This result can be obtained by elementary methods, being just the free space radiation field of an electric dipole of moment $2\bar{c}$. The factor 2 arises from the imaging of the primary dipole in the perfectly reflecting surface. The ratio

$$F(p)=E_z/E_z^\infty \tag{35}$$

is by definition the complex attenuation factor and is a measure of the efficiency of transmission of waves along the interface for a vertical-electric-dipole source.

The behavior of $F(p)$ is very dependent on the phase of p, and since

$$P=|p|e^{ib}=-\frac{i\beta\rho}{2}\Delta^2=-\frac{i\beta\rho}{2}\left(\frac{Z}{120\pi}\right)^2, \tag{36}$$

the surface impedance, Z, plays an important role. For example, in the case of a homogeneous ground of conductivity σ and dielectric constant ϵ,

$$\Delta=\frac{Z}{120\pi}=\frac{1}{N}\left(1-\frac{1}{N^2}\right)^{1/2} \tag{37}$$

with

$$N=\left[\frac{\epsilon-i\sigma/\omega}{\epsilon_0}\right]^{1/2}.$$

The refractive index, N, is usually large compared to unity with a phase near, but always less than $-45°$. Correspondingly, for a homogeneous half-space, the phase b lies between $0°$ and $-90°$. This is precisely the case that has been treated in detail by Norton, who gives numerical results of $F(p)$ as a function of $|p|$ for b varying from 0 to $-180°$.[4] In all cases for $|p|>0$, $|F(p)|$ was less than unity. In other words, the field E_z was never greater than E_z^∞ for the perfectly conducting ground plane. For purposes of numerical work, the error-function complement can be expanded in an ascending power series, as is well known. This leads to the following series formula for $F(p)$:

$$F(p)=1-i(\pi p)^{1/2}e^{-p}-2p+\frac{(2p)^2}{1\cdot3}-\frac{(2p)^3}{1\cdot3\cdot5}+\ldots, \tag{38}$$

which is absolutely convergent.

The second term of this series, the quantity $-i(\pi p)^{1/2}e^{-p}$, is rather interesting if it is considered by itself. The vertical electric field, E_z^s, which would result by ignoring the other terms, is

$$E_z^s=-2\bar{c}\beta^2\frac{e^{-i\beta\rho}}{\rho}i(\pi p^{1/2})e^{-p} \tag{39}$$

$$=\bar{c}e^{-3\pi i/4}\beta^2\frac{\sqrt{2\pi}}{\sqrt{\beta\rho}}\Delta e^{-i\beta\left[1-\frac{\Delta^2}{2}\right]}\rho. \tag{40}$$

[4] Norton used a time factor $e^{-i\omega t}$, whereas $e^{i\omega t}$ is employed in the present paper.

This field has the characteristics of a Zenneck surface wave; it varies inversely with the distance along with an exponential attenuation, and it has a phase velocity greater than that of light. By retracing the steps in the derivation it is not difficult to show that E_z^s is the residue at the pole α_0 in the complex α plane. Taken by itself, E_z^s could easily exceed E_z^∞ by a great amount if b was near $-90°$ corresponding to the phase of Z (or Δ) being near zero. This corresponds to a small conductivity in the lower half space.

The above argument would indicate that the Zenneck surface wave is excited by a vertical dipole source on a homogeneous half-space. Of course, when the other terms in the series for $F(p)$ are considered, the total field does not have the attenuation characteristics of a Zenneck surface wave. For example, if the asymptotic expansion for the complement of the error function is employed, the following series for $F(p)$ results:

$$F(p)=-\frac{1}{2p}-\frac{1\cdot 3}{(2p)^2}-\frac{1\cdot 3\cdot 5}{(2p)^3}-\frac{1\cdot 3\cdot 5\cdot 7}{(2p)^4}-\ldots, \tag{41}$$

which are also asymptotic and valid for large values of p and $-2\pi<b<0$. This would indicate that the field E_z at large ranges varies inversely as the square of distance, whereas the Zenneck surface wave varies inversely as the square root of the distance. This viewpoint is confirmed by the work of Wise [26] and Rice [27], who develop rigorous expansions for the Hertz potential on a homogeneous earth.

The absence of any features associated with a trapped surface wave on a homogeneous earth is due to the restricted range of b (namely between 0 and $-\pi/2$) for a homogeneous earth. It is of interest to note that Sommerfeld in his 1909 paper had an error in sign which was finally pointed out by Norton [3]. This error is equivalent to the interchanging of the b and $-b$. In other words, the complex conjugate of p is used in place of the proper quantity. Rolf [4] employed Sommerfeld's formulas along with the incorrect sign. Rolf's series expansions for $F(p)$ would correspond to eq (38) with b replaced by $-b$. His calculations therefore correspond to values of $F(p)$ for b from 0 to $+90°$. The appearance of his curves is indeed weird. As will be indicated below, the function $F(p)$ can exceed unity in certain instances when b is positive. This is indicated in Rolf's curves. The irregularities and dips to zero, however, must be attributed to errors in computation. The series formula for $F(p)$, although mathematically convergent, takes a great number of terms when p is greater than 5 or so. And, furthermore, the asymptotic expansion of $F(p)$ is not accurate for the real part of p less than about 15. The anomalous features in Rolf's curves occur just where the accurate computation of $F(p)$ would require tens or hundreds of terms in the power series formula. This viewpoint is confirmed when more elaborate calculations are carried out [21].

The nature of the attenuation function $F(p)$ when b is positive can be best seen from an asymptotic development. This is obtained by noting that

$$erfc(ip^{1/2})=\frac{2}{\sqrt{\pi}}\int_{ip^{1/2}}^{\infty}e^{-x^2}dx=2-\frac{2}{\sqrt{\pi}}\int_{ip^{1/2}}^{\infty}e^{-x^2}dx. \tag{42}$$

The latter integral asymptotically vanishes for $p\to\infty$ if the real part of $ip^{1/2}$ is less than zero. Therefore

$$erfc(ip^{1/2})\cong 2-\frac{ie^{+p}}{\sqrt{\pi p}}\left(1+\frac{1}{2p}+\frac{1\cdot 3}{(2p)^2}+\frac{1\cdot 3\cdot 5}{(2p)^3}+\ldots\right) \tag{43}$$

for $2\pi>b>0$ and $|p|>>1$. Utilizing this result, it then follows that

$$\begin{aligned} F(p)&=1-i\sqrt{\pi p}\,e^{-p}erfc(ip^{1/2}) \\ &\cong -2i\sqrt{\pi p}\,e^{-p}-\frac{1}{2p}-\frac{1\cdot 3}{(2p)^2}-\frac{1\cdot 3\cdot 5}{(2p)^3}-\ldots \end{aligned} \tag{44}$$

in the asymptotic sense. The term $-2i\sqrt{\pi p}\ e^{-p}$ has all the characteristics of a surface wave.

It is not present in the asymptotic development for $F(p)$ when b is negative. Of course, for dissipative media such as a stratified conductor, the real part of p is large and the surface-wave term almost vanishes compared to the term $-1/2p$.

The most interesting case is when the surface impedance is purely inductive. For example, if a flat perfectly conducting ground plane is coated with a thin layer (of thickness h) of pure dielectric (with refractive index N), then the surface impedance, Z, is given to a good approximation by [19]

$$Z \cong i\mu\omega h\left[1-\frac{1}{N^2}\right]. \tag{45}$$

Another example is when a flat metal surface is corrugated in the form of periodic rectangular slots of width d and depth D with a separation w between slot centers. The surface impedance for the magnetic vector parallel to the directions of the corrugations is then

$$Z=i\frac{d}{w}\eta_0 \tan \beta D, \tag{46}$$

provided that there are at least five corrugations per wavelength along the surface [13]. For $D<\lambda/4$, the surface impedance is purely inductive, and since

$$p=-\frac{i\beta\rho}{2}(Z/\eta_0)^2, \tag{47}$$

$p+i|p|$ and $b=\pi/2$. The attenuation function then has the asymptotic development,

$$F(p)\cong -2e^{i3\pi/4}\sqrt{\pi|p|}\,e^{-i|p|}+\frac{i}{2|p|}+\frac{3}{4|p|^2}-\frac{15i}{8|p|^3}\cdots, \tag{48}$$

where

$$|p|=\frac{\beta\rho}{2}\frac{X^2}{\eta_0^2} \text{ and } X=|Z|.$$

The vertical electric field at $z=0$ is then given by

$$E_z\cong 2c\beta^2 e^{-i\beta\rho}\rho^{-1}F(p). \tag{49}$$

The surface wave term now varies as

$$\frac{1}{\sqrt{\beta\rho}}e^{-i\beta\left(1+\frac{X^2}{2\eta_0^2}\right)\rho},$$

which *is not a Zenneck surface wave* since the phase velocity, v, given by

$$v=\frac{1}{1+X^2/(2\eta_0^2)}\frac{1}{\sqrt{\mu_0\epsilon_0}}, \tag{50}$$

is less than the velocity of light, $1/\sqrt{\mu_0\epsilon_0}$.

If the surface is purely capacitive such that $Z=-iX'$, the argument of the error function is

$$ip^{1/2}=e^{-i\pi/4}\sqrt{\beta\rho/2}(X'/\eta_0)^2, \tag{51}$$

so that $erfc(ip^{1/2})$ can be expanded directly to lead to the asymptotic representation

$$F(p)\cong -\frac{i}{2|p|}+\frac{3}{2|p|^2}+\frac{15i}{8|p|^3}\cdots, \tag{52}$$

which contains no surface-wave term.

5. Height-Gain Functions

It is desirable now to return to the general formula for $F(p)$ which is a (modified) saddle point approximation for the field of a vertical dipole over the impedive surface. For $h=0$, it is

$$W=1-i\sqrt{\pi p}e^{-w}erfc(iw^{1/2}), \tag{53}$$

where

$$w=p\left(1+\frac{z}{\Delta r_2}\right)^2\cong p\left(1+\frac{z}{\Delta p}\right)^2.$$

For small heights and receiver it is of interest to develop W in a power series in z. For example,

$$W(z)=W(0)+z\left(\frac{dW}{dz}\right)_{z=0}+\frac{z^2}{2}\left(\frac{d^2W}{dz^2}\right)_{z=0}+\cdots \tag{54}$$

Now

$$\frac{dW}{dz}=\left[-\frac{p}{w}+i\sqrt{\pi p}\,e^{-w}erfc(iw^{1/2})\right]\frac{dw}{dz} \tag{55}$$

and

$$\frac{dw}{dz}=2p\left(1+\frac{z}{\Delta\rho}\right)\frac{1}{\Delta\rho}.$$

Therefore

$$\left[\frac{dW}{dz}\right]_{z=0}=ik\Delta W(0)=ik\Delta F(p)$$

and, to a first order in z,

$$W(z)\cong F(p)\ [1+ik\Delta z]. \tag{56}$$

The generation of higher-order terms using this method is cumbersome, and it is really better to return to the original integral for the Hertz potential $\Pi(z)$ given by

$$\Pi(z)=2\overline{c}\int_0^\infty\frac{\lambda J_0(\lambda\rho)}{u+i\beta\Delta}\,e^{-uz}d\lambda \tag{57}$$

for $h=0$. Expanding the exponential, this is rewritten

$$\Pi(z)=2\int_0^\infty[1-uz+u^2z^2/2-\ \cdots\ ]\,\frac{\lambda J_0(\lambda\rho)}{u+i\beta\Delta}\,d\lambda \tag{58}$$

$$=2\overline{c}\left[\Pi(0)+i\beta\Delta\,\Pi(0)+\frac{z^2}{2}\left(\frac{\partial^2\Pi(z)}{\partial z^2}\right)_{z=0}+\ \cdots\ \right].$$

Now since $\Pi(z)$ satisfies the wave equation, $\partial^2/\partial z^2$ can be replaced by

$$-\beta^2-\frac{1}{\rho}\frac{\partial}{\partial\rho}\,\rho\,\frac{\partial}{\partial\rho}$$

so that

$$\Pi(z)=\left[1+i\beta\Delta z-\frac{z^2}{2}\left(\beta^2+\frac{1}{\rho}\frac{\partial}{\partial\rho}\,\rho\,\frac{\partial}{\partial\rho}\right)+\ \cdots\ \right]\Pi(0). \tag{59}$$

Since

$$\Pi(0)=2\overline{c}e^{-i\beta\rho}\rho^{-1}F(p), \tag{60}$$

the contribution from the second-order term is

$$\frac{z^2}{2}\left[\beta^2+\frac{1}{\rho}\frac{\partial}{\partial\rho}\rho\frac{\partial}{\partial\rho}\right]\Pi(0)=\frac{2\bar{c}e^{-i\beta\rho}}{2\rho}F(p)\left\{\frac{z^2}{\rho^2}+\frac{i(\beta z)^2}{(\beta\rho)}-\frac{z^2}{2\rho}\frac{F'(p)}{F(p)}-i\beta z^2\frac{F'(p)}{F(p)}+\frac{z^2}{2}\frac{F''(p)}{F(p)}\right\}, \quad (61)$$

where the prime(s) indicate a derivative(s) with respect to ρ. It is not difficult to see that for $2\pi<b<0$, $F(p)$ is slowly varying compared to other factors and the term in curly brackets is much less than unity if $\beta\rho>>1$ and $\rho^2>>z^2$. In the case of the inductive surface (i. e., $2\pi>b>0$), it is convenient to write

$$F(p)=F_s(p)+F_a(p), \quad (62)$$

where asymptotically

$$F_s(p)\cong -2i\sqrt{\pi p}\,e^{-p} \quad (63)$$

is the surface wave term and

$$F_a(p)\cong -\frac{1}{2p}-\frac{3}{4p^2}-\frac{15}{8p^3}-\cdots \quad (64)$$

is the remaining (nonsurface) contribution. [For the case $-2\pi<b<0$, $F(p)\cong F_a(p)$].

Now

$$\frac{F_a'(p)}{F_a(p)}\sim -\frac{1}{\rho}+0\left(\frac{1}{p^2}\right)$$

and

$$\frac{F_a''(p)}{F_a'(p)}\sim -\frac{2}{\rho}+0\left(\frac{1}{p^2}\right)$$

but

$$\frac{F_s'(p)}{F_s(p)}\sim\frac{i\beta\Delta^2}{2}$$

and

$$\frac{F_s''(p)}{F_s(p)}\sim\left(-\frac{i\beta\Delta^2}{2}\right)^2.$$

Therefore, the Hertz potential $\Pi_s(z)$, corresponding to the surface-wave field, is given by

$$\Pi_s(z)\cong\Pi_s(0)\left[1+i\beta\Delta z+\frac{(i\beta\Delta z)^2}{2}+\cdots\right] \quad (65)$$

$$\cong\Pi_s(0)e^{i\beta\Delta z}$$

whereas

$$\Pi_a(z)\cong\Pi_a(0)[1+i\beta\Delta z]. \quad (66)$$

In the case of a purely inductive surface ($Z=iX$), the exponential factor for the surface term is given by

$$e^{i\beta\Delta z}=e^{-(X\beta/\eta_0)z}=e^{-\epsilon\omega Xz}, \quad (67)$$

indicating a rapid decay of the field with height.

By a slight extension of the above, the case of both transmitter and receiver raised yields

$$\Pi_s(z,h)\cong\Pi_s(0,0)e^{i\beta\Delta(z+h)} \quad (68)$$

and

$$\Pi_a(z,h)\cong\Pi_a(0,0)(1+i\beta\Delta z)(1+i\beta\Delta h). \quad (69)$$

Still another approach to the effect of raised antennas, which is particularly appropriate for large heights, is now considered. In general,

$$\frac{\Pi}{\overline{c}}=\frac{e^{-i\beta r_1}}{r_1}+\frac{e^{-i\beta r_2}}{r_2}-2P, \tag{70}$$

where

$$P=\frac{p}{w}\,[1-F(w)]\,\frac{e^{-i\beta r_2}}{r_2} \tag{71}$$

with $F(w)=F_a(w)+\epsilon F_s(w)$, where $\epsilon=0$ for $-2\pi<b<0$, $\epsilon=1$ for $2\pi>b>0$, and $w=p(1+C/\Delta)^2$, $C=(z+h)/r_2$. Asymptotically,

$$F_s(w)=-2i\sqrt{\pi w}\,e^{-w} \tag{72}$$

and

$$F_a(w)=-\frac{1}{2w}-\frac{3}{4w^2}-\frac{15}{8w^3}-\cdots. \tag{73}$$

After some algebraic manipulations,

$$\Pi=\Pi_a+\epsilon\Pi_s$$

$$\frac{\Pi_a}{\overline{c}}\cong\frac{e^{-i\beta r_1}}{r_1}+\frac{C-\Delta}{C+\Delta}\,\frac{e^{-i\beta r_2}}{r_2}+\left\{-\frac{1}{p(1+C/\Delta)^3}-\frac{1\cdot3}{2p^2(1+C/\Delta)^5}-\frac{1\cdot3\cdot5}{4p^3(1+C/\Delta)^7}\cdots\right\}\frac{e^{-i\beta r_2}}{r_2} \tag{74}$$

and

$$\frac{\Pi_s}{\overline{c}}\cong\frac{-2\Delta}{\Delta+C}\,[2i\sqrt{\pi w}\,e^{-w}]\,\frac{e^{-i\beta r_2}}{r_2}. \tag{75}$$

The first term in the expression for Π_a is, of course, the direct or primary influence. The second term is the secondary influence modified by a Fresnel reflection coefficient. The terms containing inverse powers of p can be considered as corrections to geometrical optics. The surface-wave term is absent when b is negative. When b is positive, it is a finite contribution to the total field Π, and for a highly inductive surface (i. e., $b=90°$) it is predominant.

The vertical electric field is simply given by

$$E_z\cong\beta^2S^2\Pi=\beta^2(1-C^2)\Pi \qquad \text{for} \qquad \beta r_1 \text{ and } \beta r_2>>1,$$

and furthermore, $r_2\cong r_1-2hC$.

6. Conclusion

It has been shown that the nature of the field radiated from a dipole over a flat surface depends markedly on the complex value of the surface impedance Z. For example, when the phase of Z is between 0 and 45°, the derived expressions for the field correspond to those of Norton and others for a dipole over a homogeneous flat ground. When the phase of Z exceeds 45° the radiated field becomes trapped by the surface. This effect is most pronounced when Z is purely imaginary, corresponding to an inductive surface. A similar unifying treatment for a dipole over a curved spherical surface will be given in a sequel to this paper.

The author thanks Kenneth A. Norton for his very helpful suggestions and Howard Bussey for his constructive criticism.

7. References

[1] J. Zenneck, Uber die Fortpfanzung ebener electromagnetischer wellen einer ebenen Leiterflache und ihre beziehung zur drahtlosen telegraphie, Ann. Physik [4] **23,** 846 (1907).

[2] A. Sommerfeld, Uber die Ausbreitung der Wellen in der Drahtlosen Telegraphie, Ann. Physik [4] **28,** 665 (1909); **62,** 95 (1920); **81,** 1135 (1926).

[3] K. A. Norton, Propagation of radio waves over a plane earth, Nature **135,** 954 (1935).

[4] B. Rolf, Graphs to Prof. Sommerfeld's attenuation formula for radio waves, Proc. Inst. Radio Engrs. **18,** 391 (1930).

[5] C. J. Bouwkamp, On Sommerfeld's surface wave, Phys. Rev. **80,** 294 (1950).

[6] K. A. Norton, The calculation of ground-wave field intensity over a finitely conducting spherical earth, Proc. Inst. Radio Engrs. **29,** 623 (1941).

[7] K. A. Norton, The propagation of radio waves over the surface of the earth and in the upper atmosphere, I, Proc. Inst. Radio Engrs. **24,** 1367 (1936); II, **25,** 1203 (1937).

[8] A. N. Sommerfeld, Uber di Fortpfanzung electrodynamischer Wellen langs eines Drahtes, Ann. Physik u. Chem. **67,** 233 (1899).

[9] G. Goubau, Surface waves and their application to transmission lines, J. Appl. Phys. **21,** 1119 (1950).

[10] G. Goubau, On the excitation of surface waves, Proc. Inst. Radio Engrs. **40,** 865 (1952).

[11] S. Atwood, Surface wave propagation over a coated plane conductor, J. Appl. Phys. **22,** 504 (1951).

[12] W. Rotman, A study of single surface corrugated guides, Proc. Inst. Radio Engrs. **39,** 952 (1951).

[13] R. S. Elliott, On the theory of corrugated plane surfaces, Trans. Inst. Radio Engrs. AP–**2,** 71 (1954).

[14] F. J. Zucker, The guiding and radiation of surface waves, Proc. Symposium on Modern Advances in Microwave Techniques, p. 403 (Polytechnic Inst. Brooklyn, Nov. 8–10, 1954) (many references are given in this comprehensive paper).

[15] C. T. Tai, The effect of a grounded slab on radiation from a line source, J. Appl. Phys. **22,** 405 (1951).

[16] D. B. Brick, The radiation of a Hertzian dipole over a coated conductor, Monograph 113, Inst. Elec. Engrs. (London), Dec. 15, 1954.

[17] A. L. Cullen, The excitation of plane surface waves, Proc. Inst. Elec. Engrs. **101,** Pt. IV, 225 (1954).

[18] H. E. M. Barlow and W. M. G. Fernando, An investigation of the properties of radial surface waves launched over flat reactive surfaces, Proc. Inst. Elec. Engrs. **103,** 307 (1956).

[19] H. E. M. Barlow and A. L. Cullen, Surface waves, Proc. Inst. Elec. Engrs. **100,** Pt. III, 321 (1953).

[20] N. Marcuvitz, Guided wave concept in electromagnetic theory, Research Rept. R–269–52 (P. I. B.–208, ONR, May 14, 1952, Polytechnic Inst. of Brooklyn, Microwave Research Inst.).

[21] J. R. Wait, Radiation from a vertical dipole over a stratified ground, I, Trans. Inst. Radio Engrs. AP–**1,** 9 (1953); II, AP–**2,** 144 (1954).

[22] J. R. Wait, Radiation from a vertical antenna over a curved stratified ground, J. Research NBS **56,** 232 (1956) RP2671.

[23] A. N. Sommerfeld, Partial differential equations (Academic Press, Inc., New York, N. Y., 1949).

[24] B. L. Van der Waerden, On the method of saddle points, Appl. Sci. Research B–**2,** 33 (1950).

[25] P. C. Clemmow, Some extensions to the method of integration by steepest descents, Quart. J. Mech. Appl. Math. **3,** 241 (1950).

[26] W. H. Wise, The physical reality of the Zenneck surface wave, Bell System Tech. J. **16,** 35 (1937).

[27] S. O. Rice, Series for the wave function of a radiating dipole at the earth's surface, Bell System Tech. J. **16,** 101 (1937).

Boulder, Colo., April 19, 1957.

Journal of Research of the National Bureau of Standards Vol. 59, No. 6, December 1957 Research Paper 2808

Cunife Wire Magnets of Small Size

Irvin L. Cooter and Robert E. Mundy

A ductile permanent-magnet alloy, having a composition of 60 percent of copper, 20 percent of nickel, and 20 percent of iron, was cold-drawn from wire, 25 mils in diameter to 5 mils in diameter. Demagnetization curves were obtained for several sizes of the wire in the cold-drawn state. These wires were then given a heat treatment and again demagnetization curves were obtained. Values of coercivity, retentivity, and maximum energy product are compared for various wire diameters. Although the magnetic properties were adversely affected by the cold-working, they were substantially improved by the heat treatment.

1. Introduction

Most of the commercially available permanent-magnet materials of high coercivity are mechanically hard and brittle and must be cast or sintered into the required shape for use. A magnet alloy of approximately 60 percent of copper, 20 percent of nickel, and 20 percent of iron (called Cunife or Cunife I by its producers in the United States) has an unusual combination of magnetic and mechanical properties. Although it has a coercivity of several hundred oersteds, Cunife is so ductile that it is possible to cold-reduce it considerably.

Several investigators [1,2,3] [1] have reported on the magnetic properties of Cunife wire and on the effects of cold-working and subsequent heat treatment. Their results have shown that even if the material is cold-worked to the point at which the magnetic properties are adversely affected, the initial magnetic properties may be recovered or improved by a simple heat treatment or baking. These reports, however, pertained only to the larger wire sizes. No data were available on the magnetic properties of Cunife drawn to wires a few thousandths of an inch in diameter.

The solution of a special magnetic problem required cylindrical magnets approximately 0.50 in. long and 0.005 in. in diameter.[2] The ductility and high coercivity of Cunife made it appear suitable for this application, and the present investigation was undertaken in order to evaluate it.

2. Material

The commercial material used in this investigation had a composition of 19.3 percent of nickel, 19.5 percent of iron, and 60.4 percent of copper, and was supplied by the maker in the form of wire with a diameter of 0.025 in. and in the heat-treated condition. This wire was cold-reduced from 0.025 to 0.020 in. through tungsten carbide dies with five passes. Diamond dies were used for the further reduction from 0.020 to 0.005 in. with 21 passes. Potassium soap was used as the lubricant for all passes, and no heat treatment was given the wire at any time during the reduction from 0.025 to 0.005 in. At various stages of reduction, samples were cut from the coil of wire for later measurement.

3. Heat Treatment

The magnetic properties of the cold-drawn Cunife wire may be markedly improved by properly heat-treating the wire. Since the maximum temperature at which the wire is heated affects the final magnetic properties, several heat-treating temperatures were tried. The resulting magnetic properties for samples of 5-mil wire when heat-treated for 1 hr at various oven temperatures are shown in figure 1. During this heat-treating process the wire was embedded in iron filings to prevent oxidation. In each case the temperature of a muffle-type oven was allowed to

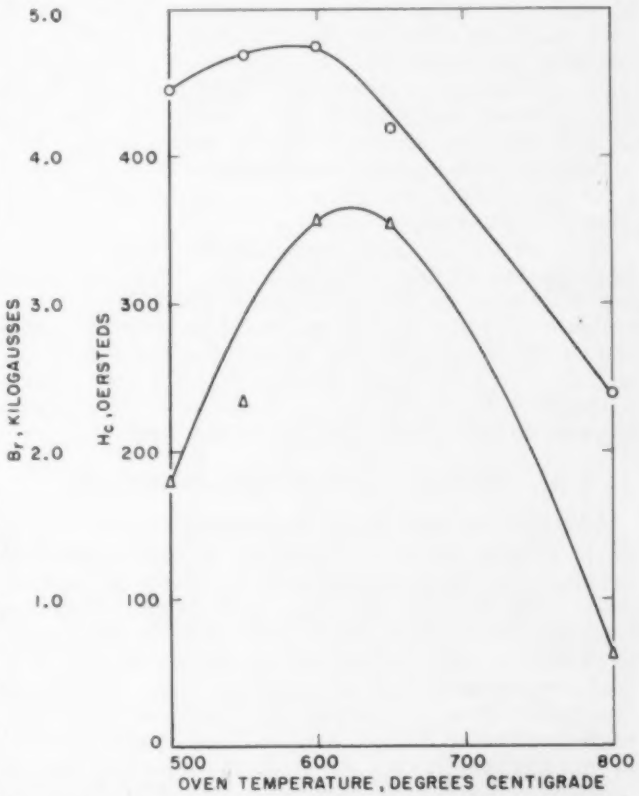

FIGURE 1. *Influence of temperature of heat treating for 1 hr on coercivity and retentivity of 0.005-in.-diameter Cunife wire.*

△, Ccercivity; ○, retentivity.

[1] Figures in brackets indicate the literature references at the end of this paper.
[2] This problem was related to a classified project of the Mine Fuze Branch Diamond Ordnance Fuze Laboratory.

reach the heat-treating temperature before the wire and iron filings were placed inside. The wire and filings remained at the heat-treating temperature for 1 hr and then the heaters were turned off, the oven door opened, and the oven allowed to cool to 300° C. This cooling usually required 20 to 30 min. The sample was then removed from the oven and cooled to room temperature.

The results in figure 1 show a definite maximum value for the coercive force of Cunife when heat-treated about 620° C. This is in accord with the results obtained by Geisler [3] with the alloy Cunico. He has shown an interesting curve for the change in coercive force of Cunico as a function of aging time when held at various aging temperatures. The maximum coercive force for the three isothermals occurs at different aging time; if the proper aging time is selected the coercive force will increase, go through a maximum, and decrease when plotted as a function of aging temperature.

In order to determine the effect of oxidation on the magnetic properties, a specimen of 0.005-in. wire was placed in an oven at 610° C in an atmosphere of air and was heated for 1 hr. The wire was then slowly cooled to room temperature. The surface of this wire was then grayish black. However, the magnetic properties were the same within 5 percent as those of wire of the same size, oxidation of which had been prevented by heating in iron filings.

It might also be expected that, since wire specimens of different sizes have had different amounts of cold-working, different heat treatment might be required to obtain the best magnetic properties of wire of each size. However, using 0.020-in. (36% cold-reduced) and 0.005-in. wire (96% cold-reduced) as test samples, no such effects were found. The maximum heat-treating temperature of 610° C and 1 hr of heating time gave the optimum results for wire of both sizes.

As a result of these experiments, all wires were heat-treated in the same manner. The procedure selected was to heat the wire specimens, while embedded in iron filings, to a maximum temperature of 610° C, to hold them at this temperature for 1 hr, and then to allow them to cool slowly to room temperature. This produced wire that was bright and showed no noticeable signs of surface oxidation.

4. Apparatus and Measurements

The normal induction and demagnetization curves of the Cunife wires were obtained by using a High-H permeameter [4] and a calibrated ballistic galvanometer. The magnetizing force was measured with a flip coil, and the flux density in the wires was measured with a coil surrounding the specimen. Air flux was compensated with an auxiliary coil. The forms for the B coil and compensator coil were of aluminum, each form being 0.75 in. long with an inside diameter of approximately 0.1 in. and a wall thickness of 0.010 in. Each coil form was wound with 15,370 turns of AWG 44 varnish-coated copper wire. The Cunife specimens were cut 0.75 in. long, and a sufficient number of wires were used to have a cross-sectional area of at least 0.00040 sq in. The demagnetization curves were obtained from a maximum magnetizing force of 3,000 oersteds.

5. Results

The dependency of the coercive force on the reduction of area of the wire is shown in figure 2. Since the 0.025-in. wire was in the annealed condition initially, the percentage reduction in area is also the percentage cold-working for the lower curve. As a result of the cold reduction of the wire from 0.025 to 0.005 in., the coercive force decreased from 550 to 50 oersteds. Subsequent heat treatment restored the initial coercive force until the wire was reduced in area more than 85 percent, or to a diameter of approximately 10 mils. Further reduction in area caused a sharp decrease in the values of the coercive force, H_c; for the heat-treated 0.005-in. wire, H_c was only 60 percent of the value for the 0.025-in. wire.

This sharp decrease in coercive force at the smallest sizes of wires studied is of special interest. Since the major role in production of coercive force in Cunife is believed to be due to strain disregistry between a precipitate and the matrix, it is quite likely that for the smaller sizes of wire the severe cold-working has so distorted the grains that some of the effects of distortion may persist even after the wire has been aged. As shown in figure 2, the coercive force of the cold-drawn wire continually decreases as the cold-working increases. However, aging will more than restore the initial coercive force because of the preferred orientations as a result of cold working [5, 6, 7]. If the cold-working exceeds the optimum amount for the small wires, then the initial coercive force of the larger wire size cannot be regained, indicating that the anisotropy of the alloy was changed.

Figure 3 shows that the value of the residual induction, B_r, remained approximately constant until the reduction in area exceeded 80 percent, then decreased sharply for further increases in cold reduction.

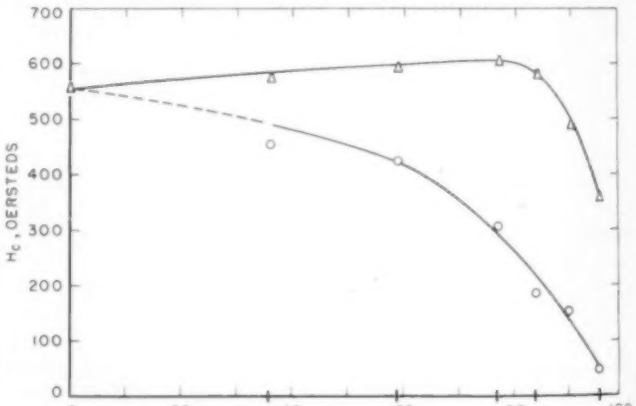

FIGURE 2. *Coercivity as affected by cold reduction and heat treatment.*

△, Heat treatment at 610° C for 1 hr; ○, cold drawn.

After the successive samples of wire were heat-treated, the residual induction, B_r, for each wire size, increased to or exceeded the initial value for the 0.025-in.-diameter wire.

The shape of the residual induction curve for the aged condition shows no dependence on wire size. This can be explained on the basis of the accepted idea that the value of residual induction for alloys depends primarily on composition and the amount of ferromagnetic phase, while strain and structure are of secondary importance.

The relationship between the maximum energy product, $(B_dH_d)_m$, and the reduction in area is shown in figure 4. For the cold-worked condition, the decrease in the maximum energy product is small until a 50-percent reduction in area of the wire is reached. For greater cold-working, $(B_dH_d)_m$ decreases quite rapidly. The heat-treated materials show a gradual increase until the reduction in area approaches 80 percent, and then the curve dips and a rapid decrease in $(B_dH_d)_m$ occurs.

The information contained in figures 2, 3, and 4 is shown in figure 5 in a different manner. The upper curve is for the ratio $(B_r)_{cw}/(B_r)_{ht}$ as a function of the diameter of the Cunife wire. Here, as well as later, the subscript *cw* designates the cold-worked condition and *ht* designates the heat-treated condition. This curve shows that the value of B_r is practically independent of the cold-working until the wire has been reduced to about 8 mils.

This figure also contains the data for the ratios $(H_c)_{cw}/(H_c)_{ht}$ and $[(B_dH_d)_m]_{cw}/[(B_dH_d)_m]_{ht}$ as functions of wire diameter. The points for both sets of data fall along the same curve and both indicate the improvement in magnetic properties that results from the proper heat treatment for the cold-worked wire.

The demagnetization curves for heat-treated Cunife wires of diameters 0.005, 0.012, and 0.020 in. are shown in figure 6.

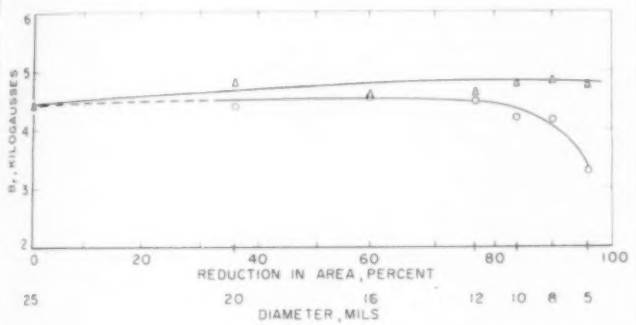

FIGURE 3. *Retentivity as affected by cold reduction and heat treatment.*

△, Heat treatment at 610° C for 1 hr; ○, cold drawn.

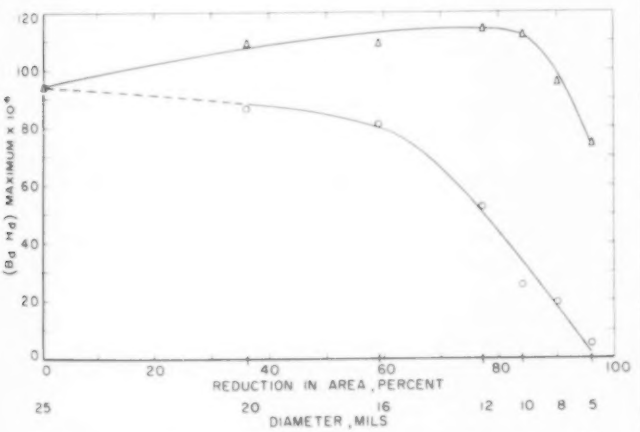

FIGURE 4. *Maximum energy product as affected by cold reduction and heat treatment.*

△, Heat treatment at 610° C for 1 hr; ○, cold drawn.

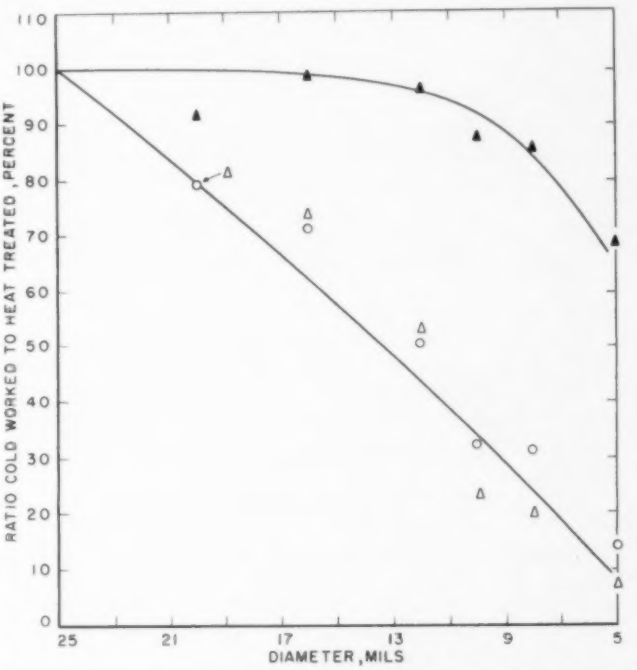

FIGURE 5. *Relative properties of cold-worked and heat-treated Cunife at different diameters.*

▲, $(B_r)_{cw}/(B_r)_{ht}$; ○, $(H_c)_{cw}/(H_c)_{ht}$; △, $[(B_dH_d)_m]_{cw}/[(B_dH_d)_m]_{ht}$.

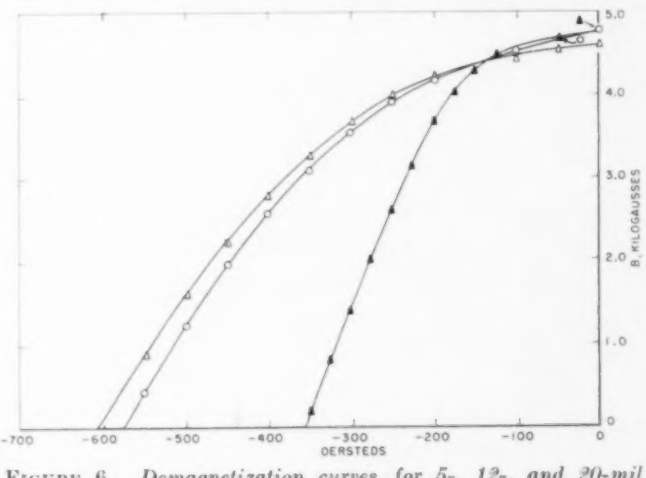

FIGURE 6. *Demagnetization curves for 5-, 12-, and 20-mil Cunife wire after heat treatment at 610° C for 1 hr.*

▲=0.005; △=0.012; ○=0.020.

It is possible to improve the magnetic properties of 0.005-in.-diameter wire by starting the drawing process from a heat-treated wire having a smaller diameter than 0.025 in. This of course will require less cold-working in reducing the wire to 0.005 in. For example, a 0.012-in.-diameter wire, in the heat-treated condition, was cold-drawn to 0.005 in. Wire samples of diameter 0.010, 0.008, and 0.005 in. were heat-treated and measurements made of their magnetic properties. The results obtained for the coercive force, H_c, and residual induction, B_r from wires drawn from 0.012 and 0.025 in. are given in the following table:

Wire diameter	H_c		B_r	
	Initial wire diameter, 0.012 in.	Initial wire diameter, 0.025 in.	Initial wire diameter, 0.012 in.	Initial wire diameter 0.025 in.
in.	*Oersteds*	*Oersteds*	*Kilogausses*	*Kilogausses*
0.010	625	580	4. 6	4. 8
.008	610	490	4. 6	4. 8
.065	520	360	4. 6	4. 8

Figure 7 shows the relative effects of cold-working and heat treatment on the small sizes of Cunife wire when the starting diameters of the heat-treated wires are 0.025 and 0.012 in.

6. Conclusions

Permanent magnets as small as 0.005 in. in diameter may be cold-drawn from commercially available Cunife wire. If the cold-drawn wire is subjected to a simple heat treatment, the permanent-magnet properties of the material are substantially improved. The magnetic properties for the smallest wire sizes, resulting from the final heat treatment, are apparently affected not only by the diameter of the wire but also by the cold-working.

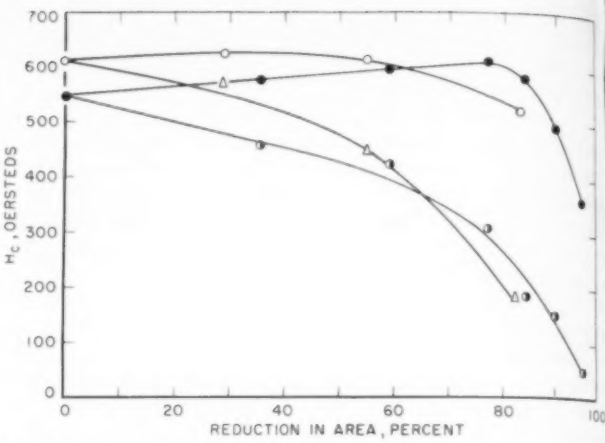

FIGURE 7. *Coercivity as affected by cold reduction and heat treatment at 610° C for 1 hr when initial wire diameters are 0.025 and 0.012 in.*

●, Heat treatment; ◑, cold drawn for 0.025-in. wire.
○, Heat treatment; △, cold drawn for 0.012-in. wire.

7. References

[1] R. M. Bozorth, Ferromagnetism (D. Van Nostrand Co., Inc., New York, N. Y., 1951).

[2] H. Newmann, A. Buchner, and H. Reinboth, Mechanisch Weiche Dauermagnetlegierungen aus Kupfer, Nickel und Eisen, Z. Metallkunde **29**, 173 (1937).

[3] A. H. Geisler, Structure and properties of the permanent magnet alloys, Elec. Eng. 69, 37 (1950).

[4] R. L. Sanford and E. G. Bennett, An apparatus for magnetic testing at magnetizing forces up to 5,000 oersteds, J. Research NBS **23**, 415 (1939) RP1242.

[5] A. H. Geisler, Structure of permanent magnet alloys, Trans. Am. Soc. Metals **43**, 70 (1951).

[6] W. R. Hibbard, Jr., Preferred orientations and magnetic properties of rolled and annealed permanent magnet alloys, Conference on Magnetism and Magnetic Materials, p. 184 (Am. Inst. Elec. Engrs., 33 W. 39th St., New York 18, N. Y., 1955).

[7] J. F. Libsch and G. P. Conrad, Metallurgy and magnetic materials, Conference on Magnetism and Magnetic Materials, p. 80 (Am. Inst. Elec. Engrs., 33 W. 39th St., New York 18, N. Y., 1955).

WASHINGTON, April 15, 1957.

Journal of Research of the National Bureau of Standards Vol. 59, No. 6, December 1957 Research Paper 2809

Interpretation of Mass Spectra of Condensates From Urban Atmospheres

E. R. Weaver,[1] E. E. Hughes, Shirley M. Gunther, Shuford Schuhmann, Nancy T. Redfearn and Ralph Gorden, Jr.

A method of interpreting the mass spectra of the very complex mixtures of substances that condense from an urban atmosphere at the temperature of liquid oxygen is described. The number of individual chemical compounds in such a mixture is greatly in excess of the number of masses recorded, and it is accordingly impossible to identify all the compounds present. However, the significant sources of pollutants are much less numerous, and if the products from each source are of substantially constant composition it is possible to obtain a representative pattern of each and to proceed thereafter to make a fairly good estimate of the character and amount of pollutants in terms of their sources. The greatest simplification is made by treating the gases associated with motor traffic as a unit.

1. Introduction

At an early stage in the study of air pollution in the Los Angeles area, it was proposed by Martin Shepherd [1] [2] that condensible gases be collected from the atmosphere by cooling and filtering at the temperature of boiling oxygen and subsequently subjected to analysis by mass spectrometer. During 1949–51, approximately 50 samples were taken in the vicinity of Los Angeles by this method, all of which gave very complicated spectra whose interpretation was undertaken with only limited success [2, 3]. Subsequently, similar samples were taken in several cities under various circumstances. All of these have shown a basic similarity, which indicates that most of the polluting gases in each urban atmosphere are the same chemical substances in much the same proportions, and are of the general character of "products of combustion."

It is fairly obvious that in any city we may expect large volumes of products of combustion to enter the air from three sources: (1) From fuel used for heating buildings and producing power, (2) from automobiles, and (3) from waste disposal. In most cities the first is important only during cold weather and the third is intermittent or localized. The second is continuous and universal. It would be desirable and may yet be possible to find distinguishing characteristics between these three sources, but their principal differences appear to depend on the completeness of combustion of the fuel rather than on its type, whether coal, petroleum products, or wood and paper. When combustion is "complete," only carbon dioxide, water vapor, and a little sulfur dioxide, nitric oxide, and nitrogen dioxide, are added to the air, and oxygen, in negligible amount, is removed from it. When combustion is "incomplete," but as nearly complete as it can readily be made under the conditions of burning, carbon monoxide is the chief component of the "products of incomplete combustion," and hydrogen and various hydrocarbons are the most easily identified of the additional products. As conditions are changed to make combustion less complete, products become more complex and more dependent on the character of the original fuel; but to the stage in which visible smoke appears, sufficient to attract attention and to induce remedial action, only moderate differences of composition occur.

The temperature at which samples can be "frozen out" without condensing oxygen from the air at the same time is too high to permit the collection of hydrogen or carbon monoxide, or methane unless it is present in explosive concentration. The amounts of other gases that escape condensation depend mainly on their vapor pressures at the boiling point of oxygen.

Most of the air in the cold trap after the initial sampling is removed by partial evacuation at the boiling point of nitrogen, and treatment is then given the sample to eliminate some of the carbon dioxide and water. The sample is then warmed, usually only to room temperature, and the vapors are admitted to the evacuated inlet reservoir of the mass spectrometer. In this procedure another portion of the pollutant may be lost, i. e., that which condensed from the gas phase but did not re-evaporate at the time of transfer to the spectrometer. This loss includes a portion, but not all, of each high-boiling compound that occurred in the initial atmosphere to or nearly to the point of saturation. The losses that occur both through failure to condense in the first place and to re-evaporate later are discussed in the next section.

The mass-spectrometer records a "spectrum" produced by the amplification of ion currents each of which is proportional to the total charge of ions having a single value of M/e, where M is the sum of the atomic weights of the atoms in the ion and e is the positive charge carried by it (the number of electrons removed in the ionization process). The charge is usually unity, and its measurable indication on the record is referred to as a "peak" designated by a "mass number," which is the weight of the ion with unit charge that would produce the peak. In this paper, the mass number enclosed in parentheses will indicate the ion current represented by a particu-

[1] Retired, present address: 6815 Connecticut Ave., Chevy Chase 15, Md.
[2] Figures in brackets indicate the literature references at the end of this paper.

lar peak, usually expressed as a percentage of the total ion current of all peaks of interest.

Chemical compounds produce ions either by the loss of an electron, leaving a "parent" peak that is only undetectably different in mass from the parent molecule, or by the loss of one or more atoms from the parent molecule, leaving a charged fragment. Each compound breaks up in a characteristic manner, producing a "pattern" by which a compound that occurs alone can almost always be identified with certainty. However, the ion currents with the same mass-to-charge ratios from a mixture of different compounds are additive. In theory at least, we could determine every compound present by the solution of an equal number of simultaneous linear equations if we had as many or more peaks on which to base the equations and patterns of all compounds involved.

All of the spectra of urban pollutants so far obtained have contained 80 or more usable peaks; but in every case there has been evidence that these peaks represented many more than 80 compounds, and their complete identification was obviously impossible. Even when a sample was separated by multiple distillations into 50 fractions, the simplest fraction still contained traces of more compounds than can be identified with certainty.

However, if we consider significant sources of pollutants, it is probable that their number is much less than that of the usable peaks, and if the products from each source are of substantially constant composition, we may be able to obtain a characteristic pattern of each and to proceed thereafter to make a fairly good estimate of the character and amount of the pollutants in terms of their sources. A procedure for making such estimates and some of the results obtained is the primary subject of this paper; but the main theme will be preceded by a discussion of sampling and laboratory procedure intended to make the analytical method understandable and essentially complete.

2. Character of Sample Submitted to Mass Spectrometry

As indicated in the introduction, the sample that enters the mass spectrometer contains everything that was in the gas phase in the atmosphere except (1) vapors below their concentration of saturation at the boiling point of oxygen, and (2) vapors condensed at that temperature but not re-evaporated at the time of introduction into the spectrometer. The second group of losses is discussed first.

The cold trap (Shepherd) that was generally used has a volume of about 300 ml. Typically about 100 liters of air are passed through the trap. If the atmosphere is initially saturated with a given compound, its condensate, when warmed to the initial temperature for introduction into the spectrometer, will be confined to about 0.3 percent of the volume occupied before sampling, and consequently only about 0.3 percent of the compound collected will immediately re-enter the vapor phase. However, this vapor is introduced into an evacuated and relatively large inlet reservoir of the spectrometer, and as pressure in the saturator decreases during the transfer, more of the condensate is evaporated. In the case most favorable for the detection of a high-boiling compound, the freezeout tube contains only as much total volatile material as will produce a pressure satisfactory for analysis in the combined volumes of tube and inlet reservoir. In this case, the compound should be detectable if the spectrometer is only as sensitive as would be necessary to show the presence of the compound in solid or liquid form in the reservoir itself. This is the condition roughly represented on figure 1 by the notation "approximate limit of detection." Actually the freezeout tube will usually contain enough material for several spectrometer runs; the inlet reservoir will be filled from it through a passage small enough to prevent much mixing between the reservoirs, and the composition of the gas entering the inlet reservoir will not change greatly during the transfer. Sensitivity for the compound is then reduced by a factor roughly equal to the number of times the inlet reservoir can be filled from the contents of the sampling tube.

Generally a compound should be "detectable" if it occurs in the atmosphere to the extent of 5 percent of saturation and if, at the temperature of delivery into the spectrometer (assumed to be 25° C), an atmosphere saturated with it would contain more than 1 part per 10 million. This statement involves a number of approximations, including the ease of forming ions from the compound, and implies that the substance contributes a measurable amount to one or more peaks that would serve for the detection and presumably the identification of the compound if nothing else were present. It does not indicate any certainty that so small a quantity of the compound can be recognized in the complicated spectrum of the total condensate.

In order to make use of this rough generalization in anticipating an indication of a compound in the mass spectrum, we need some knowledge of its approximate vapor pressure at 25° C. Relatively few observations of vapor pressure include this temperature and those that do are scattered in the scientific literature. On the other hand, tables of boiling points for thousands of compounds occur in several commonly available textbooks. The boiling point is closely enough related to the vapor pressure at another temperature for our purpose provided there is not a change of phase between the two temperatures. Accordingly, the vapor pressure at 25° C was plotted with respect to the boiling point for enough substances to permit the construction of a satisfactory but entirely empirical curve, shown in two sections in figure 1.

The compounds included in this curve were chosen almost at random, and many of the vapor pressures at 25° C were obtained by extrapolating a formula given by the observer, often much beyond the limit of applicability specified by him. Little can be said for the plot except that the regularity shown is great

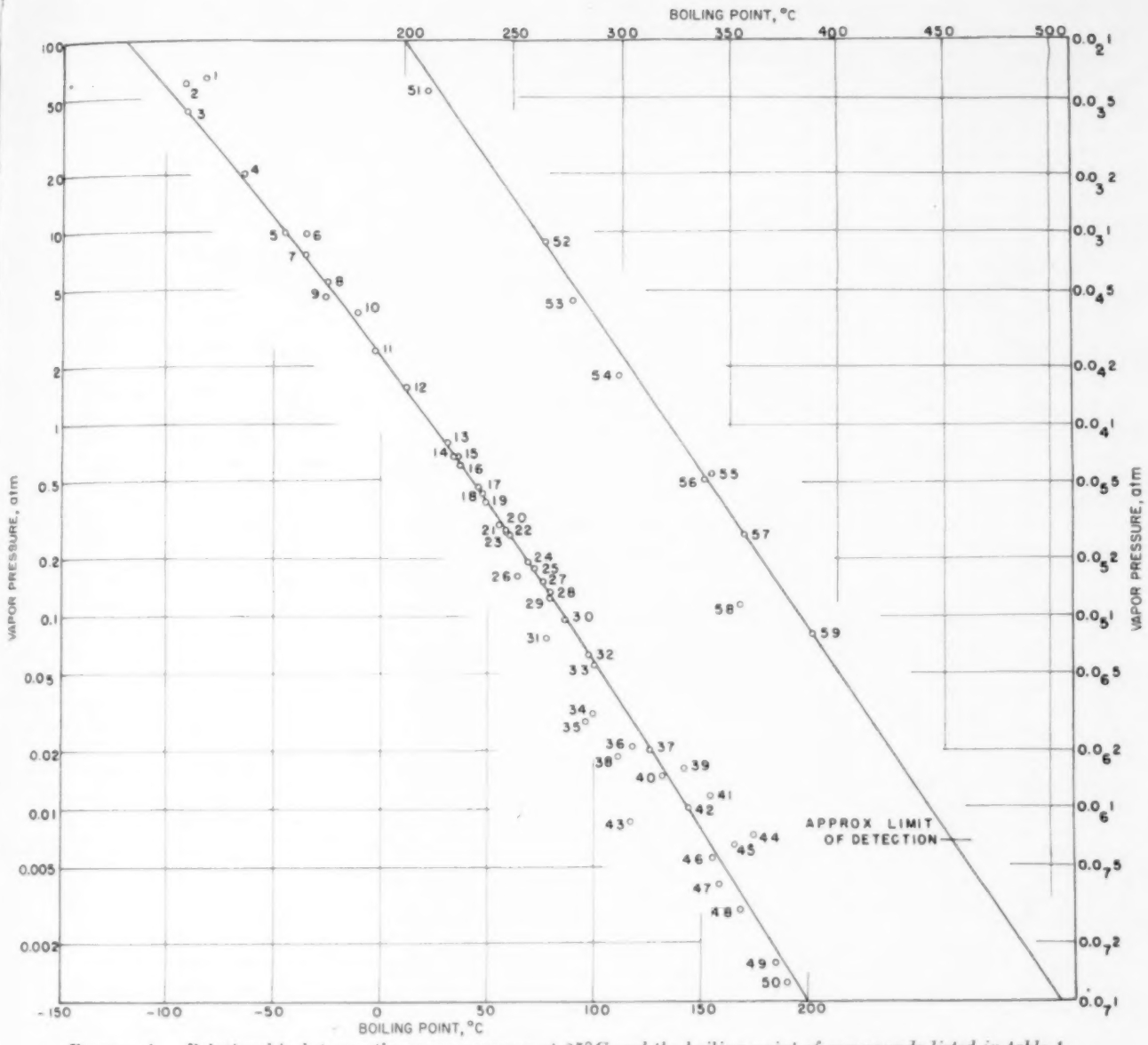

FIGURE 1. *Relationship between the vapor pressure at 25°C and the boiling point of compounds listed in table 1.*

enough to serve the purpose intended. Unfortunately, it applies only to compounds that are liquid both at the temperatures at which their vapor pressures reach 1 atm and at 25° C. Table 1 is a list of the substances included in making the chart. Elements, hydrocarbons, and organic halides, fall surprisingly close, considering the accuracy claimed by the observers of the original data, to a smooth curve that is a straight line below about 0.05 atm. Vapor pressures are notably less than would be read from the curve in the case of water, the simpler aliphatic alcohols, and some other polar compounds.

Of the 6,175 organic compounds listed in the "C-table" of International Critical Tables, not one that is liquid at 25° C has a boiling point high enough to indicate that failure of its condensate to vaporize in the sampling tube would seriously interfere with the determination of its vapor in the atmosphere. Both because they are rare and because they would have to be widely dispersed to approach saturation in a significant portion of the atmosphere, it is improbable that high-boiling liquids not on the ICT list would occur as vapors in the atmosphere and then be lost in sampling. Unless all condensed liquids including water are completely vaporized in the sampler, solution would complicate the situation somewhat.

The case is different with solids. No vapor pressure data were found for any solid that did not appear below the line of figure 1 by a factor in the range from 1.5 (camphor) to 2×10^5 (red phosphorus). All but a few chemical substances may be expected to be in the solid form when collected at −183° C, and a great many of them will remain solid at room temperature. Some of these may readily escape detection although initially present in the atmosphere in greater quantity than more volatile substances that can be determined.

TABLE 1. *Compounds used in constructing figure 1*

Number	Formula	Name
1	CO_2	Carbon dioxide.
2	N_2O	Nitrous oxide.
3	C_2H_2	Ethane.
4	H_2S	Hydrogen sulfide.
5	C_3H_8	Propane.
6	NH_3	Ammonia.
7	Cl_2	Chlorine.
8	CH_3Cl	Methyl chloride.
9	$(CH_3)_2O$	Methyl ether.
10	SO_2	Sulfur dioxide.
11	C_4H_{10}	Normal butane.
12	C_2H_5Cl	Ethyl chloride.
13	$HCOOCH_3$	Methyl formate.
14	$(C_2H_5)_2O$	Ethyl ether.
15	C_5H_{12}	Normal pentane.
16	C_2H_5Br	Ethyl bromide.
17	CS_2	Carbon disulfide.
18	$C_2H_2Cl_2$	*cis*-Dichloroethylene.
19	C_6H_{14}	2,2-Dimethylbutane.
20	C_2H_4O	Acetaldehyde.
21	Br_2	Bromine.
22	$C_2H_2Cl_2$	*trans*-Dichloroethylene.
23	$CHCl_3$	Chloroform.
24	C_6H_{14}	Hexane.
25	C_2H_5I	Ethyl iodide.
26	CH_3OH	Methyl alcohol.
27	CCl_4	Carbon tetrachloride.
28	C_4H_8O	Methyl-ethyl ketone.
29	C_6H_6	Benzene.
30	C_2HCl_3	Trichloroethylene.
31	C_2H_5OH	Ethyl alcohol.
32	C_7H_{16}	Heptane.
33	CH_2O_2	Formic acid.
34	H_2O	Water.
35	C_3H_7OH	Normal propyl alcohol.
36	$C_2H_4O_2$	Acetic acid.
37	C_8H_{18}	Normal octane.
38	CCl_3NO_2	Chloropicrin.
39	$(CH_3)_2C_6H_4$	*ortho*-Xylene.
40	C_6H_5Cl	Chlorobenzene.
41	C_9H_{12}	Propyl benzene.
42	$C_2H_2Cl_4$	Tetrachloroethane.
43	C_4H_9OH	Normal butyl alcohol.
44	$C_{10}H_{14}$	Cymene.
45	$C_{10}H_{14}$	Isobutyl benzene.
46	C_6H_5Br	Bromobenzene.
47	$C_{10}H_{22}$	Dimethyl octane.
48	$C_5H_{10}O_2$	Isobutyl valerate.
49	C_6H_7N	Aniline.
50	C_6H_5I	Iodobenzene.
51	$C_6H_5NO_2$	Nitrobenzene.
52	$C_{13}H_{12}$	Diphenyl methane.
53	$C_{12}H_{10}$	Acenaphthene.
54	$C_{13}H_{10}$	Fluorene.
55	$C_{14}H_{10}$	Anthracene.
56	$C_{14}H_{10}$	Phenanthrene.
57	Hg	Mercury.
58	$C_{12}H_9N$	Carbazole.
59	$C_{14}H_8O_2$	Anthraquinone.

When a compound is identified, the question arises whether the percentage found in the sample that enters the spectrometer is the same as that in the original sample. If, from a knowledge of the total pressure in the sampler and the best available information on the vapor pressure of the compound at the working temperature, the sample in the cold trap appears to be saturated or nearly so, the amount shown by the mass spectrometer may be low by as much as two orders of magnitude. If saturation is not indicated in the cold trap, no loss through failure to vaporize need be assumed, but there is still to be considered the amounts of highly volatile constituents of the atmosphere that were not collected in the first place or were lost during the subsequent removal of air.

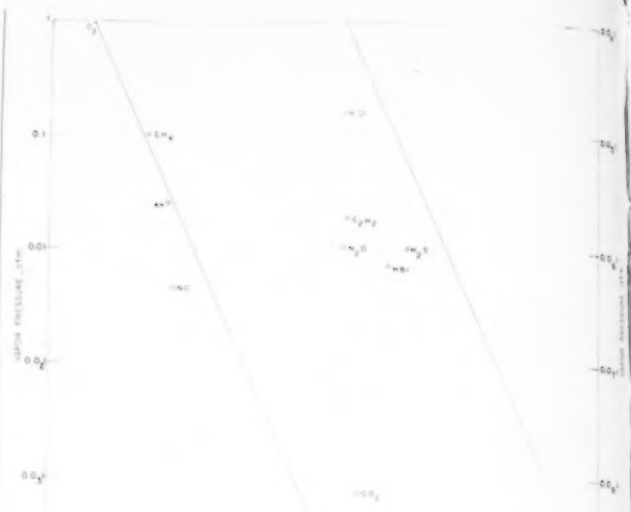

FIGURE 2. *Relationship between the vapor pressure of the liquid at −183°C and the boiling point.*

The vapor pressure of solid substances at −183° C related to the boiling point is indicated by the identified points.

The problem of loss of substance through failure to condense in the cold trap was attacked in the same way as that of failure of the condensate to vaporize, that is, by constructing a plot relating vapor pressure at −183° C to the boiling point. Nearly all vapor-pressure data that could be used, even by extrapolation, relate to the liquid phase and nearly all substances are solid at the boiling point of oxygen. Liquid phase equations were extrapolated, and, as in figure 1, they gave a very consistent curve, which is a straight line within the limits of error of the data. This line has been drawn in two sections in figure 2. Extrapolated data regarding the vapor pressure of solids have been added. With the exception of methane, they lie well below the plotted line, and solution and adsorption may reduce them further. They give a rough guide for estimating the probable loss of material by failure to condense. Thus, we should not expect to collect methane unless 10 percent is present in the atmosphere. The limit for the collection of ethylene is about 30 ppm and for ethane 10 ppm. However, we should expect to lose only about 0.2 ppm of acetylene, 0.1 ppm of hydrogen sulfide, and less than a part per billion of carbon dioxide. The loss of enough of anything that boils above −20° C to be measurable with the mass spectrometer is improbable.

It is concluded that the delivery to the spectrometer of the vapors (1) of all substances that boil above about −20° C, and are liquid at 25° C, and (2) of substances that are solid at 25° C and boil between −20° and 300° C, is substantially complete. Outside this classification there may be significant loss of material at both ends of the scale of volatility.

3. Treatment of Sample Before Introduction Into the Mass Spectrometer

Samples of atmospheric condensates have been treated in various ways before introduction into the mass spectrometer. The data and conclusions reported in this paper will not differentiate between the various treatments because the differences that resulted from them did not produce certainly significant changes in the interpretation of the samples to be considered. In all cases, the significant portion of the condensate must be separated from a much greater quantity of air and of condensed carbon dioxide and water. These major constituents of the unpolluted atmosphere are to be considered primarily as diluents of the sample rather than as interfering substances. As diluents they carry most of the ion current at a few mass peaks and leave the remainder of the spectrum too feeble for use. Otherwise their interference is limited to a small number of peaks shared with pollutants that can be identified in most cases, by ions of other masses.

Air is removed by evacuation while the cold trap is immersed in liquid nitrogen. Because it is impossible to remove oxygen and nitrogen completely without losing low-boiling pollutants, the evacuation is carried only far enough to control dilution. Carbon dioxide and water have been reduced to workable concentrations in several ways. These include the use of absorbing reagents ahead of the cold trap when sampling the atmosphere, freezing out a portion of water ahead of the cold trap, and the use of absorbants in the path of all of the sample between the cold trap and the spectrometer.

The treatment preferred is the following: After removing the air from the cold trap, it is allowed to warm to about −120° C while connected through an Ascarite tube to a receiver immersed in liquid nitrogen. When most of the carbon dioxide has been removed in this way, the Ascarite tube is bypassed and the transfer of the sample is continued at a higher temperature, but one low enough to leave most of the water behind as ice. Preferably the ice is sublimed at least once to permit the escape of anything trapped in the original precipitate of frost. Later a higher-boiling fraction may be taken through a drying tube in the same way that the first fraction was taken through Ascarite.

4. Numerical Arrangement of Analytical Data for Study

The curves plotted by the mass spectrometer are reduced to numerical form by reading the "peak heights" in terms of scale divisions. The heights of the peaks considered useful are then "normalized," that is, they are added together and each peak height is expressed individually as a percentage of the total. For this purpose, certain omissions and corrections are made. The volumes of air, carbon dioxide, and water left in the sample after preliminary treatment are each still greatly in excess of the total volume of "pollutants," and their principal peaks are sometimes too high for the available scale. Even if these peaks are readable, they indicate nothing about the sample except variations in the success of the pretreatment. If they are included in the spectrum when it is normalized, two samples that contain identical pollutants will appear to be substantially different if different quantities of air, carbon dioxide, or water escaped removal. It is, therefore, convenient to include in the total for normalizing only the peaks that are subsequently to be used as significant of pollutants. For this reason Shepherd and his coworkers normalized the California samples with the omission of all peaks below (25), those between (27) and (37), and (44), (45), (46), (99), (101), and (102). To make subsequent observations comparable without recalculating the voluminous California data, the same omissions have been made in the total used in normalizing, but several peaks not included in that total are sometimes used in the interpretation of the results. These include especially (20), (22), (31), (35), (36), (45), and (46). Actually, in most cases, it makes little difference whether this group of peaks is included in the normalizing total or not as together they seldom constitute more than a fraction of 1 percent.

The omission of the principal peak of nitrogen and carbon monoxide (28), of oxygen (32), and of carbon dioxide (44) from the normalizing total and from other steps in the interpretation of the results, especially the plotting of figures, is unquestionably desirable. Little use has been made of (29) and (30), which are large peaks but seem to be nearly constant in substantially all the spectra of urban atmospheres so far studied. They are affected by isotopes related to (28) and not readily corrected for because (28) is an important peak of nitrogen, carbon monoxide, and carbon dioxide. Peak (29) represents ethyl ions which are possible fragments of a great number and variety of heavier compounds and have very little diagnostic value. Peak (30) has been given much attention, without practical result, because it contains the principal identifying peak of the nitrogen oxides and acids, and the parent peaks of ethane and formaldehyde. Figure 2 shows that nitric oxide, NO, like methane, is too volatile to be collected in the trap at any probable concentration but N_2O, most of which is dissociated to NO^+ in the spectrometer, may be indicated. The peak is usually equal to about 9 percent of the normalizing total, and we have been unable to attach any definite significance to its variations. Peak (40) is an important one in the spectra of many potential pollutants and is the parent peak of argon, for which a correction must be made if it is to represent pollutant and not air. The correction is based on (32). A correction of (45) and (46) for isotopes in carbon dioxide is based on (22), a doubly charged ion that distinguishes carbon dioxide from propane. Usually (99), (100), and (102) are neglected because of interference by the doubly charged isotopes of mercury that are always present. Occasionally one or more of these peaks is useful. It can usually be ascertained which peaks are significant in the study of pollution because, in the absence of pollution, they

should all appear in the constant ratios of the mercury isotopes.

Although several attempts have been made to simplify the study of pollutants by fractionating the condensate [2], they have not been very useful because the separations are not sharp and the spectra of the fractions are almost as complex as those of the total condensates. Although further study of fractionation is planned, all data in this paper refer to total condensates only.

5. Graphic Arrangement of Data for Study

A great deal of use has been made of the suggestion of Sibyl Rock of the Consolidated Electrodynamics Corporation that comparisons be made between spectra by plotting them with the peaks arranged in the order of descending height in one of the spectra, called the "Reference." The peak heights are plotted on a logarithmic scale.

This method of plotting has several desirable features. The reference spectrum approaches a fairly smooth curve without maxima or minima. A spectrum compared with it shows differences of composition by deviations from the curve which, if they are at all large, take the form of a series of maxima and minima. A third spectrum shows similarities to the second by the location of the high and low points. At any peak the linear distance between the two plots represents a ratio between the abundances of the constituents that produce the ion represented. If several peaks, the (117), (119), and (121) peaks of carbon tetrachloride for example, represent only a single compound in both the reference and the sample compared with it, they all stand out equally from the reference line although they may be of greatly different magnitude. The logarithmic scale makes relative quantities of rare ions in two spectra as prominent as those of more abundant ions. This is especially important because the peaks most useful in identification are often small. These features help greatly in the identification of compounds in what seems otherwise a hopeless tangle of data. Plots are made on tracing paper so that two or more can be read when superposed, and punchings facilitate accurate registration.

In order to make convenient intercomparisons between them, all the spectra from the California samples were plotted in the order of a single spectrum designated "Ref." Ref was chosen as representative of the very similar spectra of condensates obtained in Los Angeles and Pasadena during the worst smogs that occurred in a period of 3 months in the autumn of 1951. The order of peaks in the original Ref was as follows: 43, 27, 41, 26, 42, 39, 57, 56, 55, 70, 25, 58, 69, 71, 38, 91, 40, 78, 83, 37, 84, 51, 50, 92, 53, 72, 45, 97, 85, 31, 98, 52, 54, 86, 67, 68, 77, 111, 82, 65, 112, 49, 63, 95, 46, 106, 79, 59, 81, 62, 130, 132, 60, 105, 74, 76, 73, 61, 47, 90, 96, 66, 93, 64, 126, 87, 89, 114, 117, 119, 48, 75, 113, 134, 94, 110, 120 109, 125, 80, 103, 107, 104, 121, 88, 115, 140.

Figure 3 represents, by an envelope, the spectra of three samples taken in Los Angeles and three in Pasadena. The envelope consists of an upper line joining points representing the highest percentage of each ion in any of the six condensates and a lower line representing the lowest percentage. The broken line between the two is Ref. The group of high peaks (117), (119), and (121), near the lower end of the plot represent carbon tetrachloride in one sample, and the peaks (64) and (48) represent sulfur dioxide in another. Both may be the result of contamination of the samples in the laboratory.

Samples taken later in various places produced other peaks below the level of detection in the samples used in the original selection of Ref. It was convenient to adopt a standard order for plotting these and other peaks, such as (29) and (30), that had been disregarded initially. This order is approximately that in which the peaks happened to become of interest, and is as follows: 128, 124, 123, 127, 138, 139, 131, 129, 142, 136, 137, 118, 133, 141, 108, 116, 147, 154, 151, 152, 156, 148, 149, 143, 153, 146, 155, 145, 29, 30, 31, 35, 36, 99, 100, 164, 165, 166, 168, 170. In the figures that follow, this order will be considered a part of the "order of Ref," not all of which is always used.

The plotting of peaks in other orders than that of Ref is frequently desirable. It is now the usual practice to plot a spectrum first in the order of Ref for comparison with plots of other mixtures in order to make as good a preliminary estimate as possible of what is present. The sample under study is then plotted in the order of magnitude of its own peaks, and the spectrum of the components thought to be present is built up as they are tentatively identified. This procedure gives most of the advantages of comparision with Ref, particularly the recognition of groups of peaks that indicate a single compound, and permits the modification of the tentative analysis as often as necessary with a minimum of replotting.

6. Regularities Found in Samples From Southern California

The most remarkable thing about the condensates obtained from the atmosphere of Southern California during smogs, was the close resemblance between their mass spectra. This is strikingly shown by the narrowness of the envelope of the six samples represented in figure 3 taken in different parts of the area during a period of 3 months. Although these samples were admittedly selected because of their close agreement, many other samples showed strong resemblances to the group and tended to show a progressive series of differences. By this is meant that the deviations from Ref were not random. Instead, differences usually appeared in much the same series of peaks, and if a certain peak height differed from that of Ref more in one sample than in another, several other peak heights showed correspondingly greater deviations in the first sample than in the second. This would, of course, necessarily be the case if the peaks considered represented a single compound; but the relationship appeared to be too general to be explained by different concentrations of 1 or 2 substances. Two explanations

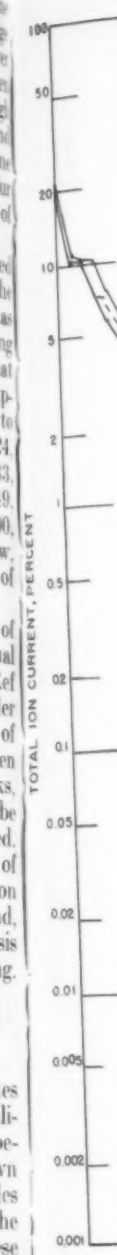

FIGUR

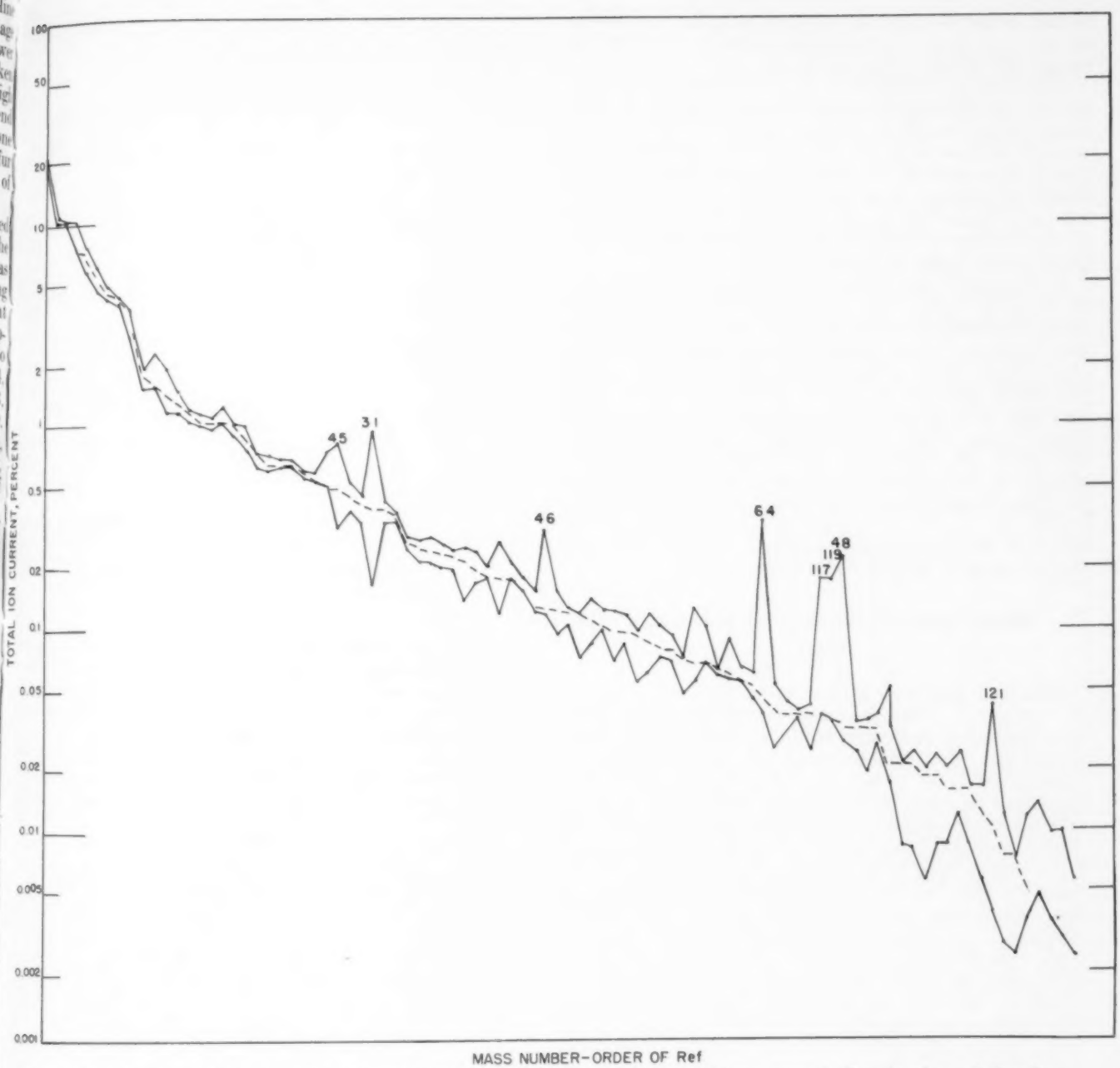

FIGURE 3. *Agreement between spectra of several condensates taken during periods of heavy smog in Los Angeles and Pasadena.*

appear probable, (1) that the atmosphere contained varying proportions of two principal groups of pollutants from different sources, or (2) that a predominant pollutant from a single source was undergoing change by reactions in the atmosphere, the progress of which was indicated by the changing spectrum. It is not surprising that local or temporary variations confused the picture considerably.

Accompanying the samples were some rather vague statements about weather conditions, visibility, eye irritation, etc., from which it was possible to arrange the numerous samples roughly in the order of apparent severity of smog. Each of numerous peaks and functions of peak heights, especially ratios between selected peaks, were plotted with respect to the numbers of the sample arranged in this order of apparent severity. Several of these plots indicated fairly definite trends; for example, the most abundant peak, (43), appears to increase during smog. However, the most positive trend appeared among the three ratios, (58)/(53), (72)/(67), and (86)/(81), all of which increased strongly and fairly consistently with increasing indications of smog. A further discussion of regularities within groups of spectra is given after the next section on "normal traffic gas." The trends mentioned in this paragraph all relate

to the composition of the mixture of pollutants in the air and not to its over-all concentration, with which no certain correlations are apparent.

When studies of pollution in other cities were begun it was immediately evident that the spectra of their atmospheric condensates usually resembled strongly those from Los Angeles. The obvious explanation is that a large part of the pollution came from a similar source or sources; and when weather conditions and places of sampling are also considered, there appears to be nothing common to the probable origin of the pollutants except automobile traffic.

Both exhaust gas and gasoline vapor are chemically so complex that their determination as individual compounds is impossible by any means now available. But because they are released from so many vehicles, they are probably much the same everywhere; and it should be possible to treat "traffic gases" (a term intended to include an average amount of gasoline vapor from filling stations, leaks, etc.) as a unit. In order to recognize pollutants of a different character and to locate their sources, it is important to differentiate them from traffic gases as a whole. Unless we can do this, by mass spectra or otherwise, we lack the information needed to deal with the control of pollution at its various sources.

7. Mass-Spectra Pattern of Normal Traffic Gas

The first step was to determine with a fair degree of certainty, though not necessarily with great accuracy, the mass spectrum we may expect from traffic gas. For this purpose we had available the spectrum (A) of a sample taken from a tunnel in Pasadena in 1951 during heavy traffic, and another (B) taken in a tunnel in Washington, D. C. in 1954 under similar conditions. The Pasadena sample represented both exhaust gases and vapors from the engines, and the generally polluted atmosphere of the city drawn into the tunnel as the cars passed through, but it was reasonable to suppose that the high concentration of traffic gas would result in the outside pollution becoming negligible or nearly so. Actually, the one or two recognizable constituents of outside smog not attributable to motors indicated that about 20 percent of the total condensate collected came from outside. The Washington sample (B) was taken in a region free of industrial contamination and was believed to be almost free of pollution from any source except automobiles. Both these samples represented continuously moving traffic. To supplement them three samples were taken; (C) from a busy intersection where traffic is interrupted by lights; and (D) and (E) from points of heavy but uninterrupted traffic in residential districts. A link of a sort was established with the Southern California samples by plotting the ratios between certain peaks previously mentioned as best indicating the appearance of smog. The several samples, including two from Detroit and four from Washington, were arranged chronologically in the order of sampling. The result is figure 4. The

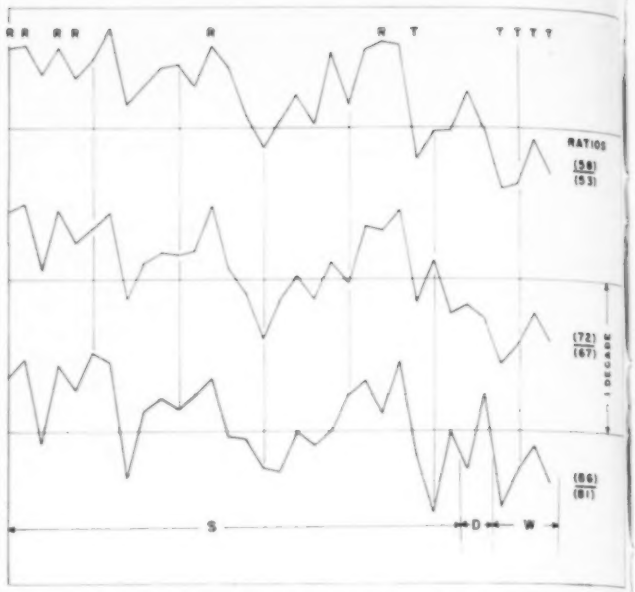

FIGURE 4. *Variation in the ratio of the peak height of three pairs of mass numbers as affected by the nature of the sample.*

S, Southern California; D, Detroit; W, Washington
Samples used in deriving patterns: R, Ref; T, NTG

ordinates are logarithmic, and the curves are separated by shifting the scale 1 decade for each. Horizontal lines represent the ordinate 1.0 for the curve that intersects it. The fact that the three ratios are closely related without regard to locality is unmistakable. The six samples used to establish Ref (fig. 3) are indicated in figure 4 by the letter R, and the five samples chosen to represent normal traffic gas, by T.

The five spectra of traffic gas were plotted and critically examined, point by point. The agreement was not as good as had been expected, and the reasons for disagreement are obscure. However, it could be assumed that if such a thing as a normal traffic gas exists, there is nothing in any of the sampling locations to remove anything from the mixture, but it is possible, even probable, that significant additions may come from other sources. On the other hand, there is the possibility that something was lost from any of the samples during handling, by reaction, solution in stopcock lubricants, or the like. In view of these possibilities it was not believed that statistical rules of probable error would have much significance, and it was decided to consider each mass number individually and to select what seemed to be a "best value" rather than to take any kind of mathematical mean. The result is plotted with peaks in the order of the customary Ref, in figure 5. The solid line is the selected spectrum, which will be referred to as normal traffic gas or NTG. Ref is shown as a dotted line. It must be admitted that initially no great confidence was placed in the accuracy of this picture of normal traffic gas, but subsequent use has caused greater significance to be attached to it.

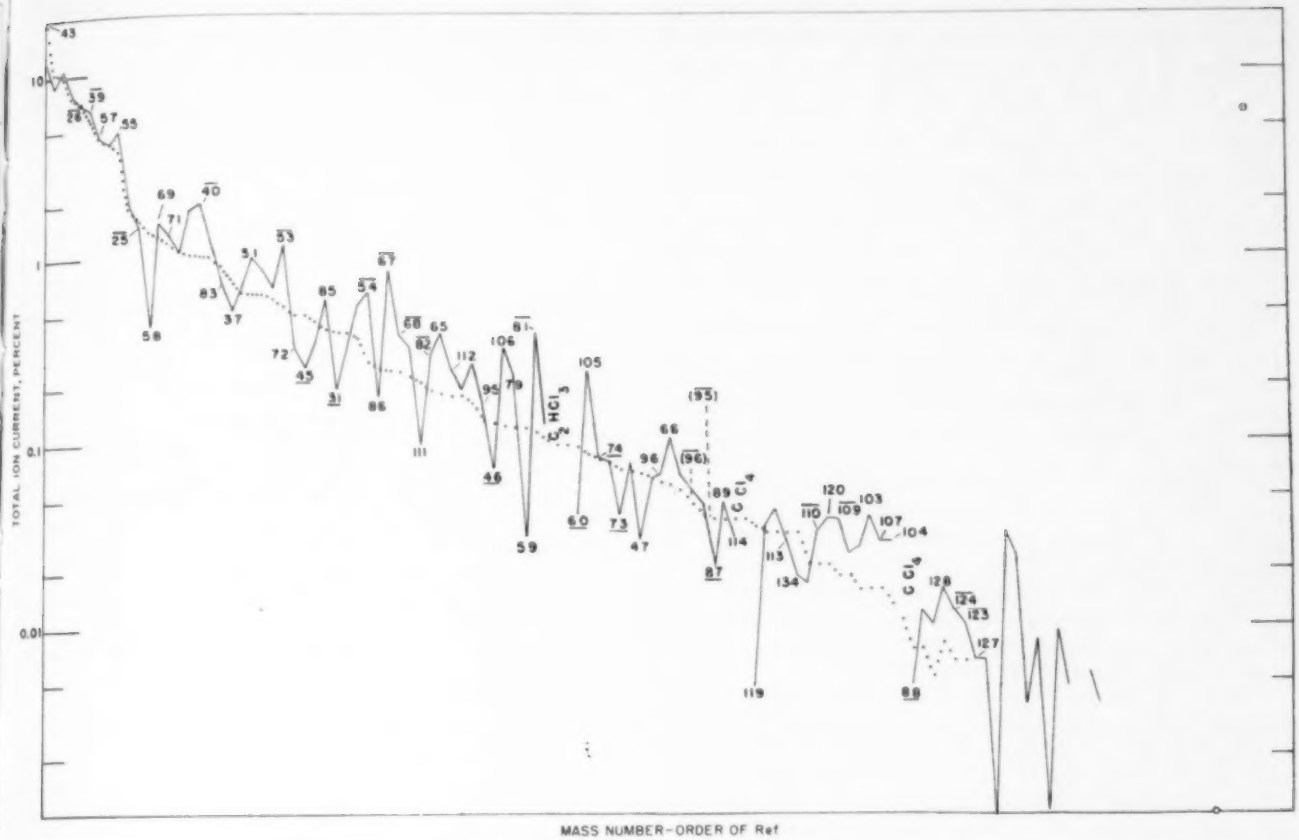

FIGURE 5. *Spectrum of normal traffic gas plotted in the same order as Ref.*
———, NTG; . . . . . , Ref.

8. Comparison of Normal Traffic Gas with Ref

A comparison of the two curves of figure 5 at once shows that compounds of certain chemical series are more abundant in one than in the other.

The members of a homologous series of compounds, for example, the paraffin hydrocarbons, differ in molecular weight by multiples of 14. Thus methane has a molecular weight of 16, ethane 30, propane 44, butane 58, etc. A positive ion formed by the loss of an electron from the molecule, called the parent ion, has the mass number of the original molecule. However, many more ions are formed from most compounds by the breaking up of molecules than by the loss of single electrons. An examination of the structural formula of any paraffin hydrocarbon will show that if it is broken in any manner into two fragments and no more, each fragment will have a mass of 1 or of 1 plus a multiple of 14; and that mass will be 1 less than one of the parent masses of the same series of compounds. Thus, when butane loses 1 hydrogen atom, mass (57) is left, if 1 carbon atom with its attached hydrogen (a methyl group) is detached, the residue has mass (43), 1 unit less than the parent mass of propane; detaching an ethyl group leaves 29, 1 unit less than the parent mass of ethane, etc. Although ions are also formed with the breaking of more than 1 bond of the molecule, the ions of the parent mass and of 1 less than the parent mass of some member of the homologous series, are predominant enough to be significant of the chemical nature of the parent compounds.

With this in mind, table 2 was prepared to afford a comparison of the chemical nature of the compounds represented by NTG (normal traffic gas) and Ref (the condensate from smog, assumed to be formed in considerable part, at least, by chemical reactions of traffic gas in the air). It should be noted that the same series of numbers may include the parent peaks of homologous series of compounds of quite different character.

In the following discussion it will be assumed that Ref is the product of reactions of NTG in air rather than a mixture with things from other sources, although this can be only roughly true, and the mixture represented by Ref will for brevity be referred to as "oxidized" as distinguished from "normal" traffic gas. Table 2a indicates that compounds of the same parent masses as the paraffins increase in relative amount as the atmospheric reactions proceed. Because all numbers in the table are percentages of a total sample, the simplest explanation for the over-all effect is that compounds other than the paraffins are disappearing, probably with the formation of nonvolatile particles or water, carbon

dioxide, carbon monoxide, etc., not included in the part of the spectrum considered, leaving the inert paraffins as a greater percentage of the total. However, we find that in the aggregate it is only the parent peaks that have increased. If the first explanation were the only one, the odd- and even-numbered peaks should have changed in proportion. A more interesting explanation than the first is that aldehydes and ketones are among the products of the smog-forming reactions. Aldehydes and ketones produce a much larger proportion of parent ions than do the easily broken paraffins.

Table 2b shows the surprising fact that in general the peaks thought to be most characteristic of the olefins remain practically constant in relative abundance. In the literature bearing on the Los Angeles smogs the unsaturated hydrocarbons, and the olefins in particular, are given a major part of the blame for smog formation, and irradiation experiments of olefins in air have shown that the blame is not misplaced. At present no adequate explanation of the relative constancy of the "olefin peaks" has been thought of by the authors. One possibility is that most of them are derived from cycloparaffin rather than olefin sources and that the cycloparaffins remain substantially inert in the atmosphere.

Table 2c shows a striking decrease during smog formation of nearly all the parent and parent-minus-one peaks of the group that includes acetylene and the dienes. The only exception is acetylene itself, which remains relatively constant as indicated by its parent peak, (26). The relatively smaller number of (25) ions in traffic gas may well be the effect of a reduced number of fragments of heavier molecules rather than a decrease in acetylene itself. It seems reasonably certain that the decided decrease in the other peaks in this group during conversion to smog is the result of reactions in which their parent molecules are used up.

Table 2d shows a decrease in the aromatic hydrocarbons only less striking than in the preceding group, especially in the higher members of the series.

Table 2e represents the peaks characteristic of a rather wide variety of oxygen-containing compounds, of which the alcohols, and particularly ethyl alcohol are likely to be the most abundant. Generally the peaks are not in the ratio that would indicate ethyl alcohol alone, however. This series shows such striking increases that it seems most probable that it is derived in large part from the products of traffic gases reacting in the air.

Many of the peaks in figure 5 have been labeled. Those of the series beginning with (25) and (26) are marked with a line above the number, those in the series beginning with (32) and (31) are underlined. With the exception of (25), all the 16 peaks of the first series are above Ref by surprisingly consistent amounts. A secondary regularity is to be seen in the fact that, on one side of peaks (53) and (54), which are about equally above Ref, the even-numbered peak is larger than its adjacent odd-numbered peak, whereas above (54) the reverse is true. Peaks (95) and (96) seemed out of

TABLE 2. *Ratios of parent and parent-minus-one peaks*

M/e		Ratio of ion currents in Ref to currents in NTG	
Parent	Parent−1	Parent	Parent−1
a. PARAFFIN SERIES (also aldehydes and ketones)			
30	29	1.30	(a)
44	43	(b)	1.81
58	57	2.60	1.00
72	71	1.51	0.91
86	85	1.41	.70
100	99	1.7	1.2
114	113	1.22	1.1
128	127	0.5	0.2
Average		1.46	0.99
b. OLEFIN SERIES (also cycloparaffins)			
28	27	(c)	1.13
42	41	1.04	0.93
56	55	1.0	.78
70	69	0.93	.64
84	83	.89	1.21
98	97	1.2	1.31
112	111	0.70	2.20
126	125	.86	0.73
140		.50	
Average		0.89	1.12
General average		1.00	
c. ACETYLENE SERIES (also dienes and cycloolefins)			
26	25	0.89	1.09
40	39	.52	0.87
54	53	.41	.45
68	67	.61	.28
82	81	.66	.31
96	95	.85	.25
110	109	.63	.48
124	123	.52	.61
Average		0.64	0.54
d. ONE-RING AROMATIC HYDROCARBONS			
78	77	0.89	0.68
92	91	.89	.57
106	105	.38	.3
Average		0.72	0.52
e. ALCOHOL SERIES (also ethers, acids, and esters)			
32	31	(d)	2.0
46	45	1.76	3.1
60	59	2.97	3.6
74	73	0.95	1.8
88	87	1.98	1.62
Average		1.92	2.42

[a] Too strong interference for use. [b] Obscured by carbon dioxide. [c] Obscured by nitrogen. [d] Obscured by oxygen.

place until it was discovered that those numbers in Ref were strongly affected by trichloroethylene. When they were corrected for the chlorine compound, they fell in the positions on the descending Ref curve marked by ( ), which makes them consistent with other members of the group.

Again with one exception, (74), the underlined numbers are all below the line. Peak (74) is probably affected by an interference, as (95) and (96) were, though the source of the interference has not been determined.

9. Estimation of the Kind and Amount of Traffic Gas in a Local Situation

It would be unreasonable to suppose that all the regularities occurring in the relation between NTG and Ref could have appeared had not the selection of the two patterns been substantially representative of two general phases of air pollution. Continuing the assumption that smog is derived primarily from traffic gas, a pollutant having the spectrum of NTG should be converted, in time, to one with the spectrum of Ref. These two spectra are so different that it is at least desirable to distinguish between them whenever a pattern for a traffic gas is used in the study of an unknown sample.

It has become a fairly well established practice in the petroleum industry to determine the various types of compounds in petroleum products, paraffins, aromatics, cycloparaffins, olefins, etc., by considering ratios between selected groups of peaks; and reported comparisons with synthetic mixtures show that high accuracy is frequently obtainable. An attempt was made to apply a similar method, using the ratios represented in figure 4, to determine the state of reaction of the pollutants from motor traffic.

The recorded values of the several peaks (with one addition) and the computed ratios are shown in table 3.

TABLE 3. *Peaks principally used in judging the extent of oxidation of traffic gas*

Peak	NTG	Ref	$\frac{\text{Ref}}{\text{NTG}}$	$\frac{\text{NTG}}{\text{Ref}}$
	%	%		
(54)	0.66	0.27	0.41	2.4
(58)	.54	1.40	2.6	0.38
(53)	1.20	0.54	0.45	2.2
(72)	0.33	.50	1.5	0.66
(67)	.88	.25	0.28	3.5
(86)	.18	.255	1.4	0.71
(81)	.40	.121	0.30	3.3
(58)/(53)	.45	2.6	------	------
(72)/(67)	.38	2.0	------	------
(86)/(81)	.45	2.1	------	------
Average	0.43	2.23	------	------

Two approximate formulas were developed for estimating the extent of oxidation, but the rigid application of neither of them was very successful for two apparent reasons, (1) pollutants unconnected with traffic gas interfere with some of the peaks used, and (2) the reactions of oxidation do not all occur at the same rate. A rough estimate of the extent of oxidation can usually be made by plotting the spectrum of the sample in the order of Ref and comparing, preferably by superposing, with the spectra of NTG and Ref as shown in figure 5.

The total percentage of traffic gas is estimated at the same time. It will be noted that the portions of Ref and NTG between ordinates 10 and 1.5 (peaks 27 and 25 in the usual order) coincide very closely. The plot of the sample is adjusted vertically to obtain as good a fit of this portion of its curve to those of figure 5 as is practicable but with one limitation, sample peaks in other parts of the spectrum must not fall so low that their explanation would require the elimination of an unreasonable fraction of the traffic gas. Peaks much higher than either Ref or NTG should not be disturbing, in fact they are what we are looking for. When the two sets of curves have been fitted together as well as practicable, the vertical distance between the indices (ordinate 1) of the two scales shows the percentage of the total sample to be attributed to traffic gas, normal or oxidized. The fraction "X," the percentage of conversion of normal to oxidized traffic gas, is estimated by noting the relation of peak heights of the sample to those of Ref and NTG that are widely separated from one another. Peaks (53), (54), (58), (67), (72), (81), and (86) appear to be the most useful for this purpose. If maxima are not noticeable at (53), (54), (67), and (81), oxidation of the sample has proceeded far. Minima at (57), (72), and (86) are less significant because the presence of interfering substances accentuates common peaks but raises low points of the spectral curve.

Some of the peaks found in the spectra of the traffic gases are indicative of known compounds with very little probable interference. This is especially true of the parent peaks of the aromatic hydrocarbons. The aromatics are important constituents of the traffic gases and should remain a part of the total spectrum of a sample until a decision has been made as to its probable content of traffic gas. However, the aromatics can be independently determined and it would be unfortunate to have the analysis affected by their amounts in Ref or NTG. Hence the patterns of the aromatics are "taken out" of the initial patterns of Ref and NTG, and are applied separately in the interpretation of the spectrum of the sample.

The chlorine compounds trichloroethylene and carbon tetrachloride were present in all samples used in the selection of Ref and in 2 or 3 of those used for NTG; but they are not considered normal constituents of traffic gas and they have also been taken out of the patterns of Ref and NTG. With somewhat less assurance, the patterns of ethyl alcohol, acetylene and sulfur dioxide were also taken out of the traffic gas patterns, but the spectra of these compounds are subject to so many interferences that they are determined only after most other identifiable constituents have been taken out.

While the spectrum of the sample is superposed on figure 5, a notation is made of any peaks that seem abnormally high, and an effort is made to identify these peaks, as far as possible, with the chemical compounds they seem most likely to represent.

Sometimes they indicate a whole group of compounds, such as gasoline vapor, in excess of that normally present in traffic gas.

The procedure is now to attempt to interpret the spectrum of the sample in the usual way except that the expurgated patterns of Ref, NTG, and other approximately known mixtures are treated as though they represented single substances. It is helpful to plot the spectrum of the sample in the order of abundance of its own peaks, and to compare with it from time to time the composite spectrum of whatever seems to have been identified. Relations among the residual peaks are more readily seen in graphic than in numerical form, and when the analyst has done the best he can, the remaining plot indicates at a glance how successful his effort has been.

10. Application of the Method to a Specific Sample, Louisville D–6

Even with the general method of approach that has been outlined, each sample presents a unique and complicated problem that is solved largely by trial and error. The interpretation of the spectrum of one sample, designated D–6, from Louisville will be followed in considerable detail to illustrate the method employed.

The spectrum of the sample was first plotted in the order Ref and the graph superposed on the patterns of both Ref and NTG, shown in figure 5. The result is figure 6, in which the spectrum of the sample is represented by a solid line and the two types of traffic gases by broken ones. From the agreement of the half dozen larger peaks, it is evident that the sample contains about the percentage of the more abundant hydrocarbons that is usually found in traffic gas. However, the plot also indicates that traffic gas contains much greater quantities of a large number of other things than are found in the sample, and these cannot be accounted for except by assuming that (1) there are great differences in the composition of the traffic gas in Louisville and elsewhere, or (2) that much of the major hydrocarbon fraction of the sample was derived from something other than traffic gas.

Rejecting the first assumption, the relative positions of the two plots were shifted to those of figure 7, in which there is as good agreement among minor constituents represented by the numerous smaller peaks as seemed readily attainable. The relation between the indexes of the two plots (ordinate 1 of NTG is in parentheses) shows that the dotted curve now represents the contribution of 30 percent of NTG to the total spectrum. Ref has been omitted from the figure because the sample was taken early in the morning when much conversion to the condition of Ref seems unlikely and because the occurrence of high and low points in the two spectra at the same mass numbers is frequent enough to indicate normal rather than oxidized traffic gas.

If only a third of the principal group of hydrocarbons is from traffic gas, it is necessary to account otherwise for the other two-thirds. It seemed most

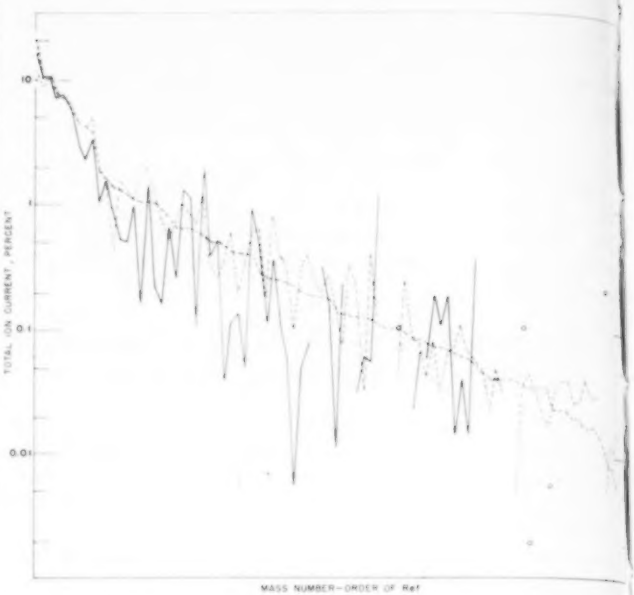

FIGURE 6. *Comparison between Louisville sample D–6 and both Ref and normal traffic gas.*

———— ○, Sample; . . . . . , Ref and NTG.

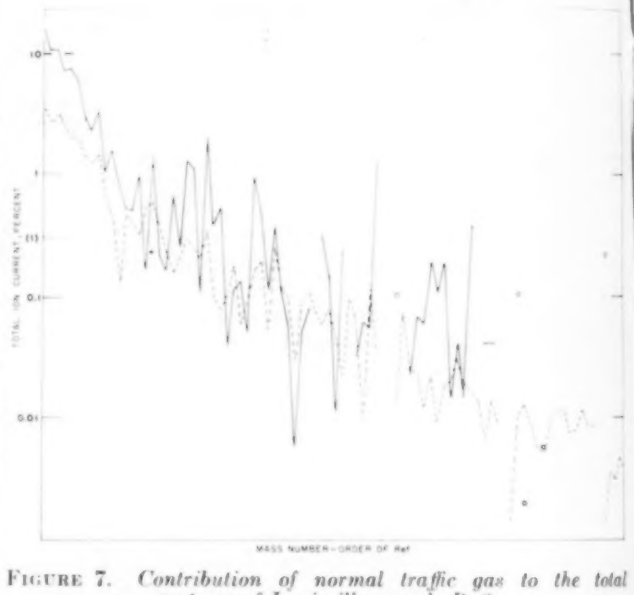

FIGURE 7. *Contribution of normal traffic gas to the total spectrum of Louisville sample D–6.*

———— ○, Sample; . . . . . , 0.3 NTG

probable that it was raw gasoline vapor from a source not at first identified. There was available for comparison the spectrum of a composite sample of "average" gasoline from Los Angeles, made in 1951. This has a strong resemblance in the proportions among its higher peaks to the spectrum of both the sample and NTG, but the percentage of these peaks is somewhat higher than in the sample. A matching of the curves as well as practicable by superposing them in the same way that the sample and Ref were previously matched, indicated an excess in the gaso-

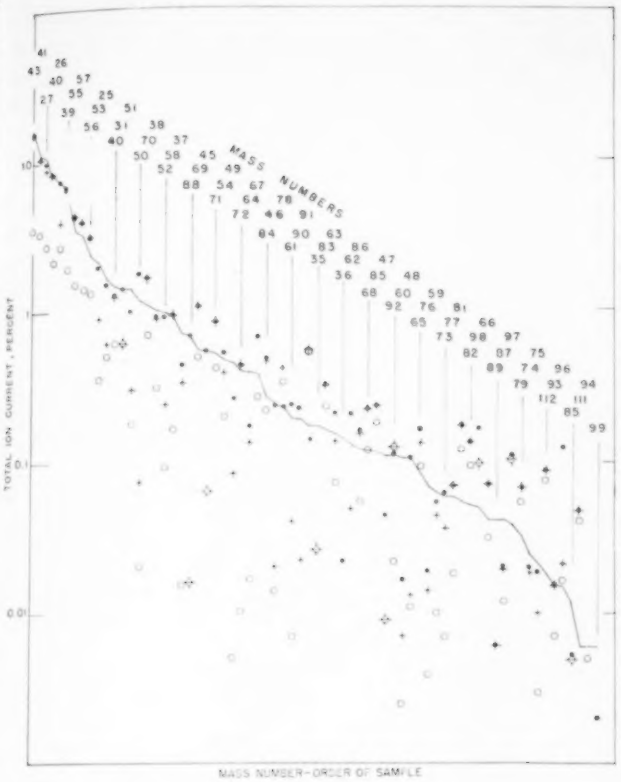

FIGURE 8. *Total contribution of identified substances to the spectrum of Louisville sample D–6.*

The mass numbers are plotted in descending order of their magnitude in the spectrum.

———, Sample. Accounted for by: ○, NTG 30%; +, NTG 30%, plus gasoline 50%; ●, total.

line of about 25 percent. From these data it appeared that in addition to 30 percent of NTG the sample should contain about 56 percent of gasoline vapor. A first calculation gave generally high values for the principal peaks that were high in the gasoline pattern, and the fraction assumed to be present was then rounded off to 50 percent.

In the remainder of this discussion the interpretation of the spectrum is represented by figure 8. The sample spectrum was replotted in the order of magnitude of its own peaks. The open circles indicate the contribution to the spectrum of 30 percent of NTG, the crosses represent the sum of 30 percent NTG and 50 percent of Los Angeles gasoline vapor, and the solid dots represent the sum of everything eventually added together in the effort to account for the entire sample.

The figure shows a great deal at a glance. The distance between a cross and the solid line indicates material to be accounted for from sources other than traffic gas and gasoline. Most of the masses at which there were large gaps to be accounted for were found to be important peaks of some of the compounds listed in advance as probable emissions from the industrial district called Rubbertown. Thus peaks (26) and (25) surely represent acetylene, (88) represents chloroprene, etc. The identification of substances that cannot be attributed to common traffic gas and gasoline, is the most important reason for assuming and applying a pattern for traffic gas. The substances identified are summarized in table 4.

It will be observed that most of the totals that are much above the line coincide with the crosses and show that the sample did not produce particular peaks as large as was expected from traffic gas and gasoline only. They are to be interpreted as meaning that the traffic gases and motor fuels whose patterns were used did not have exactly the composition of those in Louisville. This is not surprising. It is gratifying that such local differences affected as little as they did the identification and approximate determination of pollutants from other sources.

The peak heights of (78), (91), and (92), obtained by adding the patterns of NTG and gasoline and indicated by crosses, are above the dots representing "accounted for." The reason for this is that (78), the parent peak of benzene, and (92) the parent peak of toluene have no probable significant interferences, and the amount recorded by the spectrometer must, therefore, be considered to be the amount in the sample. The dot was therefore placed on the line representing the sample. None of the aromatic peaks higher than (92) was reported; accordingly (91) accounted for was calculated from (92) and the pattern of toluene. It falls somewhat below the line, indicating that there was a certain amount of aromatic material of higher molecular weight, but not enough to be reported. It is much below the (91) to be expected from NTG alone. Peaks (67) and (81) are high, possibly because the butadiene which was one of the gases from Rubbertown may have contained some higher homologs. With two exceptions, (71) and (85), the other peaks notably above the line are, in the order in which they occur in the figure, (55), (56), (70), (69), (83), (68), (98), (82), (97), (79), (112), (96), and (111). All of these could be olefin peaks, but are more likely to be peaks of the cycloparaffins. Their scarcity in Louisville probably results from the fact that the California petroleums and those of Venezuela from which Washington is probably largely supplied, have high cycloparaffin contents that are lacking in the midcontinent petroleums. It was found that samples from Detroit and Cincinnati showed a similar dearth of cycloparaffin peaks, though not to the same extent as this sample which was so largely raw gasoline. It was noted that the ratio of accounted for peaks to those of the sample tends to increase with increasing mass. A possible explanation for this is the fact that most of the gasoline in Louisville probably came from a tank farm in which the vapor escaped above the liquid and was generally lighter than the liquid left behind, whereas the gasoline used as a pattern in the accounted for spectrum was completely vaporized.

Three chlorine compounds, chloroprene, vinyl chloride, and dichloroethylene, were easily identified. The first two were on the list, with hydrogen chloride and chlorine itself, of compounds to be expected from Rubbertown. Because acetylene and chlorine readily form dichloroethylene, this compound may be the product of reaction in the atmosphere.

The dots significantly below the line represent portions of the sample spectrum, (37), (49), (64), (35), (36), (47), (76), (87), and (89) still not completely accounted for, but all or nearly all of them are peaks that occur more abundantly in the spectra of chlorine compounds than elsewhere, and they seem to represent a background of numerous chlorine derivatives present only in very small traces.

Conclusions regarding sample D–6 are summarized in tables 4 and 5.

The relative sensitivities of compounds are usually given in the tables of their patterns, hence relative concentrations of the identified chemical compounds need not be much in doubt. They are shown for sample D–6 in table 5. It is a major weakness of the method of analysis that no definite sensitivity can yet be assigned to the patterns of traffic gas and gasoline, and this makes it impossible to determine with accuracy even the relative mole fractions of these mixtures and of the individually identified compounds. In preparing table 5, it was assumed that the 13.74 percent of the ion current carried by "identified" compounds represented a 20 mole percent of the sample, and that the remaining 86.26 percent of the ion current represented an 80 mole percent of traffic gas and gasoline. It follows that for the traffic gas and gasoline BC=1.08; that is, unit volumes of their mixture contribute as much to the ion current in the spectrometer as 1.08 volumes of butane.

TABLE 4. *Interpretation of Louisville sample D–6*

General fractions:			*Mole percent*
Traffic gas			30.00
Gasoline vapor			50.00
Identified compounds	Principal identifying peak	Peak height, % of total spectrum	
One-ring aromatic hydrocarbons:			
Above C_8H_{10}	105	None	None
Xylene, C_8H_{10}[a]	106	Trace	Trace
Toluene, C_7H_8	92	0.109	0.17
Benzene, C_6H_6	78	.223	.23
Terpenes	93	None	None
Styrene, C_8H_8	104	None	None
Carbon tetrachloride, CCl_4	117	None	None
Trichloroethylene, C_2HCl_3	130	None	None
Chloroprene, C_4H_5Cl	88	0.665	3.71
1,3-Butadiene, C_4H_6	54	.298	0.74
Acrylonitrile, C_3H_3N	53	.051	.16
Vinyl acetylene, C_4H_4	52	.423	.66
Vinylchloride, C_2H_3Cl	62	.095	.25
Dichloroethylene, $C_2H_2Cl_2$	61	.151	.29
Acetylene, C_2H_2	26	6.79	10.31
Ethanol, C_2H_6O	31	1.32	2.43
Sulfur dioxide, SO_2[b]	48	0.106	0.67
Hydrogen chloride, HCl[b]	36	.141	.38
Chlorine, Cl_2[b]	35	.156	———

[a] Includes ethyl benzene.

[b] Not quantitatively significant of concentration in the original atmosphere because a large fraction is lost with the carbon dioxide. Chlorine and sulfur dioxide are entirely incompatible in aqueous solution and their coexistance in the sample to the point of introduction into the spectrometer is in some doubt. Although chlorine and hydrogen chloride were on the list of pollutants discharged into the air by industrial plants, it is also uncertain that (35) and (36) represent these two gases rather than unidentified organic compounds containing chlorine.

TABLE 5. *Approximate concentrations of identified compounds in Louisville sample D–6*

Column A—Height of identifying peak (% of total ion current).
Column B—Ratio of sensitivity of identifying peak to base peak.
Column C—Ratio of sensitivity of base peak to base peak of butane.
Column D—A number proportional to mole fraction of identified compound=A/BC.
Column E—Mole fraction of pollutant if identified compounds are assumed to aggregate 20%.

Compound	A	B	C	D	E
Toluene	0.109	0.77	1.17	0.12	0.17
Benzene	.223	1.00	1.36	.16	.23
Chloroprene	.665	1.00	0.26	2.55	3.71
1,3-Butadiene	.298	0.88	.67	0.51	0.74
Acrylonitrile	.051	.90	.50	.11	.16
Vinyl acetylene	.423	1.00	.95	.45	.66
Vinyl chloride	.095	0.76	.74	.17	.25
Dichloroethylene	.151	1.00	.74	.20	.29
Acetylene, total	6.79	1.00	.96	7.08	10.31
(from industrial sources)					
Ethanol, total	1.32	1.00	.79	1.67	2.43
(from industrial sources)					1.34
Sulfur dioxide	0.106	0.49	.47	0.46	[a] 0.67
Hydrogen chloride	.141	1.00	.54	.26	[a] .38
Chlorine	.117	----	----	----	----
			Total	13.74	20.00

[a] Not quantitatively significant for the reason stated in footnote (b) of table 4.

11. Louisville Sample ST–1

Other samples from Louisville can be reported in much less detail. Several of them present points of special interest, however.

Sample ST–1 was taken from 9 to 10 p. m. in the West End of Louisville at a time of very little air movement, the direction of which was not definitely determined. The ratios plotted for other samples in figure 4 and often used in judging the percentage of change from NTG to Ref, were all lower than for NTG itself. This, and the fact that the sample was taken after sunset combine to make any previous photochemical reaction in the atmosphere improbable. From a comparison of a plot of the sample with one of NTG, it was estimated that 85 percent of the sample was traffic gas, but as the interpretation of the spectrum progressed this estimate was changed to 75 percent.

The procedure illustrated in figure 4 was followed. The spectrum of the sample was plotted in the order of its own peak heights and initially compared with the sum of NTG and the aromatic hydrocarbons indicated by their parent peaks. Among the peaks prominent as "unaccounted for" at this stage were (93), (94), (107), and (108) which were thought to represent phenolic compounds; (47), (49), and several other pairs of peaks two mass units apart, interpreted to represent chlorine compounds; and (55), (56), (69), (70), and others that seemed to represent a concentration of olefin or naphthene compounds much too great to be explained by traffic gas.

It appeared probable that the prominent (108) and (93) peaks should be attributed to cresol, $CH_3C_6H_4OH$. No pattern was available until a sample of commercial "Cresol, U. S. P." was run to provide one. This gave a spectrum containing some ions too heavy for pure cresol and much more (94) than seemed likely to be formed in quantity from a compound with a parent mass of (108). It was, therefore, decided to take out the pattern of phenol from that of the Cresol, U. S. P. and to consider the remainder to be the pattern of everything in cresol heavier than phenol. Phenol and cresol, based on (94) and (108), were then taken out of the spectrum of the sample. There still remained a large (93) to be accounted for. Terpenes, in particular the pinenes, seemed to offer the only patterns that would account for (93) without large deficits in other peaks, and the (93) was accordingly attributed to pinene.

Two other easily recognizable but complex groups of compounds were obviously present: (1) Chlorine derivatives and (2) unsaturated hydrocarbons, apparently mostly of the olefin series, but with some acetylene or diene members. These were clearly not from the same sources in Rubbertown that supplied the chief pollutants of sample D–6; for example, chloroprene was present only as a trace, if at all, and there was no evidence of acrylonitrile, vinyl compounds, or of gasoline in excess of that to be attributed to traffic gas.

The possible number of compounds that might have been constituents of either the chlorinated or the unsaturated groups of pollutants is many times greater than the number of peaks available for their identification; a complete analysis in terms of individual chemical compounds is accordingly out of the question, just as is that of the hydrocarbons of traffic gas. However, some of the constituents are almost certainly identifiable, and the general nature of the two groups seems fairly certain to be that indicated in table 6, both in chemical character, and approximate molecular weight.

The actual order of taking out the various substances was as follows: Cresol, phenol, C_9H_{12}, and other aromatic hydrocarbons heavier than xylene, C_8H_{10} representing the xylenes and ethylbenzene, styrene, toluene, benzene, NTG, a mixture of alpha- and beta-pinene in equal proportions, ethanol, dichloroethylene, dichloromethane, methyl chloride, trichloromethane, dichloroethane, dichloropropane, 3-methyl-1-pentene, 3-hexyne, *cis*-2-pentene, and finally isohexane (2-methyl pentane). After the last of the unsaturated hydrocarbons had been taken out, there remained prominent peaks at (86) and (71) in a ratio that corresponds to isohexane, which was then taken out. To have attributed (86) and (71) to gasoline vapor of the composition assumed in the case of sample D–6 would have produced serious deficits in other peaks, particularly (72). Several other possibilities were considered but led to similar difficulties. It seemed most likely, therefore, that there existed some source of fairly isolated isohexane, perhaps used as an intermediate in chemical manufacture or as a solvent.

TABLE 6. *Interpretation of spectrum of Louisville sample ST–1*

Substance	Principal identifying peak	Peak height, % of total spectrum	Mole fraction %
Normal traffic gas	.....	.....	75
Phenolic compounds:			
Cresol, C_7H_8O	108	0.552	1.84
Phenol, C_6H_6O	94	.151	0.66
One-ring aromatic hydrocarbons:			
Above, C_9H_{10}	105	.973	.97
Xylenes, C_8H_{10} and ethyl benzene	106	.369	.67
Toluene, C_7H_8	92	1.68	2.95
Benzene, C_6H_6	78	1.79	1.32
Styrene, C_8H_8	104	0.030	0.027
Terpenes:			
Pinenes, $C_{10}H_{16}$	93	.801	.78
Unsaturated hydrocarbons not accounted for by NTG:			
3-Methyl-1-pentene, C_6H_{12}	84	.460	1.80
3-Hexyne, C_6H_{10}	82	.336	0.61
cis-1-2-Pentene, C_5H_{10}	70	.500	1.67
Isohexane, C_6H_{14}	71	.500	1.20
Ethanol, C_2H_5OH	31	1.92	2.94
Aliphatic chlorine compounds:			
Methyl chloride, CH_3Cl	50	0.40	0.76
Dichloromethane, CH_2Cl_2	49	.250	.42
Chloroform, $CHCl_3$	93	.281	1.23
Dichloroethane, $C_2H_4Cl_2$	62	.303	0.51
Dichloropropane, $C_3H_6Cl_2$	111	.126	.13
Dichloroethylene, $C_2H_2Cl_2$	61	.10	.14

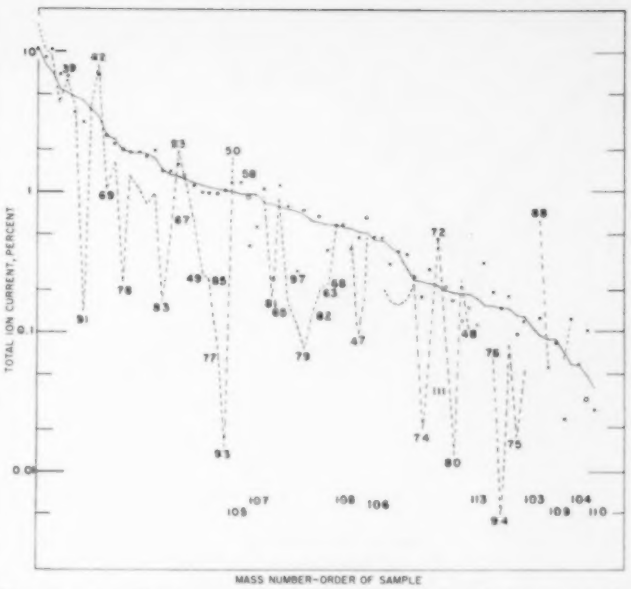

FIGURE 9. *Total contribution of identified substances to the spectrum of Louisville sample ST–1.*

....., Accounted for; ○ ....., sample D–6–Fo; ————, sample S T–1

Other residuals are either too small to be of probable significance, are of uncertain origin, or are probable fragments of parent molecules too heavy to have been included in the recorded spectrum. Thus (58) may represent propionaldehyde, acetone, or unaccounted for butane; (81) is probably a fragment of an unidentified diene or acetylene derivative with a molecular weight of (96) or more; and (95) and (97) are probably derived largely from unidentified chlorine compounds with at least 2 carbon and 3 or more chlorine atoms.

Figure 9 shows the degree of agreement reached in accounting for the sample, in this case by the relation of solid dots to the unbroken line. As a matter of interest, a broken line was added to show the spectrum of D–6 plotted in the same order. The large differences between these two samples is in striking contrast to the generally close agreement among southern California samples, illustrated in figure 3. The numbers above the solid line identify peaks much higher in D–6 than in ST–1, those below the line those that were much lower. Numbers below breaks in the dotted curve represent mass numbers not reported in sample D–6. It is probable that the small peaks attributed to fragments of unidentified chlorine compounds in D–6 came from the same general source as the aliphatic halogen derivatives in ST–1 during a brief shift of wind direction.

12. Analysis of Louisville Sample X–1

Sample X–1 (fig. 10) shows several points of interest. Whereas the major hydrocarbons' pattern of ST–1 is well accounted for by normal traffic gas,

FIGURE 10. *Total contribution of identified substances to the spectrum of Louisville sampe X–1.*

————, Sample; . . . . . , accounted for.

and that of D–6 indicates the presence of a major amount of raw gasoline vapor, the pattern of X–1 is best accounted for by the use of Ref and the assumption that oxidation of traffic gas had proceeded nearly as far as in the Los Angeles smogs. The analysis was eventually based on the assumption that the sample was two-thirds traffic gas which had undergone a 75 percent conversion to Ref.

Industrial impurities included the group of pollutants, in sample D–6, attributed to Rubbertown, ethyl alcohol, and a definite though not large portion of phenol and cresol, presumably from the same source as the same compounds in ST–1. The amount of (93) unaccounted for by toluene, phenol, and cresol was negligibly small and much less in proportion to these compounds than in ST–1. This may indicate that the terpenes in ST–1 were from a source other than that of the cresol, although it was at first assumed that they represented effluents from the same plant. Evidence of either the numerous group of chlorinated aliphatic compounds or the olefins in ST–1 is lacking in X–1.

Table 7 lists the compounds identified in X–1. Both normal butane and normal pentane are undoubtedly constituents of Ref. Their inclusion in the accounting as additional to the usual pattern of Ref is an accounting device and does not necessarily indicate that they were isolated pollutants. They may indicate some admixture of gasoline vapor from the same source as that in D–6 but not distinguishable as such, and the evidence of butane could be almost as well interpreted as acetone. However, a strong indication of butane occurs in several Louisville samples, and it may be an industrial pollutant distinct from gasoline. The identifications of carbon disulfide, fluorotrichloromethane (Freon 11), tertiary-butyl alcohol, and pentyl benzene are based each on a single peak and may be

TABLE 7. *Interpretation of Louisville sample X–1*

Substance	Principal identifying peak	Peak height, % of total spectrum	Mole fraction or %
NTG	.....	.....	16
Ref	.....	.....	50
Pentyl benzene, $C_{11}H_{16}$	148	0.073	0.45
C_9H_{12}	120	.018	.06
Xylene, C_8H_{10}	106	.291	.73
Toluene, C_7H_8	92	.304	.55
Benzene, C_6H_6	78	2.19	3.02
Cresol, $CH_3C_6H_4OH$	108	0.053	0.08
Phenol, C_6H_5OH	94	.080	.11
Styrene, C_8H_8	104	.015	.02
Chloroprene, C_4H_5Cl	88	.031	.06
Vinyl chloride, C_2H_3Cl	62	3.164	8.51
1,3-Butadiene, C_4H_6	54	0.408	1.76
Acrylonitrile, C_3H_3N	53	.267	0.91
Normal pentane, C_5H_{12}	72	.078	.12
Normal butane, C_4H_{10}	43	2.502	3.80
Ethyl alcohol, C_2H_5OH	31	1.309	2.24
Acetylene, C_2H_2	26	5.142	10.70
Carbon disulfide, CS_2	76	0.125	0.13
Fluorotrichloromethane, $CFCl_3$	103	.013	.03
Tertiary butyl alcohol, C_4H_9OH	59	.073	.14

in error. The first three are products commonly used in chemical industry, and their occurrence in detectable amounts seemed more probable than that of other compounds found to have patterns that could be fitted readily into the picture. No pattern was available for pentylbenzene, and its assignment was based on the following facts: (1) There was a small but significant peak at (148) but none were observed at (133) or (119); (2) mass (148) is one of the series of parent peaks of benzene rings with paraffin side chains, with which there is usually very little interference from other compounds; (3) from the parent molecular weight, there must be five side-chain carbons; (4) an inspection of the patterns of other benzene-paraffin hydrocarbons shows that they tend to fragment by breaking away alkyl groups. They are prone especially to lose the alkyl group or, in the case of toluene, hydrogen from the carbon attached to the benzene ring; (5) if a methyl group were attached to the ring we should expect a major peak at (133), if ethyl, at (119). The absence of both these peaks indicates that the side chain must be pentyl; (6) the (91) peak which we should expect to be the most prominent in the case of the pentyl benzene is not otherwise fully accounted for. Sensitivity was estimated from sensitivities of the parent peaks of other aromatic hydrocarbons.

Peaks that are significantly over-accounted for again contain a disproportionate number that are attributable to cycloparaffins in the traffic gas patterns. The excess of peak (40), which includes argon based on oxygen in the sample, may have been affected by the initial liquefaction of a small amount of oxygen when the sample was taken. Among the ions not completely accounted for, (49) and (50) are prominent. This is of interest because the same two peaks appear prominently in the unaccounted-for portions of several Louisville samples. They suggest the presence of biacetylene, C_4H_4, but this is a relatively rare compound that would not be expected to appear in significant amount.

13. Other Louisville Samples

Several other samples taken in different parts of Louisville during a period of clear weather with little wind are summarized in table 8, and the result of the final accounting is presented in figures 11 to 15.

Sample G–1, figure 11, was very largely traffic gas, apparently a little less than half oxidized, with the addition of a rather large amount of acetylene. Although the aromatics and alcohol were reported separately because their determination is independent of traffic gas, they were less than are usually found in traffic gas. The only evidence of pollution from Rubbertown consisted of traces of vinyl chloride and dichloroethylene such as might have been carried by an atmospheric swirl of short duration. Of the peaks not fully accounted for, (49) and (50) were again the most prominent, and cycloparaffins as indicated by peaks (69), (70), (83), (84), (97), (98), (111), and (112) were again overaccounted for. Difluorodichloromethane was introduced into the sample during laboratory operations and will not be mentioned in the discussion of other samples in which it occurred; but the small amount of carbon tetrachloride is believed to have been from a Louisville source. The sample, on the whole, was a typical traffic gas almost free of industrial contamination.

Sample G–2, figure 12 was almost like G–1. The sample was traffic gas apparently about one-eighth oxidized and entirely without evidence of industrial pollution, if we except a small amount of tetrachloroethylene and the unidentified constituent represented by peaks (49) and (50). To permit a comparison of some constituents computed directly from the spectrum of G–2 and independently from the patterns used for traffic gas, the latter have been marked with X at masses (78), (92), (106), and (31), masses which are usually significant of benzene, toluene, xylene, and alcohol, respectively.

Sample G–3, figure 13, was again traffic gas only slightly oxidized and free of the usual industrial contamination of the city, but strongly polluted with carbon tetrachloride and a little chloroform. Peaks (49) and (50) were again high, though not much so, and (59), attributed to tertiary butyl alcohol in sample X–1, was again prominent.

The traffic gas of G–5, figure 14, was about 40 percent oxidized. There was evidence of industrial pollution and on the basis of previous samples, it was thought to come from at least four separate sources. The industrial pollutants identified were cresol, phenol, chloroprene, carbon tetrachloride, and dichloromethane. Acetylene and alcohol were not in excess of the usual content amount in traffic gas.

Sample G–6, figure 15, appeared to have a base of about 40 percent of completely oxidized traffic gas (Ref), and 15 percent of gasoline vapor. It contained small amounts of the Rubbertown pollutants, chloroprene, butadiene, acrylonitrile, and acetylene, less of cresol, phenol, and pinene. There were methyl chloride, carbon tetrachloride, tetrachloroethylene, and some evidence of carbon disulfide. There was less benzene, toluene, and alcohol than expected from traffic gas. The listed paraffins,

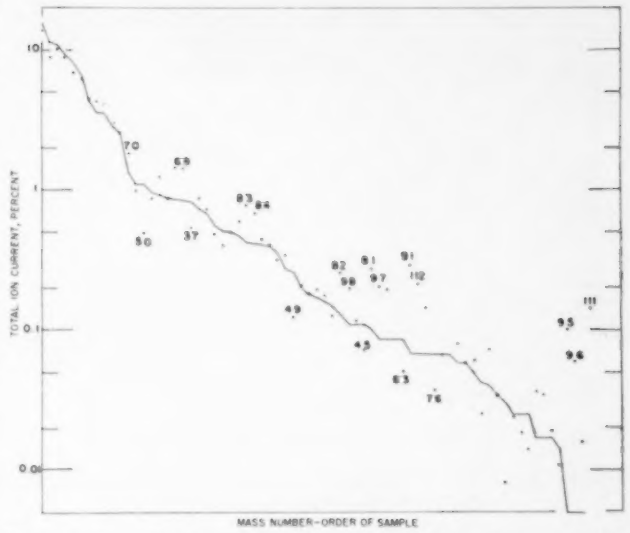

FIGURE 11. *Total contribution of identified substances to the spectrum of Louisville sample G1–L.*

———, Sample; . . . . . , accounted for.

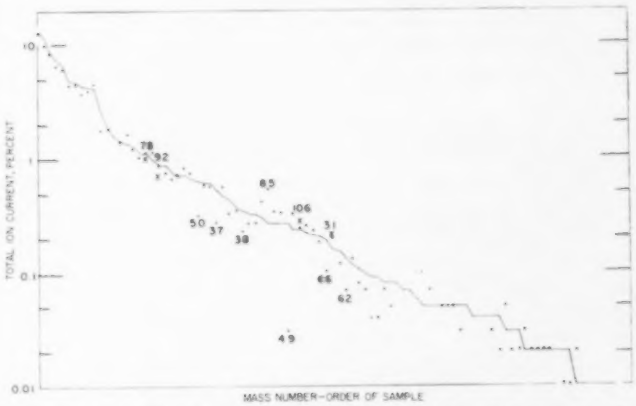

FIGURE 12. *Total contribution of identified substances to the spectrum of Louisville sample G2–L.*

———, Sample; . . . . . , accounted for; ×, accounted for by NTG only.

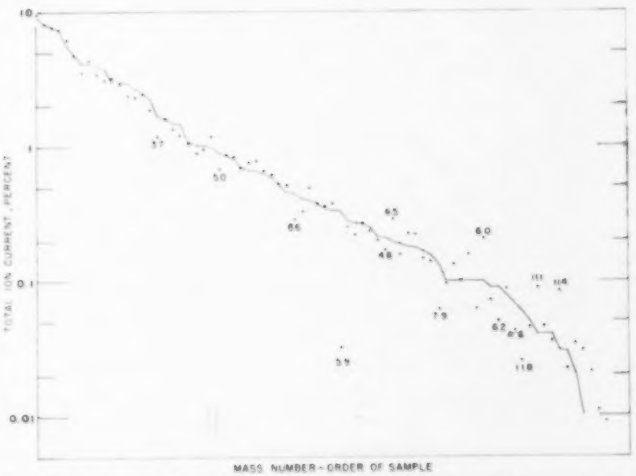

FIGURE 13. *Total contribution of identified substances to the spectrum of Louisville sample G3.*

———, Sample; . . . . . , accounted for.

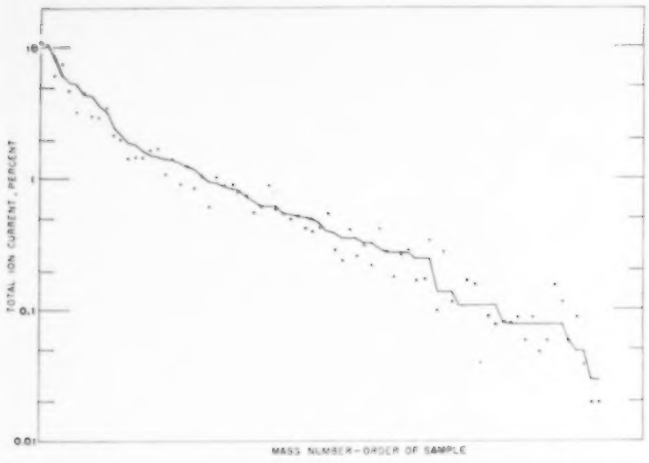

FIGURE 14. *Total contribution of identified substances to the spectrum of Louisville sample G5.*

———, Sample; . . . . . , accounted for.

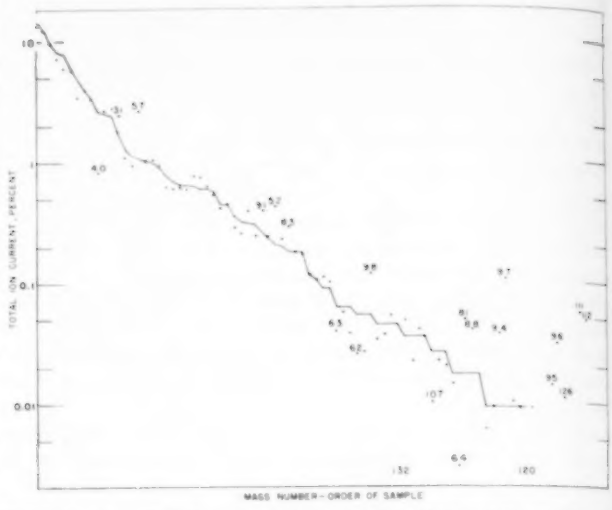

FIGURE 15. *Total contribution of identified substances to the spectrum of Louisville sample G6.*

———, Sample; . . . . . , accounted for.

TABLE 8. *Interpretation of condensed pollutants from Louisville*

(Corrected for difluorodichloromethane)

Sample	Mole fraction x100							
	D-6	ST-1	X-1	G-1	G-2	G-3	G-5	G-6
Traffic gas:								
NTG	30	75	16	48	75	65	50	------
Ref	------	------	50	34	10	22	20	53
Gasoline vapor [a]	50	------	------	------	------	------	------	31
Paraffin hydrocarbons: [b]								
Normal butane	------	------	3.80	------	------	------	------	------
Isobutane	------	------	------	------	------	------	------	2.3
Normal pentane	------	------	0.12	------	------	------	------	1.2
Isohexane	------	1.2	------	------	------	------	------	1.3
Olefins: [b]								
cis-2-Pentene	------	1.67	------	------	------	------	------	1.1
1-Hexene	------	1.21	------	------	------	------	------	------
3-Methyl-1-pentene	------	1.80	------	------	------	------	------	0.7
Other aliphatic hydrocarbons:								
Acetylene [c]	10.31	(e)	10.70	15.4	11.0	2.1	0.6	3.1
3-Hexyne	------	0.61	------	------	------	------	------	0.64
1,3-Butadiene [b]	0.74	------	1.76	------	------	------	------	.17
Vinyl acetylene	.66	------	------	------	------	------	------	------
Benzene homologs: [a]								
Benzene	.23	1.32	3.02	1.2	1.8	0.66	1.23	.31
Toluene	.17	2.95	0.55	0.03	1.6	.66	1.38	.02
Xylene and ethyl benzene	------	0.67	.73	------	0.9	.17	0.43	------
Above C_8H_{10}	------	.97	------	.12	------	.13	.25	------
C_9H_{12}	------	------	.06	------	.2	------	------	------
Above C_9H_{12}	------	------	------	------	------	------	------	------
$C_{11}H_{16}$	------	------	.45	------	------	------	------	------
Other hydrocarbons:								
Styrene	------	.03	.02	------	------	------	------	------
Pinenes	------	.78	------	------	------	------	------	------
Phenols:								
Phenol	------	.66	.11	------	------	------	4.84	.02
Cresol	------	1.84	.08	------	------	------	9.40	.02
Chlorine derivatives:								
Methyl chloride	------	0.76	------	------	------	------	------	1.2
Dichloromethane	------	.42	------	------	------	------	3.94	------
Chloroform	------	1.23	------	------	------	1.92	------	------
Carbon tetrachloride	------	------	------	.2	------	11.10	0.19	0.17
Dichloroethane	------	0.51	------	.2	------	------	------	.51
Dichloropropane	------	.13	------	------	------	------	------	.13
Vinyl chloride	.25	------	8.51	.09	------	------	------	------
Dichloroethylene	.29	.14	------	.2	------	------	------	------
Tetrachloroethylene	------	------	------	------	1.1	------	------	.07
Chloroprene	3.71	------	0.06	------	------	------	11.4	------
Difluorodichloromethane [d]	------	------	------	4.06	20.0	2.25	22.4	10.9
Fluorotrichloromethane	------	.03	------	------	------	------	------	------
Acrylonitrile	0.16	------	.91	------	------	------	------	0.21
Ethyl alcohol [e]	2.43	2.94	2.24	0.24	0.44	0.51	0.54	.45
Tertiary butyl alcohol	------	------	0.14	------	------	------	------	------
Carbon disulfide	------	------	.13	------	------	------	------	.05
Approximate total pollutant in atmosphere, ppm [f]	------	------	------	.31	.73	.47	1.0	.18

[a] In addition to gasoline represented by patterns of NTG and Ref.
[b] In addition to any of compound represented in patterns of NTG, Ref, and average gasoline.
[c] Total of compound in sample.
[d] Laboratory contamination, not included in computed percentages.
[e] Acetylene from this sample lost in pretreatment of sample.
[f] These values calculated from measured pressure of the total condensate.

normal butane and 2-methyl-pentane, were more likely a portion of the gasoline vapor than relatively pure materials from other sources. Their appearance in the accounting probably results from the fact that the pattern of Los Angeles gasoline was derived from completely vaporized fuels of somewhat different general composition. Vapors from stored gasoline must contain a higher fraction of the lower-boiling constituents, and pentane and hexane are underestimated when the regular gasoline pattern is used. There is some evidence of additional olefins, accounted for as isobutene and 1-hexene. They may have been a part of the gasoline vapor, but they may also have come from the same sources that provided the olefins in sample ST–1 that could not be attributed to gasoline. Of the over-accounted-for peaks in this sample, (83), (98), (97), (111), (112), and (126) are evidence of the cycloparaffins in the Los Angeles gasoline pattern; and (81), (94), (95), and (96) are also accounted for entirely by the patterns of gasoline and Ref used. The spectrum actually obtained showed a large quantity of dichlorodifluoromethane which was probably introduced in the laboratory and was, therefore, taken out of the spectrum in advance of the accounting represented by table 8 and figure 15. The Freon was based on the total (87), part of which must have come from something else, for there was not enough (31) and (88) to complete the pattern.

14. Pasadena Sample S–23

Among the many old spectra of samples from Southern California, one was of special interest because it was taken during a period of what appeared to be, from the vague description available, one of severe smog; but from a formula based on ratios of certain peaks (see fig. 4), the percent oxidized was only 49.6. Even if the concentration of pollutant was unusually high, a relatively slight effect would have been anticipated from the extent of its oxidation.

The problem was attacked by taking out from the spectrum the pattern of an equal mixture of Ref and NTG, followed by the separation of individual compounds. It was soon evident that the peaks relatively high in NTG were being "over-accounted for." In effect, the procedure from then on was one of trial and error that resulted in the interpretation shown in table 9 and represented by figure 16. Table 9 indicates relative concentration only in terms of the percent of total ion current occurring at the principal identifying peak. From this it appears that the sample consisted of traffic gas about 90 percent oxidized to Ref, some aromatic hydrocarbons heavier than benzene, a complex group of cycloparaffins in much greater proportion than is usual even in Southern California, and a number of substances too varied and in too small quantity for identification. Although the cycloparaffins are represented in the table by a half dozen compounds that have a combined spectrum substantially like that of the otherwise unaccounted for residue, it is not to be supposed that they are the only cycloparaffins present. Residues of (125) and (126) probably represent cycloparaffins that could not be fitted by known

TABLE 9. *Interpretation of Pasadena smog No. S–23*

Substance	Principal identifying peak	Peak height, % of total spectrum
Aromatic hydrocarbons:		
$C_{11}H_{16}$	133	0.005
$C_{10}H_{14}$	134	.045
C_9H_{12}	120	.061
C_8H_{10}	106	.331
C_7H_8	92	.912
C_6H_6	78	1.094
Tetrachloroethylene, C_2Cl_4	129	0.012
Trichloroethylene, C_2HCl_3	130	.124
Carbon tetrachloride, CCl_4	117	.058
Acetylene, C_2H_2	25	.906
Ethanol, C_2H_5OH	31	.244
Cycloparaffins:		
$C_{10}H_{20}$	140	.028
C_9H_{18}	111	.326
C_8H_{16}	112	.154
C_7H_{14}	98	.129
C_6H_{12}	97	.068
C_5H_{10}	70	.839
NTG 10%	----------	----------
Ref 75%	----------	----------

patterns without an excess of lower masses. The catalogs of spectra contain patterns of more than 50 cycloparaffins in the range of molecular weight involved, and a much larger number is possible. The chlorine compounds, alcohol, acetylene, and benzene are present in about their usual proportions in the atmosphere of the region.

It seems probable that the heavy aromatics and the cycloparaffins that distinguish this sample came from a common source that may have been crude oil or a heavy petroleum residue. Because this was a unique sample among many from the same location, it is suggested that a job of paving or road oiling may have been in progress in the neighborhood when the sample was taken. The numerous small unaccounted for residues probably represent slight pollution from varied industrial or domestic sources, including waste disposal.

15. Detroit Sample No. 5

A sample taken in Detroit during a period of smog is interpreted so far as seemed practicable in table 10 and figure 17. The plot, arranged in the order of descending peak heights of the sample, shows excellent agreement with a mixture of 60 percent of NTG and 40 percent of Ref down to a peak height of about 0.1 percent of the total ion current. Beyond that, there are nearly 50 small peaks that are in major part unaccounted for. They indicate a very complicated mixture of pollutants, none of which can be present to the extent of more than a few tenths of 1 percent of the total condensate. In this, they resemble the less numerous unaccounted for residues of Pasadena sample S–23 previously discussed. In the figure the points representing the accounted for portion of these peaks have been labeled, and ions not accounted for at all are indicated by numbers near the bottom of the figure.

The amount of benzene present is a little less than that normally found in traffic gas; toluene is nearly normal, but all the other aromatics much above normal. Alcohol and acetylene are each a little

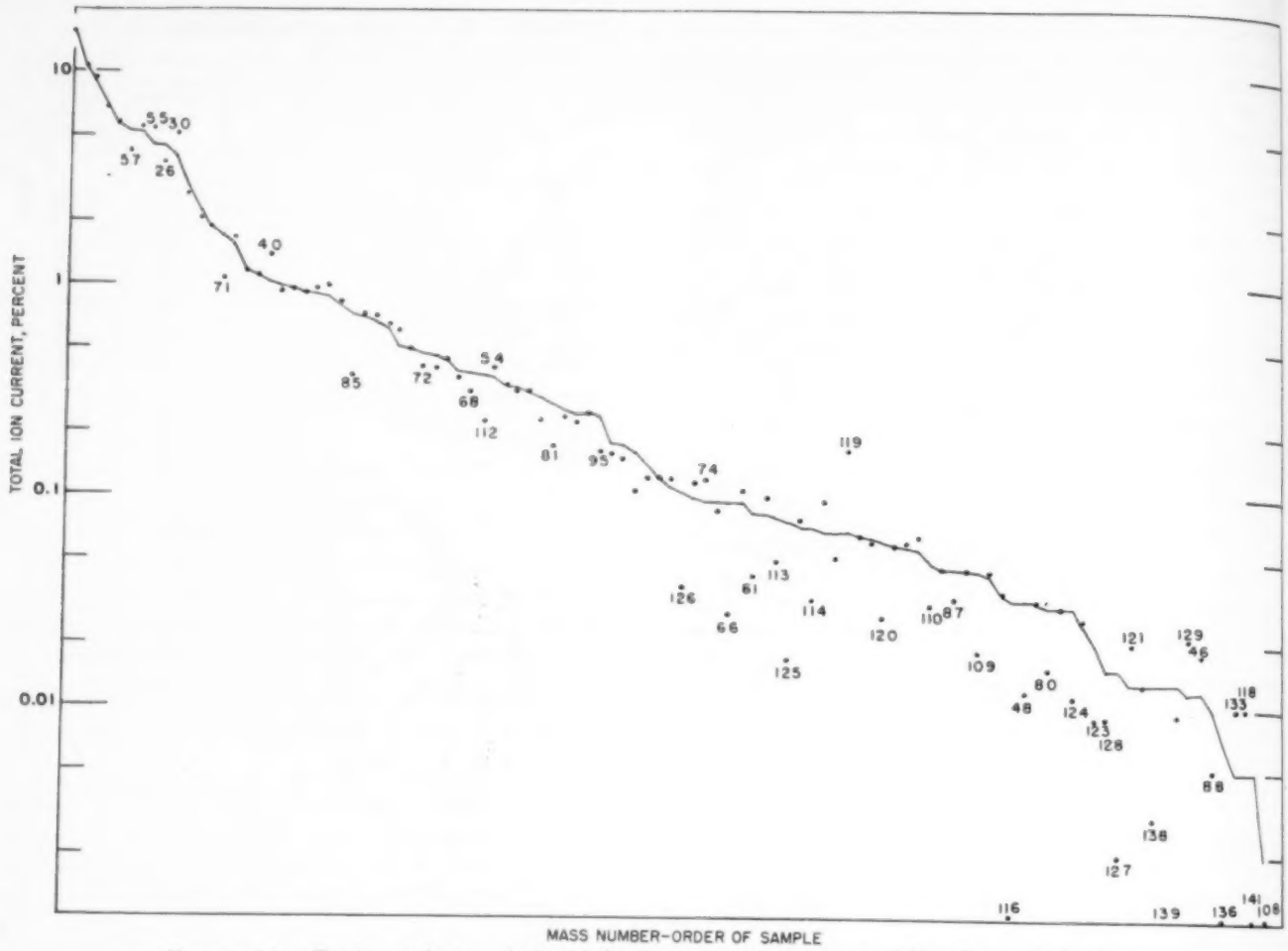

FIGURE 16. *Total contribution of identified substances to the spectrum of Pasadena sample S–23.*
————, Sample; ....., accounted for.

TABLE 10. *Composition of Detroit smog No. 5*

Substance	Principal identifying peak	Peak height, % of total spectrum
Aromatic hydrocarbons:		
$C_{12}H_{18}$	147	0.021
$C_{11}H_{16}$	148	.009
$C_{10}H_{14}$	134	.058
C_9H_{12}	120	.024
C_8H_{10}	106	.437
C_7H_8	92	.499
C_6H_6	78	.629
Carbon tetrachloride, CCl_4	117	.052
Ethanol, C_2H_5OH	31	1.107
Acetylene, C_2H_2	25	0.647
NTG 57%	.....	.....
Ref 38%	.....	.....

less than would be expected for traffic gas. Butadiene appears from (53) and (54) to be about normal for traffic gas, but compounds with six or more carbon atoms and with two double or one triple bond appear in unusual quantity and are indicated by underscored (81), (82), (95), (96), (109), (123), (124), (137), and (138). Identifying connections have not been established between the many small peaks of high mass and their fragments have not been identified among the traffic gases. It is hence impossible to say with certainty what they represent. A reasonable guess can be made at some of them, however, on the ground that some compounds are more commonly used or more volatile than others. For the first reason, (58) is more likely to represent acetone or butane than acetaldehyde, and for both reasons, (116) is more probably from an ester than from an acid or alcohol. Butyl acetate, of parent mass (116), is a widely used solvent in plastic and lacquer industries. As in Louisville, peak (111), which seems always to be the most prominent peak of the cycloparaffins when heights are plotted logarithmically, is more than accounted for by traffic gas alone.

16. Cincinnati Samples

Two samples taken in Cincinnati during a period of high barometric pressure, were found to be unique among urban air samples in that they consisted basically of halogen compounds instead of hydrocarbons. One sample is represented by table 11 and figure 18. Hardly more than trace amounts of cresol and phenol were recognized, and no more than the normal amounts of the individually determinable

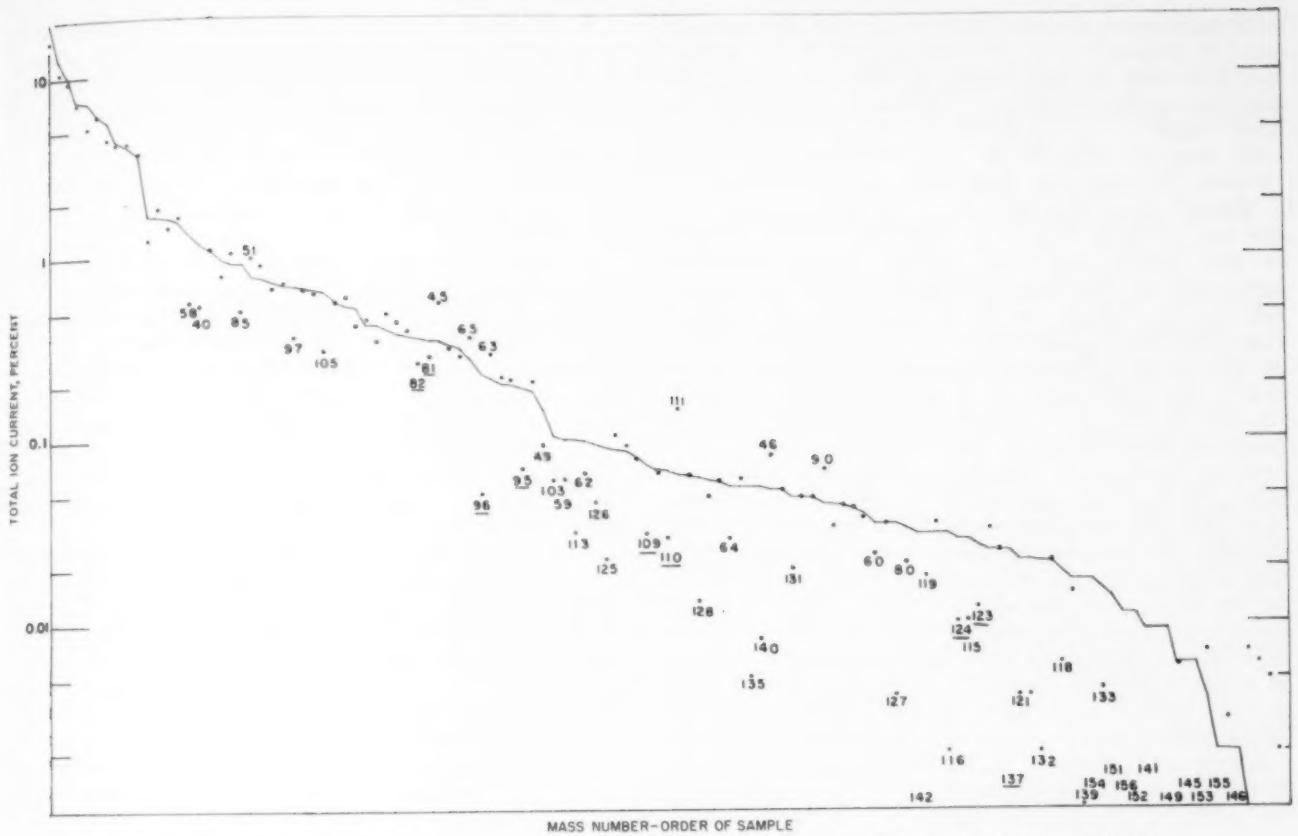

FIGURE 17. *Total contribution of identified substances to the spectrum of Detroit sample, Smog No. 5.*
———, Sample; ....., accounted for.

TABLE 11. *Composition of Cincinnati smog No. 1*

Substance	Principal identifying peak	Peak height, % of total spectrum
Tetrachloroethylene, C_2Cl_4	166	0.07
Carbon tetrachloride, CCl_4	117	16.46
Chloroform, $CHCl_3$	83	4.92
Freon-12, CCl_2F_2	87	1.23
Cresol, C_7H_8O	108	0.02
Phenol, C_6H_6O	94	.04
Toluene, C_7H_8	92	.04
Benzene, C_6H_6	78	1.91
Tertiary butyl alcohol, $C_4H_{10}O$	59	0.56
Acetylene, C_2H_2	25	.31
Ref 20%	----	----

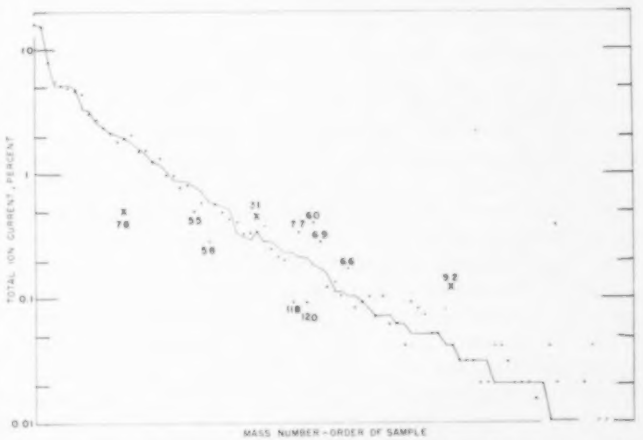

FIGURE 18. *Total contribution of identified substances to the spectrum of Cincinnati Smog No. 1.*
———, Sample; ....., accounted for; ×, accounted for by traffic gas.

constituents of traffic gas, aromatics, acetylene, and alcohol. As in Detroit, there were numerous but very small unidentified peaks that indicated slight and extremely varied industrial pollution not closely enough related to suggest a common source.

In addition to the difluorodichloromethane believed to have been introduced at the time of analysis, the samples contained carbon tetrachloride, chloroform, tetrachloroethylene, and fluorotrichloromethane. The source of the halogen compounds and its relation to the sampling point is unknown, but it is incredible that halogen derivatives in such quantity can be widespread in the city. A point of general interest is that the portions of the sample attributed to traffic gas were of the approximate composition of Ref in one sample and at least half Ref in the other. As in Louisville and Detroit, it was evident that the traffic gases had a smaller cycloparaffin content than the traffic gases of Los Angeles and Washington.

17. Summary and Conclusions

The composition of the condensate, at liquid oxygen temperature, from any urban atmosphere is too complex for resolution into its individual components; but by considering pollutants from each of

various sources as substantially constant in composition, it is possible to identify many of the sources and to determine approximately how much each has contributed to the total. This method of study has been applied to condensates from seven cities: Los Angeles, Pasadena, and Wilmington, Calif.; Detroit, Washington, Louisville, and Cincinnati.

The samples from the California cities were numerous and enough alike to be treated, for the purpose of this paper, together. When minor variations have been allowed for, substantially all the samples fall readily into a series of mixtures of regularly changing composition that could be regarded either as blends in different proportions of two basic and nearly uniform mixtures, or as various stages in the transformation of one basic mixture by chemical reactions into another. At one end of the range of composition found in Southern California is a sample taken from a highway tunnel in which it is probable that the pollutant was nearly all from moving automobiles, and at the other end are samples, very much alike, taken at different places during periods of severe smog. If we assume that mixtures of the second type are derived from the first by chemical reactions, it is evident that they are not end products of those reactions, but are the result of an approximately steady state that is approached while the initial substances are regularly poured into a steadily reacting mixture. As a matter of convenience the first stage is referred to as "normal" and the second as "oxidized" traffic gas without implying that these terms tell the whole story. The term "traffic gas" is intended to include engine exhaust gases and the amount of gasoline vaporized in the ordinary handling and use of the fuel.

Condensates from the atmospheres of eastern cities reveal basic pollution, very much like that of southern California, in which variations in the proportions between normal and oxidized traffic gas are clearly discernible. With these traffic gases, which are of substantially constant but virtually unknown chemical composition, a variety of other pollutants occur in relatively small amount. These minor pollutants usually come from local industrial sources. Typical mass-spectral patterns have been selected for the initial and final stages of traffic gas, and when these are taken out of the spectra of condensates under study, the principal pollutants not attributable to automobile traffic are much more easily recognized and determined.

From the studies so far made by this method the following conclusions may be drawn:

1. The pollutants in the air of Washington, D. C., which has almost no chemical industry and in the summer no obvious source of appreciable pollution except traffic gases, resemble the pollutants of Los Angeles very closely. However, the traffic gases are seldom or never in an advanced state of oxidation.

2. As a corollary, we may conclude that industrial pollution in the Los Angeles area is minor or that it is of a character, a mixture of fuel vapors and products of combustion, not readily distinguishable from traffic gas.

3. A group of mass peaks, believed to represent cycloparaffin compounds, is much more prominent in California and Washington traffic gases than in those of Louisville, Detroit, and Cincinnati. This is attributed to the derivation of the motor fuels on the coasts and in the interior from petroleums of different types. With this exception, no general distinction has appeared between traffic gases in various places.

4. Some compounds that occur in all traffic gases have identifying peaks that are relatively free of interference by other compounds ordinarily encountered. They include benzene and toluene as individual compounds, and heavier aromatic hydrocarbons as groups of the same molecular weight, acetylene, and ethyl alcohol. They are determined and taken out of the spectrum of a sample as individual compounds, not as part of traffic gas. Concentrations much greater than normal for traffic gases are noticeable and are attributed to other sources.

5. In contrast to the uniformity of samples from southern California, samples from Louisville have shown large variations that cannot be attributed to traffic gas. Most of the chemical materials responsible for the larger variations could be identified. Some could be identified only partly or not at all; but essentially the same pattern, repeated in several samples, indicated pollution from a common source which it should be possible to locate by further study.

6. Repeated joint occurrences of the same pollutants in samples from Louisville indicate that they originate in the same plant or nearly adjacent plants.

From the analytical data alone, the following grouping appears to be probable:

a. A source of gasoline vapor in large quantity.

b. A source or neighboring sources of acetylene and vinyl chloride.

c. A source or neighboring sources of butadiene, acrylonitrile, chloroprene, vinyl acetylene, and dichloroethylene.

d. A source of benzene.

e. A source of cresol, phenol, and styrene.

f. A source of pinene.

g. A source or sources of ethyl alcohol.

h. A source of aliphatic chlorine derivatives in considerable variety.

i. A source of olefins in variety.

j. A source of carbon tetrachloride.

k. A source of ion (59) tentatively attributed to tertiary butyl alcohol.

l. A source of ions (49) and (50) not certainly identified with any compound.

18. References

[1] Martin Shepherd, Method for identifying and estimating gases and vapors in air pollution, Air Pollution, Proc. 1st U. S. Tech. Conf. on Air Pollution, p. 228 (1952).

[2] Martin Shepherd, S. M. Rock, Royce Howard, and John Stormes, Isolation, identification, and estimation of gaseous pollutants in air, Anal. Chem. **23**, 1431 (1951).

[3] E. R. Weaver and Shirley Gunther, Condensible impurities in the air of Los Angeles and vicinity, Proc. 3d Natl. Air Symposium, Pasadena, p. 86 (1955).

WASHINGTON, May 20, 1957.

Journal of Research of the National Bureau of Standards Vol. 59, No. 6, December 1957 Research Paper 2810

Infrared Emission Spectrum of Silicon Carbide Heating Elements *

James E. Stewart [1] and Joseph C. Richmond

A method for determining the spectral emittance of a silicon carbide heating element (Globar) was devised and data were obtained over the wavelength range 1.25 to 15.25 μ for four different temperatures. The spectral emittance at all four temperatures, 482°, 649°, 816°, and 982° C (900°, 1,200°, 1,500°, and 1,800° F), was found to be approximately constant except for a gradual rise in emittance from 1.25 to about 4 μ and two minimums in the curves at longer wavelengths. The first of these minimums, which occurred at about 9 μ, was ascribed to minor amounts of SiO_2 present on the surface of the silicon carbide heating element, whereas the second at about 12.5 μ corresponds to one of the strong Raman lines for SiC.

1. Introduction

There is much current interest in heat-transfer processes at high temperatures. The extreme temperatures encountered in jet aircraft engines have long presented problems; but in modern aircraft performing at supersonic velocities even skin temperatures are well into the range where metals show undesirable creep and corrosion properties. Because radiative processes play a primary role in the transfer of heat to and from such parts it is desirable to obtain data on the thermal emission of various metals and coatings of engineering interest in a temperature range from 482° to 982° C (900° to 1,800° F).

Some work has been done in measuring the total emittances of various materials of interest. Total emittance, the ratio of the total radiant energy per unit area emitted by a specimen to that emitted by a black body at the same temperature, is not a satisfactory measure of the amount of radiant energy emitted or absorbed by a specimen for use in heat-transfer computations because (1) the spectral distribution of the radiant energy emitted by all surfaces, including black bodies, varies with temperature, (2) the spectral distribution of the radiant energy emitted by a surface may be markedly different from that of a black body at the same temperature, and (3) air and other gases absorb radiant energy at certain wavelengths that are characteristic of the gas.

Spectral emittance is the ratio of the radiant energy per unit area emitted by a surface at a given wavelength to that emitted by a black body at the same temperature and wavelength, for all wavelengths at which the specimen or black body emits a significant amount of energy. The radiant energy transmitted from a hot to a cold surface can be computed if the temperature of both surfaces, their spectral emittances at their respective temperatures, and the spectral absorption of any material through which the radiant energy passes between the surfaces, are known.

Absolute measurements of infrared radiation are difficult to make. The spectral distribution of energy emitted by a black body as a function of temperature has been known for many years, hence most emission measurements today are referred to a black body as standard. By definition, black bodies absorb all radiation incident upon them, and emit according to the Planck radiation law. A cavity with its walls at uniform temperature, having an appropriately small opening, furnishes a close approximation to the required conditions, and is not only the best standard for laboratory use, but also, under the proper conditions, is very nearly ideal in its physical characteristics. However, a small opening focused on a spectrometer requires that the spectrometer slit also be kept small, and this in turn requires a high amplifier gain and slow scanning speeds. It also makes focusing more difficult. To circumvent these difficulties it was decided to measure the spectral emission of the various test surface with respect to a secondary standard and then to adjust the resulting data to emittance after measuring the secondary standard against a black body.

A recrystallized silicon carbide rod (Globar) was believed suitable as the secondary standard because of its ruggedness, resistance to oxidation, and the ease with which the temperature can be controlled when the material is resistance heated by passing a current through it.

The present paper describes the method used for measuring the spectral emittance of test bodies and for calibrating the Globar, used as a secondary standard, to a sufficient degree of accuracy to permit the comparison of emission properties of test bodies. Values given below for the spectral emittance of Globar are not to be taken as standard emittance data for silicon carbide for reasons to be discussed.

2. Review of Earlier Work

The total emittance of silicon carbide powder bonded with 25 percent of clay was reported by Pirani [1] [2] to be nearly 1.0 at 200° C, dropping to about 0.75 at 900° C. The spectral emittance of a

* This project was under the sponsorship and with the financial assistance of the National Advisory Committee for Aeronautics.

[1] Present address: Beckman Instruments, Inc., Fullerton, Calif.

[2] Figures in brackets indicate the literature references at the end of this paper.

silicon carbide heating element (Globar) was first reported by Silverman [2] for the range 2 to 15 μ and for a single temperature of 1,102° C (approximately 2,015° F). Silverman used a specially prepared hollow cylinder of silicon carbide with a large outside diameter. An axial slot cut through the wall permitted radiation from the cavity to be compared with radiation from the surface of the source. His emittance curve shows a gradual rise from about 0.73 at 2 μ to about 0.84 at 5 μ, a fairly constant level to about 9.4 μ where a shallow minimum occurs followed by a stronger minimum at about 12.5 μ. He identified the minimum and maximum of the emittance curve at about 12.5 and 10 μ with the maximum and minimum, respectively, of the reflectivity curve at 12 and 10 μ.

Brügel [3] measured the spectral emittance of a standard spectrometer source of silicon carbide (Globar) in the 0.6 to 15 μ region for a series of temperatures from 727° to 1,527° C (approximately 1,340° to 2,780° F), with a comparison cavity black body at 727° C and instrument deflections calculated from those obtained at 727° C for measurements at other temperatures. He shows an emittance curve for 970° C (1,778° F) which rises from 0.75 at 2 μ to a maximum of about 0.87 at 8 μ and falls to about 0.77 at 15 μ. His curve shows a minimum at about 12.2 μ but none near 9.4 μ, probably because his measurements were made at 0.5 μ intervals. Brügel reports a linear temperature dependence of spectral emittance ranging from about 3×10^{-5} per degree Kelvin at 2 μ and 14 μ to a maximum of about 12×10^{-5} per degree Kelvin at 10 μ.

The reflectance spectrum of silicon carbide was first measured by Coblentz [4] and repeated by Schaefer and Thomas [5], who also measured the infrared absorption spectrum of a plate. The reflectance spectrum showed only the strong peak at 12 μ and the minimum at 10 μ mentioned above.

Ramdas [6] recently redetermined the absorption spectrum between 1 and 20 μ for a number of modifications of silicon carbide, using plates ranging between 0.14 and 1.0 mm in thickness. He found a very strong band probably centered near 12 μ and numerous weaker combination tones. Ramdas assigns the 12 μ band to a vibration mode involving an asymmetric stretching of C—Si bonds.

The Raman spectrum of silicon carbide has been observed by Narayanan [7], who reported a strong line at 818 cm^{-1} (12.2 μ).

3. Experimental Method

A Perkin-Elmer model 21 double-beam infrared spectrophotometer [8] was used with a sodium chloride prism for all measurements. Ordinarily the Perkin-Elmer instrument is used for transmission measurements and is arranged as shown schematically in figure 1. A Nernst glower source, N, is viewed by two pairs of mirrors which produce images, magnified two times on the monochromator slits. The instrument records the ratio of the radiance [3] of the two images and this ratio depends on the absorption of a transmission specimen placed at S.

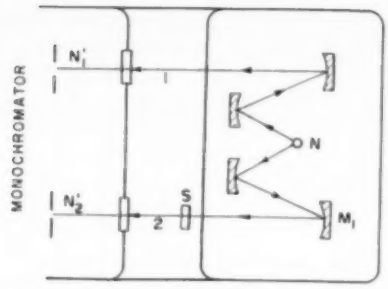

FIGURE 1. *Schematic drawing of double-beam infrared spectrophotometer when arranged for transmission measurements.*

N, Nernst glower source; M, mirror; S, specimen.

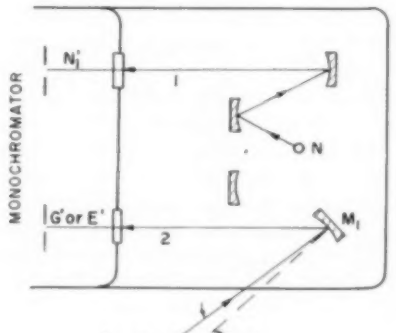

FIGURE 2. *Same instrument as in figure 1 as modified for measuring the relative emission from a black body (B) as compared to a Globar (G).*

For emission measurements the equipment is modified as shown schematically in figure 2. The mirror, M_1, is rotated as indicated so as to produce an unmagnified image of either the Globar source, G, or the black body, B, on the slit.[4] Because the path lengths of the two beams are approximately the same, the absorption by atmospheric water vapor and carbon dioxide will be nearly balanced.

The design of the black body is shown in figure 3. The core is made of graphite and the two electrodes (not shown in the figure), one at each end of the core, are connected to a welding transformer of variable power input. During a test, nitrogen is permitted to flow into the Vycor cylinder surrounding the cavity in the graphite. This prevents rapid oxidation of the graphite. An asbestos baffle serves to prevent the nitrogen from impinging directly on the graphite, which might otherwise produce a cool spot at this area.

[3] Radiant flux per unit surface area.

[4] The images of both the Globar and the opening in the black body are sufficiently large to fill the slit and hence require no magnification.

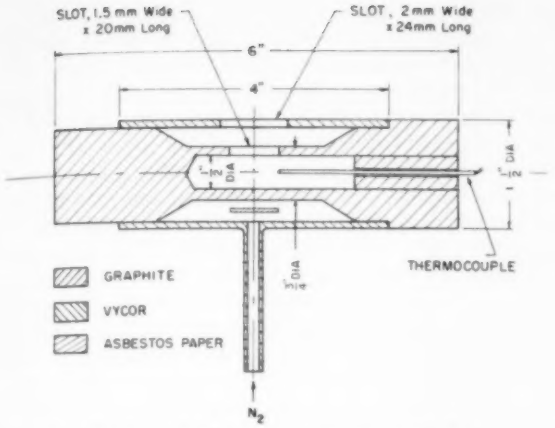

FIGURE 3. *Design of black-body source used for measuring spectral emittance of silicon carbide heating element.*

Nitrogen flowing through Vycor cylinder prevents rapid oxidation of graphite during determinations at elevated temperatures.

The temperature at the inside of the cavity of the graphite core was measured with a Chromel-Alumel thermocouple. During operation neither the thermocouple bead nor the ceramic insulator could be observed through the slit, thus indicating good temperature uniformity within the cavity. In each test the temperature was maintained within $\pm 1.7°$ C of that desired by manually adjusting the power input.

The temperature of the silicon carbide heating element was measured by a Chromel-Alumel couple inserted into a hole that was drilled into the side of the element with a Cavitron [9]. The temperature of this element was also maintained to within $\pm 1.7°$ C of that desired.

In making a determination, the silicon carbide element and graphite core were brought to the same temperature. Mirror M_1 in figure 2 was adjusted so as to focus the image of the element on the slit of the monochromator and a trace representing emission with respect to the Nernst glower source was obtained over the wavelength region 1.25 to 15.25 μ. Next, mirror M_1 was rotated slightly so as to fill the slit with radiation from the black body and a second trace was obtained. The ratio of the heights of the two curves at any point, corrected for the difference introduced by the slight shift in angle of mirror M_1, was then taken as the emittance of the silicon carbide surface at that particular wavelength. In making these calculations, the angular variation in reflectivity of the aluminum coating on the mirror as well as the effect of changing optical aberrations with angle were assumed negligible for the small changes in angles involved.

4. Results and Discussion

Figure 4 is a plot of the emittance of silicon carbide as a function of the wavelength of emitted energy for 482°, 649°, 816°, and 982° C (900°, 1,200°, 1,500°, and 1,800° F). The results are in qualitative agreement with those of Silverman [2] and of Brügel [3],

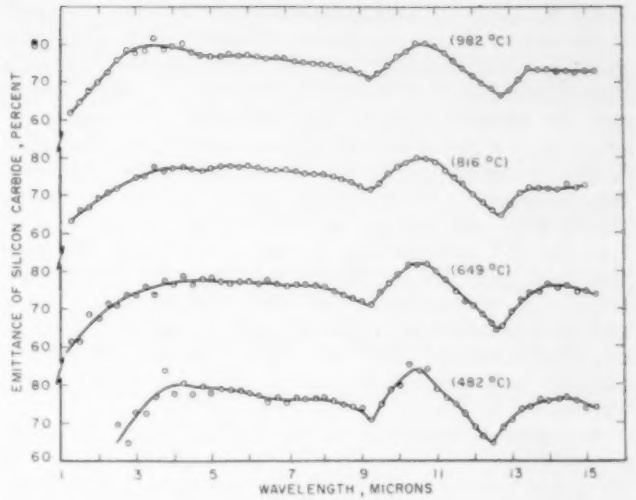

FIGURE 4. *Spectral emittance of Globar heating element at four temperatures.*

but the values tend to be somewhat lower than those reported by these two investigators. The change in spectral emittance with temperature is small; therefore, the lower values obtained in the present series of measurements are probably not due to differences in the range of temperatures in the three laboratories.

The measurements were reproducible within a range of about ± 2 percent at the shorter wavelengths ($\lambda < 5$ μ) and about ± 1 percent at the longer wavelengths. Fluctuations in the temperature of the Nernst glower are probably responsible for much of the uncertainty. Within these experimental limits no temperature dependence of emittance was found for regions sufficiently remote from the minimums near 9 and 12 μ. The minimums however, were definitely temperature sensitive. As seen in figure 4, they shift to longer wavelengths as the temperature is increased, and in fact appear to do so as linear functions of temperature: $\lambda_1 = 8.97\ (1+4.1\times10^{-5}T)$ and $\lambda_2 = 12.17\ (1+5.08\times10^{-5}T)$. ($T$=temperature in °K.) This temperature dependence was investigated further by determining the positions of the peaks at additional temperature of 193°, 260°, 316°, 398°, and 1,115° C (380°, 500°, 600°, 749°, and 2,039° F). The broadness of the peaks, particularly at the lower temperatures, makes accurate determinations of the minimums difficult. It is clear, however, that the 12 μ peak should occur at about 12.2 μ at room temperature, in excellent agreement with the Raman observation. The other peak should be found at about 9.0 μ at room temperature. McMahon [8] has observed a similar temperature shift of the peak observed near 9.5 μ in the emission spectra of glasses. He attributes this to an increase in the Si—O bond distance as a result of thermal expansion.

Because no band had been observed at 9 μ in the infrared reflection or absorption spectra, or in the Raman spectra of silicon carbide, the appearance of a peak there in the emission spectra is puzzling

Both Ramdas [6] and Schaefer and Thomas [5] made their observations on plates oriented with the basal plane perpendicular to the incident radiation. Hence vibrations perpendicular to the basal plane might not be observed [10]. An attempt was made to observe the infrared absorption spectrum of a randomly oriented sample of silicon carbide by suspending some very fine powder in a potassium iodide disk. The differences in refractive indices (about 1.65 for KI and 2.6 for silicon carbide at 750 mμ) were too great to permit observation of a good spectrum. A broad band was observed at about 12 μ and a Christiansen window [11] occurred at 9.5 μ, no doubt where the refractive indices of silicon carbide and potassium iodide coincide. No band was found at 9 μ.

A plausible explanation of the 9 μ band is that it arises from an impurity. The various forms of silica are known to have strong reflection bands near 9 μ, due to an asymmetric stretching of the Si—O—Si bonds. Furthermore, these bands seem to shift to longer wavelengths as temperature is increased [12]. Silica is a likely impurity in silicon carbide because the material is prepared by reduction of silica with carbon at high temperature and also because X-ray [13,14] and electron diffraction [13] studies have shown that cristobalite is formed by oxidation of silicon carbide at temperatures encountered by heating elements in ordinary use. β-Cristobalite, the high temperature form, has its reflection maximum at about 8.8 μ at 300° C [12]. Because a peak in the reflection curve is influenced by both the refractive index and the absorption coefficient, it does not necessarily coincide with a vibrational frequency of the material. The true frequency of the vibration producing the 8.8 μ reflection peak in the β-cristobalite has not been measured, but by analogy with α-cristobalite and quartz it probably lies at a wavelength longer than 8.8 μ by a few tenths of a micron. In addition, the bonding material in Globar is likely to produce its own emission peaks.

No change in the cristobalite peak, or in the entire Globar spectrum, was detected during the period of time (about 50 hr) these and other measurements required. Nevertheless, because of the known changes in emitting properties of Globar sources with time it is necessary to compare the Globar with the black body at intervals during a series of measurements.

The discrepancy between the results reported here and the earlier observations could be due to differences in the composition or aging of the specimens studied or to experimental difficulties associated with temperature equilibrium and measurement. The spectral emittance of the Globar used in this study was checked in the region between 1.0 and 2.5 μ by R. G. Johnston and E. D. Tidwell, using a spectrometer and black body furnace of the Radiometry Section of the Bureau. Agreement was obtained throughout the region only by adjusting the temperature of the Globar to obtain agreement at 2.5 μ. The instrument used had very short slits (3 mm) which permitted the observation of energy emitted from different parts of the Globar. In this way the existence of a steep thermal gradient along the Globar was demonstrated, with the ends of the Globar perhaps as much as 10 percent cooler than the middle. An averaged intensity is observed with a spectrometer having longer slits.

The peak in Brügel's curve showing the temperature rate of change of emittance as a function of wavelength is produced, or at least augmented, by the shift in the 9 and 12 μ peaks. The observations by Pirani [1] that total emittance of a mixture of silicon carbide and clay decreases with increasing temperature is consistent with a spectral emittance that is independent of or even slightly increasing with temperature, for as the temperature is increased the peak of the black body emission curve moves to shorter wavelengths where the emittance of silicon carbide is decreasing. The clay in Pirani's sample also undoubtedly affects the emission properties.

As the purpose in measuring the spectral emittance of the silicon carbide heating element is to be able to determine the emittances of coated metal specimens, a typical example of this application is shown in figure 5. The upper curve is the emission, normal to the surface, from a sand-blasted stainless-steel strip coated with A–418, a material consisting of chromic oxide, barium borosilicate glass, and clay, relative to silicon carbide at 982° C (1,800° F). The lower curve is the emittance adjusted to be relative to a black body.

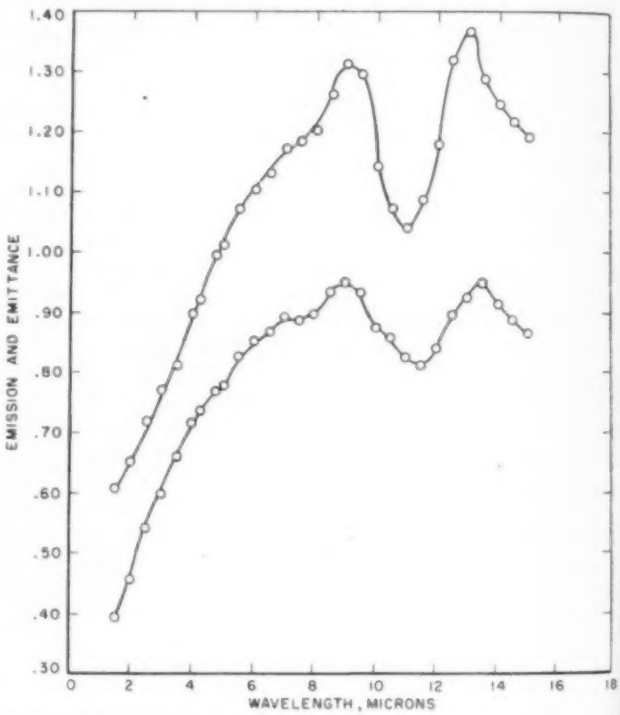

FIGURE 5. *Spectral emission (upper curve) and spectral emittance (lower curve) of a barium borosilicate coating on stainless steel.*

Coating A–418 on stainless steel.
982° C (1,800° F).

5. Conclusion

The spectral emittance of silicon carbide seems to be independent of temperature in the range 482° to 982° C (900° to 1,800° F) within the experimental error of the measurements, except for two minimums near 9 and 12.2 μ. The wavelengths of these peaks appear to vary nearly linearly with temperature and to fall at longer wavelengths at higher temperatures. The peak near 12.2 μ undoubtedly arises from a vibration of the silicon carbide itself, whereas the peak near 9 μ probably is contributed by cristobalite which is known to form when silicon carbide oxidizes.

The observed variation in emission from different regions along the Globar rod leads to the conclusion that a Globar source is not a precise standard for emissivity measurements unless the emittance from a fixed portion of its surface is determined by comparison with a black-body source.

The authors express their gratitude to R. G. Johnston, E. D. Tidwell, and E. K. Plyler of the Radiometry Section, and to D. G. Moore and W. N. Harrison of the Enameled Metals Section for helpful discussions and assistance.

6. Appendix. Emission, Emittance, and Emissivity

The use of the words emission, emittance, and emissivity in this paper follows the recommendations of Worthing [15].

Emission is the act or process by which radiant energy is emitted by a body as a consequence of its temperature only. This term is also used for the rate of such emission in units of energy per unit area and unit time. It is influenced by the composition, thickness, and surface texture of the specimen.

Emittance is a property of a specimen, regardless of its composition, thickness, or surface texture, and is the ratio of the emission of the specimen to that of a black body at the same temperature.

Emissivity is a property of a material, and is the emittance of a specimen of the material having a polished surface, of sufficient thickness to be opaque. It represents a minimum value of emittance as regards the effect of surface texture, and a maximum value as regards the effect of thickness (opacity) of the specimen.

7. References

[1] M. Pirani, Radiation properties of different substances within the temperature range 250° C to 800° C, J. Sci. Inst. **16,** 372 (1934).
[2] S. Silverman, The emissivity of Globar, J. Opt. Soc. Am. **38,** 989 (1948).
[3] W. Brügel, Strahlungsmessungen an Elektrisch Geheitzen SiC-Stäben, Z. Physik **127,** 400 (1950).
[4] W. W. Coblentz, Radiometric investigations of infrared absorption and reflection spectra, Bul. BS **2,** 457 (1906) S45.
[5] C. Schaefer and M. Thomas, Oberschwingungen in Ultraroten Absorption-spektren, Z. Physik **12,** 330 (1923).
[6] A. K. Ramdas, The infrared absorption spectrum of silicon carbide, Proc. Indian Acad. Sci. [A] **37,** 571 (1953).
[7] P. S. Narayanan, Raman spectrum of Carborundum, Current Sci. **21,** 239 (1952).
[8] H. O. McMahon, Thermal radiation characteristics of some glasses, J. Am. Ceram. Soc. **34,** 91 (1951).
[9] G. H. DeGroat, Soft steel and ultrasonics machine carbide, Am. Machinist **96** (19) 141 (September 15, 1952).
[10] J. E. Stewart, Use of partially oriented solid samples and unpolarized radiant energy in the analysis of infrared absorption spectra, J. Chem. Phys. **23,** 986 (1955).
[11] R. B. Barnes and L. G. Bonner, The Christiansen filter effect in the infrared, Phys. Rev. **49,** 732 (1936).
[12] I. Simon and H. O. McMahon, Study of the structure of quartz, cristobalite, and vitreous silica by reflection in infrared, J. Chem. Phys. **21,** 23 (1953).
[13] G. Heine and P. Scherer, Untersuchung der Oberflächenschicht von Siliciumcarbid und Umwandlung von SiC in Cristobalit, Helv. Phys. Acta **13,** 489 (1940).
[14] T. H. Elmer, Silicon carbide heating elements-development, uses, chemical and physical investigations, Bul. Am. Ceram. Soc. **32,** 23 (1953).
[15] A. G. Worthing, Temperature radiation emissivities and emittances. Temperature, Its Measurement and Control in Science and Industry, p. 1164 (American Institute of Physics, 1941).

Washington, December 3, 1956.

Journal of Research of the National Bureau of Standards Vol. 59, No. 6, December 1957 Research Paper 2811

Increased Chemical Reactivity of the Surface Compared With That in the Bulk Volume of Britton-Robinson Universal Buffers

Robert G. Pike and Donald Hubbard

A direct comparison of the chemical reactivity at the surface with that in the bulk volume of buffer solutions over the range *p*H 7 to *p*H 11.8 was made, using Corning 015 glass as the indicator. By observing interferometrically the surface alterations of optically flat specimens brought about by exposures to aqueous buffer solutions under controlled conditions of time, temperature, and *p*H it was possible to evaluate, at least semiquantitatively, the difference between the chemical reactivity of the surface and the bulk volume of the solutions. For the buffer at *p*H 7 the surface reactivity appeared to correspond to a hydrogen ion activity of *p*H 9.4. The apparent concentration differential between the surface and bulk volume falls off sharply for buffers of increased *p*H, amounting to only 0.2 *p*H unit for the buffer at *p*H 11.0, and becomes nondetectable at *p*H 11.8. Unfortunately the chemical durability characteristics of the glass were such that no differentiation could be made between the hydrogen ion activity of the surface and the bulk volume in solutions more acid than *p*H 7.

1. Introduction

Although direct experimental verification is often difficult, there is abundant theoretical evidence that the concentration at the surface of a solution may differ considerably from the bulk-volume concentration. J. Willard Gibbs emphasized this point when he derived his mathematical relation between surface concentration and surface tension [1].[1] This relation, as simplified and expanded by Wolfgang Ostwald is $u=-c/RT\cdot d\gamma/dc$, where u is excess solute in unit surface, c is concentration or activity, and γ is surface tension [2].

Inspection of this equation reveals that if the surface tension γ increases with the concentration then u is negative and the surface concentration is less than the concentration of the bulk of the solution. However, if γ decreases as the concentration increases, u is positive and the surface concentration is greater than the concentration of the bulk volume. Finally, if the surface tension is independent of the concentration, then the concentration of the solute in both the surface layer and the bulk of the solution will be the same.[2]

In a previous investigation into the relation between chemical durability of glass and the voltage anomalies of the glass electrode, a pronounced increased reactivity on optical glass flats by the surface of Britton-Robinson universal buffer solutions had been noted [5]. The present investigation was undertaken to study these effects systematically over an extended *p*H range.

2. Experimental Procedure

Instead of using surface tension as an uncertain and uninterpretable indicator of concentration difference in the complex buffers used, the increased chemical activity at the surface compared with that in the interior of the solution (bulk volume) was studied on a glass of known durability characteristics in order to obtain direct comparison of the hydrogen ion activity [H^+] at the surface and in the bulk volume. A glass sensitive to attack in alkaline solutions and having a composition near the lowest melting eutectic of the soda-lime-silica ternary phase equilibrium diagram, viz., 23% of Na_2O, 5% of CaO, and 72% of SiO_2 (Corning 015 glass) was selected as the indicator in this study [6, 7, 8]. Glass was chosen primarily because its use eliminated oxygen as a possible contributing factor in the interpretation of the results.

Small specimens of this glass having surfaces sufficiently flat and well polished to give satisfactory interference bands when placed beneath a fused silica optical flat, were exposed by partial immersion in a series of buffer solutions under controlled conditions of time, temperature, and *p*H. This procedure leaves a portion of the specimen unexposed to either the surface or the bulk volume of the test solution. The excess chemical activity of the surface (attack on the glass) compared with that of the bulk volume of the solution was obtained from the alteration of the interference pattern caused by exposures of 6 hours at 80° C.

The solutions employed were Britton-Robinson universal buffers, because with these a controlled *p*H range from *p*H 2 to *p*H 11.8 could be obtained without introducing any new ionic species [9]. Basically, these buffers consist of a mixture of phosphoric, acetic, and boric acids in which the desired *p*H is obtained by adding the proper amount of sodium hydroxide.

The experiments were performed with a thin layer of liquid petrolatum on the surface of the buffers to minimize evaporation during the period of the test. This simplified procedure was accepted and adopted only after ascertaining that exposure in a closed

[1] Figures in brackets indicate the literature references at the end of this paper.
[2] Gibbs' equation has been verified experimentally [3] and the difference in concentration between the bulk of the liquid and the surface determined for different substances by several methods [4].

system without an oil layer did not give appreciably different results.

3. Results and Discussion

Figure 1 shows typical examples of interference patterns obtained for specimens of Corning 015 after partial immersion in buffers of different *p*H values for 6 hours at 80° C. In each of the photographs the lower part of the field is that of the immersed portion of the specimen, which when compared with the unexposed portion of the field gives the surface alterations of the specimen brought about in the main bulk and at the surface of the buffer. For the portion of the specimen exposed to the buffer at *p*H 4 (fig. 1,A) the displacement of the fringes to the left indicate a swelling of about 2/10 fringes. Such swelling is characteristic of many glasses in acid buffers [10, 11]. At *p*H 7 (fig. 1,B) and at *p*H 9 (fig. 1,C) a perceptible swelling for the portion of the specimen exposed is evident in the bulk solution, but a distinct attack or surface cut (i. e., a displacement of the fringes to the right) appears at the surface of the solution. Such surface cuts were noted and briefly discussed in an earlier publication [5]. At *p*H 10 (fig. 1,D) the specimen exhibits attack for the immersed portion with additional attack at the buffer surface.

Figure 2 shows the composite curve obtained when these and additional data from table 1 were plotted with surface alterations as the ordinates and *p*H as the abscissa. The closed circles represent the values found for alteration of the specimen occuring in the bulk volume of the solution. The open circles give the accompanying attack (surface cut) attributable to the chemical activity of the surface of the solution. Inspection of figure 2 reveals that these surface cuts may be interpreted directly in terms of the effective *p*H for the surface of the buffer solutions. For example, for the buffer at *p*H 7 the alkalinity of its surface has caused an attack on the glass equal to the bulk-volume attack caused by a buffer at

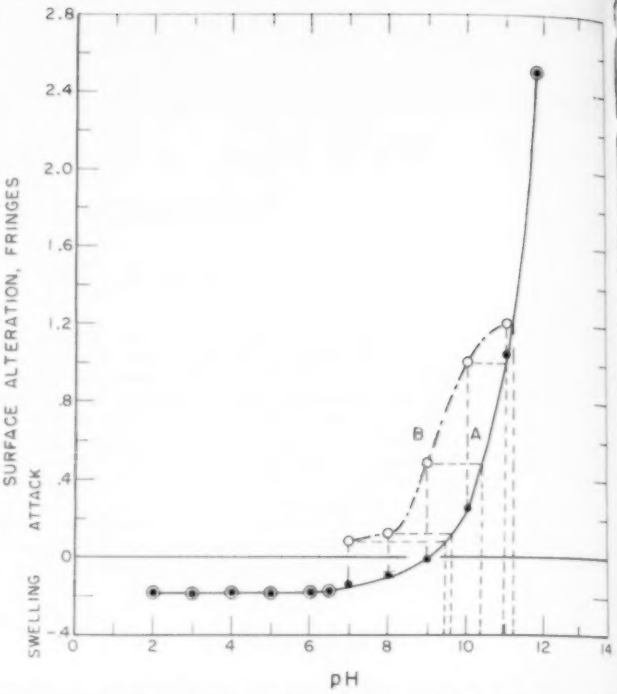

FIGURE 2. *Chemical durability characteristics of Corning 015 glass over the range p*H *2 to p*H *11.8*

Exposure 6 hours at 80° C. A, Surface alteration of the specimens in the bulk volume of the buffers; B, surface alteration of the specimens brought about by the increased surface reactivity of the buffers.

*p*H 9.4. In other words the surface of the buffer at *p*H 7 appears to be more alkaline than the bulk-volume value by at least 2.4 *p*H units. Similarly for the buffers at *p*H 8 to *p*H 11.8, the observed differences are given in table 2.

At *p*H 11.8 the effective reactivity of the buffer and that of its surface either approach the same value, or the use of this glass as an indicator loses its effectiveness. This latter suggestion can be dismissed, because from the ascending shape of the chemical durability curve it is evident that the glass

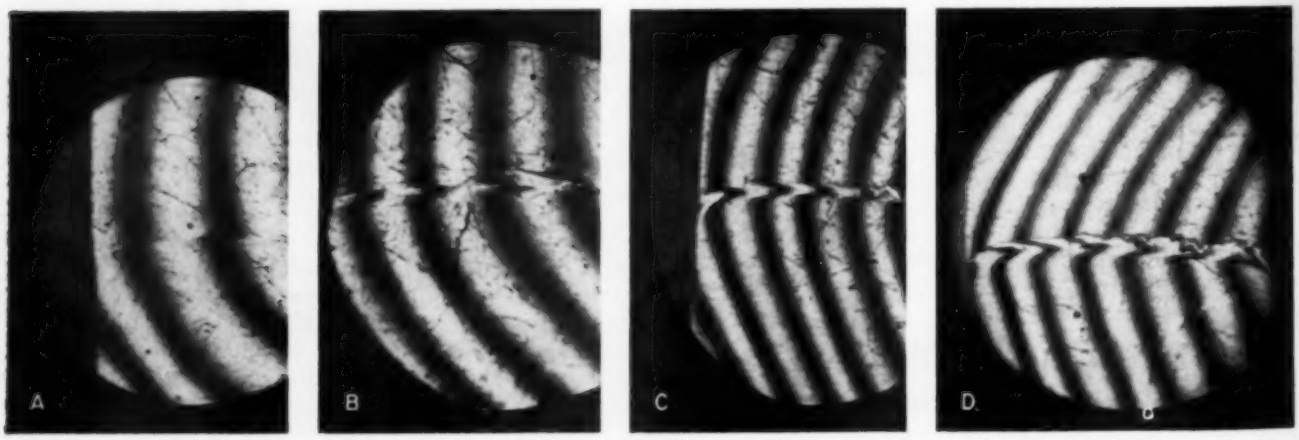

FIGURE 1. *Interferometric patterns illustrating the chemical durability characteristics of Corning 015 glass for exposures of 6 hours at 80°C.*

A, Pattern for *p*H 4, illustrating the swelling generally initiated by acid buffers; B, pattern for *p*H 7 showing slight attack at the buffer surface and swelling below; C, pattern for *p*H 9 illustrating liberal attack at the buffer surface and swelling below; D, pattern for *p*H 10 exhibiting attack for the immersed portion with additional attack at the buffer surface.

TABLE 1. *Chemical durability of Corning 015 glass over an extended pH range*

Buffers	Alteration of the specimens after exposure to the following buffers for 6 hours at 80° C		
	Swelling	Attack	Surface cut
pH	*Fringes*	*Fringes*	*Fringes*
2.0	<0.2	.....	.....
3.0	<.2	.....	.....
4.0	<.2	.....	.....
5.0	<.2	.....	.....
6.0	<.2	.....	.....
6.5	<.2	.....	.....
7.0	<.1	.....	<0.1
8.0	.1	.....	>.1
9.0	(a)	.....	<.5
10.0	.....	0.25	1
11.0	.....	>1	1.2
11.8	.....	2.5	2.5

[a] Detectable swelling.

TABLE 2. *Indicated surface pH of various buffers in the alkaline range*

Compiled from figure 2

Bulk-volume alkalinity	Surface alkalinity	Difference
pH	*pH*	*pH*
7	9.4	2.4
8	9.6	1.6
9	10.4	1.4
10	10.9	0.9
11	11.2	.2
11.8	11.8	.0

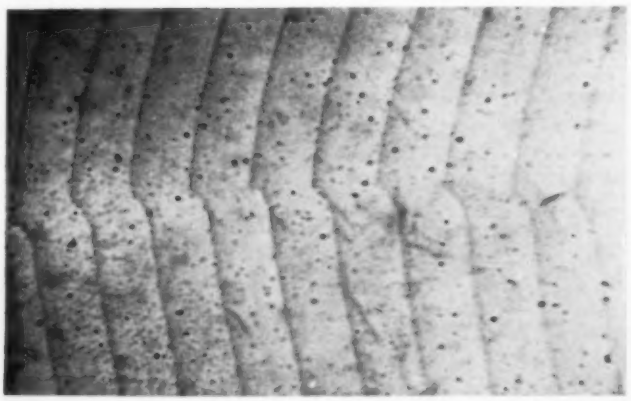

FIGURE 3. *Fabry-Perot interferometric pattern for specimens exposed at pH 11.8 for 1 hour at 80° C, showing the absence of any excess surface reactivity at this high alkalinity.*

should be a very sensitive indicator at this high alkalinity. The attack by the bulk volume for 6 hours at *p*H 11.8 was so large, it was feared that any accompanying surface cut might have been obscured. To ascertain for sure if such a cut did or did not exist another specimen was given a 1-hour exposure at *p*H 11.8. Inspection of figure 3 obtained with the Fabry-Perot interferometric technique [12] reveals no indication of an excess surface attack. The reason for the surface and the bulk volume of the buffers exhibiting equal activities at high alkalinities may be (a) that the surface approaches saturation or (b) that the same molar change for the surface at *p*H 11.8 that appeared at *p*H 7 would be a very small *p*H change indeed at the higher concentration.

Unfortunately no data were obtainable in the acid range because this glass gives a small uniform swelling over the range *p*H 2 to *p*H 6.5, making any differentiation of activity between the surface and bulk volume impossible.

4. Concluding Remarks

The difference in chemical reactivity at the surface and in the bulk volume of buffer solutions has been examined over a broad *p*H range using Corning 015 glass as the indicator. This glass served as an acceptable indicator over the range *p*H 7 to *p*H 11.8, but was ineffective for buffers more acid than *p*H 6.5. The increased chemical reactivity of the surface of buffers may be interpreted in terms of an increase in the effective *p*H at the surface of the buffer solution. This difference in effective *p*H between the surface and bulk volume was greatest near *p*H 7 where it was to be expected, and decreased with increasing *p*H.

Liquid-line corrosion has been observed on many substances other than glass. Examples are calcite in hydrochloric acid, sucrose and sodium carbonate in water [13], and metals in aqueous solutions [14]. Several theories have been advanced to account for the surface cuts in the cases cited, but none of these theories alone are compatible with the data obtained in the present study. For example: (1) Increased oxygen content at the surface of the liquid can be eliminated from consideration because a material was used that was already oxidized; (2) increased diffusion rate of active ions, increased reaction at the surface, or protection of the main body of the specimen by the downward streaming of reaction products might explain the increased surface attack in some systems, but for the Corning 015 glass a change from swelling in the body of the solution to attack at the surface (as shown at *p*H 7) can be accounted for only by a change in alkalinity at the surface of the liquid.

In analyzing these results, it is important to point out that knowledge of the value of the *p*H of a solution is not sufficient to predict its chemical reactivity. The attacking ions must be of a type that will form soluble compounds with the constituents of the glass network. For example, most glasses are inert to an aqueous solution of NH_4OH at *p*H 13.3 [15]; yet these same glasses will be attacked rapidly by NaOH prepared at an equivalent *p*H. Thus, the results obtained in the present study do not apply to all alkaline solutions of varying *p*H but only to the particular series of buffers used.

From inspection of the photographs it can be seen that some gain in accuracy and increase in sensitivity of the method can be obtained by improving the quality of the polish and optical flatness of the surfaces of the specimens. It was shown that further refinement could be brought about by increasing the

sensitivity of the interferometer by employing the Fabry-Perot [12] or the Saunders' multiple reflection techniques [16].

There is at least one other particularly interesting observation from these data that is not primarily concerned with the surface versus bulk-volume concentration of buffer solutions, but should not be overlooked. For example, inspection of the interference patterns of figure 1 shows at a glance why glass specimens partially immersed in aqueous solutions should be mechanically weakened at the liquid-air interface.

5. References

[1] J. Willard Gibbs, Trans. Conn. Acad. **3**, 439 (1876).

[2] F. H. Getman and Farrington Daniels, Outlines of theoretical chemistry, p. 236 (John Wiley & Sons, Inc., New York, N. Y., 1931).

[3] James W. McBain and C. W. Humphreys, The microtome method of the determination of the absolute amount of adsorption. J. Phys. Chem. **36**, 300 (1932).

[4] W. C. M. Lewis, An experimental examination of Gibbs' theory of surface-concentration, regarded as the basis of adsorption, with an application to the theory of dyeing, Phil. Mag. 6th series **15** (1908).

[5] Donald Hubbard, E. H. Hamilton, and A. N. Finn, The effect of the solubility of glass on the behavior of the glass electrode, J. Research NBS **22**, 339 (1939) RP1187.

[6] Malcolm Dole, Glass electrode, p. 68 (John Wiley & Sons, Inc., New York, N. Y., 1941).

[7] D. G. MacInnes and M. Dole, The behavior of glass electrodes of different compositions, J. Am. Chem. Soc. **52**, 29 (1930).

[8] G. W. Morey and N. L. Bowen, The ternary system sodium metasilicate-calcium metasilicate-silica, J. Soc. Glass Tech. **9**, 232 (1925).

[9] T. S. Britton, Hydrogen ions, 2d ed. table 57 (c) p. 225 (D. Van Nostrand & Co., Inc., New York, N. Y., 1923).

[10] Donald Hubbard, Mason H. Black, Sylvanus F. Holley, and Gerald F. Rynders, Electrode function (pH response) hygroscopicity, and chemical durability of soda-potash-silica glasses, J. Research NBS **46**, 168 (1951) RP2189.

[11] Donald Hubbard and Given W. Cleek, Deuterium and hydrogen electrode characteristics of lithia-silica glasses, J. Research NBS **49**, 267 (1952) RP2363.

[12] Jenkins and White, Fundamentals of optics, 2d ed, p. 264, Fabry-Perot Interferometer (McGraw-Hill Book Co., Inc., New York, N. Y., 1950).

[13] W. Spring, Uber eine zunahme chemischer energie an der freien oberflache flussiger korper, Z. Physik. Chem. **4** (1889) 658.

[14] E. H. Hedges, Liquid-line corrosion, J. Chem. Soc., p. 831 (1926).

[15] Donald Hubbard and Gerald F. Rynders, Voltage anomalies of the glass electrode and the chemical durability of the glass, J. Research NBS **39**, 561 (1947) RP1848.

[16] J. B. Saunders, High sensitivity interferometer for measurement of phase shifts and for other applications, Proceedings of a symposium on gage blocks held at the National Bureau of Standards, Aug. 11 and 12, 1955.

Washington, May 10, 1957.

Journal of Research of the National Bureau of Standards Vol. 59, No. 6, December 1957 Research Paper 2812

Photometric Determination of Tungsten in Steel and Titanium Alloys With Dithiol

Lawrence A. Machlan and John L. Hague

A method is described for the direct photometric determination of tungsten in steels. The sample, 0.1 to 0.2 g in weight, is dissolved in aqua regia, and a sulfuric-phosphoric-perchloric acid mixture is added. The solution is evaporated to fumes of sulfuric acid and diluted to volume with diluted sulfuric acid (1+3). An aliquot portion of the solution is treated with dithiol in diluted sulfuric acid solution (1+3) containing sulfur dioxide, and molybdenum and certain other potential interferences are removed by extraction with chloroform. Copper and other elements forming insoluble dithiolates are removed by filtration. The tungsten-dithiol complex is then formed, after the addition of hydrochloric acid, stannous chloride, and dithiol, and extracted with butyl acetate. The absorbancy of the tungsten complex is determined at approximately 635 mμ. An accuracy of 0.005 percent of tungsten, or better, is indicated in the range 0.05 to 0.50 percent of tungsten, and of about 0.001 percent for amounts of less than 0.05 percent of tungsten. The application of the method to titanium alloys is described in an appendix section.

1. Introduction

Tungsten is finding an increased usage, in the range of 2 percent or less, as an alloying element in ferrous metallurgy. Typical of some of these alloys are the "nondeforming" die and chisel steels (usually carbon-chromium-tungsten alloys), age-hardening chromium-nickel-tungsten alloys, low-tungsten tool steels such as the AISI types M 1 and M 7, and alloys finding application in the high-temperature field such as the 19–9DL types of stainless steels. Aside from alloy addition, many steels, through the use of scrap, contain residual amounts of tungsten, which may vary from a few thousandths to several tenths of a percent.

Gravimetric procedures are not well adapted to the determination of small percentages of tungsten. Iron and molybdenum retard the precipitation of small quantities of tungsten by the usual cinchonine procedure. Titanium, niobium, tin, and tantalum are often encountered, and any procedure devised must provide for their presence. Of the reactions available for the photometric determination of tungsten, the most commonly employed are those that use thiocyanate, hydroquinone, and dithiol as reagents. The thiocyanate reaction [5][1] has found acceptance [11, 12] primarily for the analysis of tool steels, but some interference is encountered with molybdenum and vanadium. The hydroquinone reaction has been used in the Bureau's Analytical Chemistry Section for some years in combination with an alpha-benzoinoxime precipitation [8], but difficulties are encountered when niobium is present. In fact, the color has been recommended [9] for the determination of niobium and tungsten in stainless steel, using photometric measurements at two different wavelengths. In any case, titanium [10] gives a much more intense color and provides a serious interference.

The dithiol (1,2-dithiol-4-methylbenzene) reagent [7, 13] appeared to offer advantages for the determination of low percentages of tungsten in spite of its obnoxious odor. Potential interferences are few, and most of these can be removed, with the same reagent, under conditions such that the tungsten color does not develop. This reagent has been applied to the determination of tungsten in titanium metal [18], in tantalum, titanium, and zirconium metals [6], and in steel [3, 14, 16, 19].

The method presented here is the result of a study of the conditions necessary to make the reaction specific for tungsten in the presence of the large number of elements encountered in ferrous metallurgical analysis. A clear solution of the sample in a sulfuric-phosphoric acid mixture can be obtained by a simple fuming operation. The resulting solution is well adapted [1, 4, 17] for the removal of molybdenum, the principal interfering element, with dithiol because considerable variations in acidity and temperature can be tolerated without tungsten reacting. Dithiol solution is added; the molybdenum and other elements that form soluble complexes are extracted with chloroform. The insoluble complexes, primarily copper, are removed by filtration. Hydrochloric acid, stannous chloride solution containing a trace of copper, and dithiol are added, and the tungsten-dithiol color is developed by heating the solution for 10 minutes on a steam bath. The solution is cooled, and the tungsten complex extracted with butyl acetate. The absorbancy of the extract is measured at 635 mμ and the tungsten determined by reference to a calibration curve or table.

The present method will not compete timewise with spectrographic methods. It was designed to provide values for tungsten, in the range 0.001 to 0.5 percent, for the standardization of a group of spectrographic steel standards containing additions of 22 elements and the rare earths. A single determination can be carried through in several hours; a group of eight determinations can be completed in a day.

2. Apparatus

Colorimeter. An Evelyn type of colorimeter, including filters, voltage stabilizer, and galvanometer

[1] Figures in brackets indicate the literature references at the end of this paper.

was used for the quantitative measurements reported. Matched test tubes (22 by 175 mm) were used as absorption cells.

Filtering Arrangement. See figure 1.

FIGURE 1. *Arrangement for filtering.*

3. Reagents

Sulfuric-Phosphoric-Perchloric Acid Mixture for Fuming. Add 100 ml of sulfuric acid [2] to 250 ml of water, cool, add 100 ml of phosphoric acid (85%) and 50 ml of perchloric acid (70%). Mix thoroughly and cool.

Dithiol Solution. Dissolve 5 g of sodium hydroxide in 50 ml of water and dilute to 500 ml. Add 1 g of 3,4-dimercaptotoluene (dithiol),[3] shake to dissolve it, and store in a refrigerator. Just before use, add 2 ml of thioglycolic acid to 125 ml of the dithiol solution, allow it to stand a few minutes, and filter through a close-textured paper. If a precipitate forms, which does not redissolve on a few minutes standing, too much thioglycolic acid has been added. Prepare a fresh portion, using slightly less thioglycolic acid. Use the turbid solution for the development of the tungsten color.

Stannous Chloride Solution. Dissolve 100 g of stannous chloride dihydrate and 5 mg of copper chloride dihydrate in 400 ml of diluted hydrochloric acid (1+1) by heating on a steam bath. Cool and dilute to 500 ml with diluted hydrochloric acid (1+1).

Sulfuric-Sulfurous Acid Mixture. Saturate diluted sulfuric acid (1+3) with sulfur dioxide gas.

Standard Tungsten Solution (1 ml≡1.00 mg of tungsten). Transfer 0.1794 g of sodium tungstate dihydrate to a 100-ml volumetric flask, dilute to the mark with water, and mix. The sodium tungstate was purified and tested by the procedure suggested by Yagoda and Fales [20], though high-purity material is not required.

Standard Tungsten Solution (1 ml≡100 μg of tungsten). Transfer exactly 10 ml of standard tungsten solution (1 ml≡1.00 mg of tungsten) to a 100-ml volumetric flask, dilute to the mark with water and mix well. This solution should be prepared as needed.

4. Procedure

Transfer 0.200 g [4] of the sample to a 125-ml Erlenmeyer flask, add 10 ml of aqua regia (3 parts of hydrochloric acid and 1 part of nitric acid), and heat gently until the sample dissolves. Add 20 ml of the "fuming acid" mixture and 1 or 2 drops of hydrofluoric acid, boil until brown fumes have been expelled, evaporate to fumes, and fume the solution vigorously for a few minutes to remove the perchloric acid. Cool, add 25 ml of diluted sulfuric acid (1+3), and heat on a steam bath to dissolve insoluble salts. Cool, transfer the solution to a 100-ml [5] volumetric flask, and dilute to the mark with diluted sulfuric acid (1+3).

Transfer 7.5 ml of diluted sulfuric acid (1+1), 5 ml. of sulfuric-sulfurous acid solution, and a suitable aliquot [6] of the sample to a 60-ml separatory funnel. Place the funnel in a water bath maintained at 30° to 40° C, add 5 ml of dithiol solution, shake the solution for 5 to 10 seconds, and allow it to stand for 5 minutes. Cool, add 10 ml of chloroform, shake it for 40 seconds, and allow the layers to separate. Drain and discard the chloroform layer. Repeat the extraction with 5 ml of chloroform, finally discarding the chloroform layer. Filter the acid layer through glass wool (see fig. 1) into a 250-ml separatory funnel. Wash the 60-ml separatory

[2] If no dilution is specified, the concentrated analytical reagent is meant. Diluted hydrochloric acid (1+1) denotes 1 volume of concentrated hydrochloric acid, sp gr 1.18, diluted with 1 volume of water. Diluted sulfuric acid (1+3) denotes 1 volume of concentrated sulfuric acid, sp gr 1.84, diluted with 3 volumes of water.

[3] A satisfactory reagent of domestic manufacture is commercially available.

[4] For materials containing more than 0.5 percent of tungsten, use 0.100 g of the sample.

[5] For materials containing from 1 to 2 percent of tungsten, transfer to a 200-ml volumetric flask.

[6] A suitable aliquot will contain up to 20 mg of sample and less than 50 μg of tungsten.

funnel twice with 2- to 3-ml portions of diluted sulfuric acid (1+3).

Place the 250-ml separatory funnel in a steam bath for 10 minutes, cool in a water bath maintained at 30° to 40° C, add 2.5 ml of dithiol solution, and shake for 5 to 10 seconds. Return the funnel to the water bath and allow it to stand for 5 minutes. Cool, add 5 ml of chloroform, shake for 40 seconds, allow the layers to separate, drain and discard the chloroform layer. Repeat the extraction with another 5 ml of chloroform, finally discarding the chloroform layer. Place the funnel in a steam bath and heat for 15 minutes.[7]

Add 50 ml of hydrochloric acid and 5 ml of stannous chloride solution to the funnel, return it to the steam bath, and heat for 3 minutes. Add 15 ml of dithiol solution, mix well, and again heat on the steam bath for 10 minutes. Cool the solution in a cold-water bath, add exactly 20 ml of butyl acetate from a pipet, shake for 20 seconds, and allow the layers to separate. Drain and discard the acid layer. Transfer the butyl acetate solution to a dry test tube and stopper the tube.

Transfer a suitable portion of the blank, or butyl acetate, to a 2-cm absorption tube or cell and adjust the photometer to the initial setting, using a light band centered at approximately 635 mμ. While maintaining this photometer adjustment, take the photometric readings of the butyl acetate extract.[8] Determine the percentage of tungsten from a calibration curve or table prepared as follows: Transfer 0.200 g of iron containing negligible quantities of tungsten and molybdenum (NBS Ingot Iron Standard Sample 55d was used) to a 125-ml Erlenmeyer flask, and continue as directed in the procedure for dissolving a sample. Add 10 ml of sodium tungstate solution (1 ml≡100 μg of tungsten) to the flask just before adding the 20 ml of "fuming acid" mixture, and continue with the procedure until the solution is diluted to volume in a 100-ml volumetric flask (1 ml≡10 μg of tungsten). Prepare a blank iron solution by the same procedure, omitting the 10-ml addition of sodium tungstate solution. Add 25 ml of diluted sulfuric acid (1+3) to five 250-ml separatory funnels. Transfer none, 1.0, 2.0, 3.0, and 5.0 ml of iron-tungsten solution (1 ml≡10 μg of W), and 5.0, 4.0, 3.0, 2.0, and none ml, respectively, of blank iron solution[9] to the funnels. Heat the solution on a steam bath, and continue with the development of the tungsten color, beginning with: "add 50 ml of hydrochloric acid and 5 ml of stannous chloride solution." Plot the photometric readings of the calibration solutions with respect to micrograms of tungsten. Beer's Law is obeyed under the conditions specified, and blanks are usually negligible.

[7] The 15-minute heating period is required to remove the sulfur dioxide, which inhibits the development of the tungsten color; and to remove the chloroform, which would increase the volume of the solvent used to extract the tungsten-dithiol complex.

[8] The absorbancy of this extract varies with temperature, about 0.2 percent per degree; measurements should be made within a range of 5° C if an accuracy of 1 percent is required.

[9] The addition of blank solution is made to provide an adequate amount of iron for the complete development of the tungsten color.

5. Discussion and Results

The results obtained by the recommended procedure on a number of synthetic mixtures are given in table 1, as well as a few values obtained on mixtures containing copper, molybdenum, and tungsten, which were not filtered. Copper in 200-μg amounts does not interfere, as is shown in experiment 1. Molybdenum in the absence of copper is removed by the chloroform extraction of the dithiol-treated solution and does not interfere, as shown in experiments 2 and 3. In mixtures containing both elements in appreciable quantities, the black precipitate formed by copper on the addition of dithiol appears to occlude molybdenum, and the extraction step does not completely remove molybdenum. The result is that on solution of the black copper precipitate during the development of the tungsten color, molybdenum is also present and causes a positive error, as shown in experiments 4 and 5. A filtration step was therefore added to the procedure.

TABLE 1. *Results of determinations for tungsten by the recommended procedure in various synthetic mixtures*

Experiment	Iron added	Molybdenum added	Copper added	Tungsten		
				Added	Found	Difference
	mg	μg	μg	μg	μg	μg
1[a]	10	------	200	------	0.1	+0.1
2[a]	10	30	------	20.0	20.0	.0
3[a]	20	50	------	50.0	49.5	−.5
4[a]	10	50	200	------	6.4	+6.4
5[a]	10	30	200	20.0	23.5	+3.5
6	------	50	------	20.0	19.4	−0.6
7	1	50	------	20.0	19.8	−.2
8	5	50	------	20.0	19.8	−.2
9	20	50	------	20.0	19.9	−.1
10	30	50	------	20.0	20.2	+.2
11	50	50	------	20.0	24.5	+4.5
12	100	50	------	20.0	33.1	+13.1
13	100	------	------	20.0	19.8	−0.2
14	10	50	200	------	0.5	+.5
15	10	50	------	1.0	1.0	.0
16	10	50	------	2.0	1.9	−.1
17	20	50	200	5.0	5.1	+.1
18	20	50	200	20.0	20.0	.0
19	20	50	50	20.0	19.7	−.3
20	24	100	10	20.0	20.0	.0
21	20	50	200	50.0	49.8	−.2
22	20	50	------	50.0	49.5	−.5

[a] Not filtered to remove copper precipitate.

Iron also inhibits the removal of molybdenum by the dithiol extraction step, and the extent of this interference is shown by experiments 7 to 12. About 30 mg of iron can be tolerated satisfactorily in the presence of molybdenum, or combinations of molybdenum and copper. The high sensitivity of the tungsten-dithiol reaction allows small amounts (0.005 percent or more) of tungsten to be determined quite satisfactorily, as shown by experiments 14 to 22. Experiment 6 shows the necessity for the presence of a small quantity of iron; a low recovery is obtained in the absence of iron [2]. As is shown by experiment 13, the accuracy of the tungsten determination is satisfactory in the presence of considerable iron if molybdenum is absent. A few experiments on 100-mg samples of NBS Ingot Iron

Standard Sample 55d indicated that an additional quantity (7 to 8 ml) of sulfuric-sulfurous acid solution and of thioglycolic acid (0.2 ml) helped in the removal of small amounts of molybdenum, and that this standard, used in preparing calibration curves, contains tungsten in amounts of the order of 1 or 2 ppm. A few experiments, in which copper and molybdenum were largely removed by treatment with hydrogen sulfide and filtration, indicated values of the same order.

The reaction of molybdenum with dithiol also appears to be sensitive to temperature. Although this particular point was not studied extensively, the reaction is too slow in the presence of iron at 10° to 15° C to be useful. The reaction temperature of 30° to 40° C was selected on the basis of convenience and a reasonable time for the removal of molybdenum.

Because the only difficulty encountered was the occasional incomplete extraction of molybdenum at the proper point (a complaint common to many of the published procedures using dithiol), photometric readings were also taken at approximately 720 mμ to detect a failure of this sort. A change in ratio of the absorbancy at 635 mμ to that at 720 mμ will indicate the presence of molybdenum; in fact, a procedure has been suggested [15] for the simultaneous determination of molybdenum and tungsten by photometric measurements at two different wavelengths. Dithiol and thioglycolic acid were ordered in small quantities and stored in a refrigerator. Difficulties were not encountered with prepared solutions of these reagents if they were stored in the refrigerator and used within a few days.

During a study of the thiocyanate photometric method for tungsten it was found that a relatively rapid and complete reduction of tungsten by stannous chloride in strong hydrochloric acid solution occurred in the presence of a trace of copper. Because this reduction is also required in the dithiol procedure, a similar technique was applied. Variations in the recovery of tungsten with several time intervals for color development, and with several amounts of stannous chloride and dithiol solutions are illustrated in figure 2. The conditions selected in the recommended procedure are about the minimum required to give a satisfactory development of the tungsten-dithiol complex in the range 1 to 50 μg of tungsten. The volume at the beginning of the color-development step is usually about 30 ml, but in handling small percentages of tungsten requiring larger sample aliquots, a larger volume is usually obtained. Volumes of up to 75 ml, containing 20 μg of tungsten, have been satisfactorily handled, as shown in figure 2.

A few experiments in which a second extraction with butyl acetate was made, indicate the tungsten-dithiol complex is completely (more than 99 percent) extracted in one treatment. The results of experiments in which extra dithiol is added to an extracted solution, followed by reheating, cooling, and extraction of any additional complex with butyl acetate, indicate that the reaction is essentially complete in the 10-minute period specified in the procedure. A

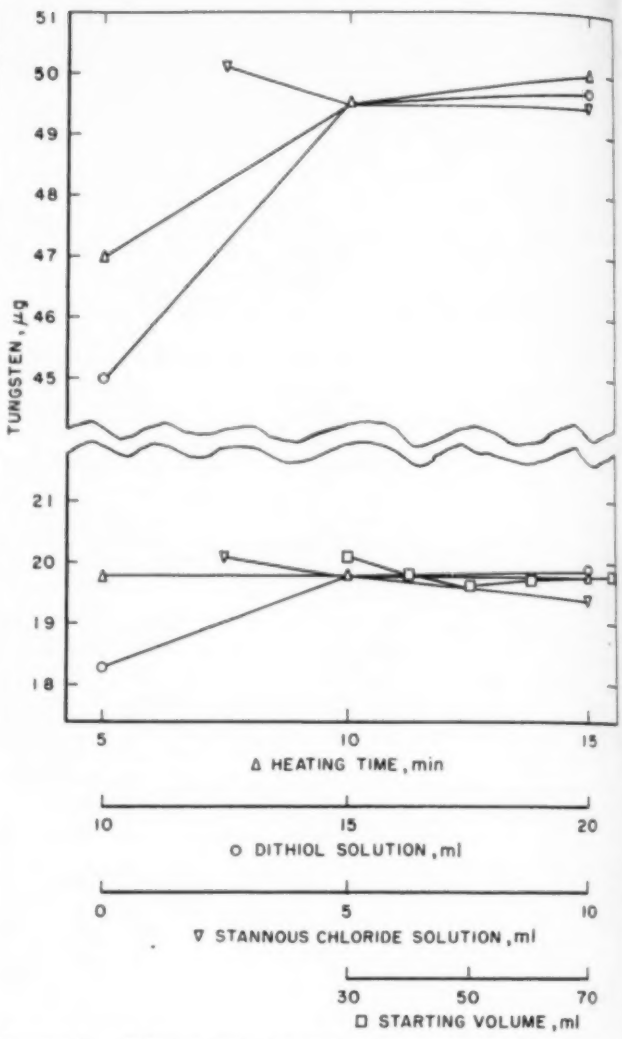

FIGURE 2. *Effect of variables on the development of the tungsten dithiol complex.*

small amount (less than 1 percent) of the tungsten present is lost during the chloroform extraction of molybdenum. This loss was checked by the evaporation of several combined chloroform extracts with sulfuric acid and hydrogen peroxide, followed by a determination of the tungsten present in the resulting solution, as described in the recommended procedure.

The results obtained on a few of the National Bureau of Standards Standard Samples of steel are shown in table 2. The values for NBS Standard Samples 159, 123, 160, and 101d have not been previously determined, because a satisfactory method for the determination of such small quantities of tungsten in these types of alloys has not been available. The values for NBS Standard Samples 123b, 155, 153, 134, 134a and the NBS Spectrographic Steel Standards 442, 443, and 444 show satisfactory agreement, considering the complexity of the materials and of the procedures used in the original analyses. The higher values given for the NBS Spectrographic Steel Standard Samples 446 and 846

TABLE 2. *Results of determinations for tungsten by the recommended procedure in various National Bureau of Standards Standard Samples*

NBS Standard Sample	Tungsten				Number of determinations	Weight of sample	Type of steel
	Certificate value	Found	Difference	Range			
	%	%	%	%		mg	
159	.....	0.005	.....	0.005	2	20	Cr 1.0, Mo 0.4, Ag 0.1.
123	.....	.005	.....	0.005 to 0.006	3	20	Cr 18, Ni 11, Nb 0.4.
160	.....	.011	.....	0.011	2	20	Cr 19, Ni 9, Mo 3.
101d	.....	.016	.....	0.015 to 0.016	3	20	Cr 19, Ni 9.
442	0.08	.078	.....	0.078	2	20	Stainless-steel spectrographic standards.
443	.09	.085	.....	0.084 to 0.087	3	20	
444	.18	.167	−0.01	0.165 to 0.169	4	10 to 20	
123b	.18	.174	−.01	0.173 to 0.175	4	20	Cr 19, Ni 11, Nb 0.8, Ta 0.2.
155	.517	.519	+.002	0.516 to 0.521	4	4 to 10	Cr 0.5, W 0.5.
153	1.58	1.55	−.03	1.54 to 1.55	6	2.5	Mo 8, Co 8, Cr 4, V 2.
134	1.82	1.87	+.05	1.87	2	2.5	Mo 7, Cr 4, V 2.
134a	2.01	2.05	+.04	2.04 to 2.06	6	2.5	Mo 8, Cr 4, V 1.
446 and 846	.....	0.043	.....	0.043 to 0.044	6	10 to 20	Cr 18, Ni 9, Mo 0.4, Cu 0.2.
446 and 846	.....	[a].048	.....	0.044 to 0.050	8	10	
446 and 846	.....	[a].055	.....	0.052 to 0.059	8	20	

[a] Not filtered to remove copper precipitate.

where the copper precipitate is not removed demonstrate the range of error that will be encountered, and the necessity for the steps in the procedure that allow for more than residual amounts of copper and molybdenum. The ranges given in table 2 show the excellent precision of the method.

Table 3 shows tests made with 15 elements mentioned as reacting with dithiol or otherwise interfering in the detection of tungsten. As will be seen, none of these elements in the amounts tested inhibit the removal of molybdenum or hinder the development of the tungsten color, and quite satisfactory recoveries of tungsten are obtained. Satisfactory determinations were also obtained in the presence of 500 mg of citric or tartaric acid.

TABLE 3. *Results of determinations for tungsten by the recommended procedure in the presence of possible interfering elements*

Experiment	Other element added	Iron added	Molybdenum added	Tungsten		
				Added	Found	Difference
	μg	mg	μg	μg	μg	μg
1	200 Sb	10	50	20.0	19.9	−0.1
2	200 As	10	50	20.0	19.8	−.2
3	200 Bi	10	50	20.0	19.9	−.1
4	5,000 Cr	10	50	20.0	19.8	−.2
5	2,000 Co	10	50	20.0	20.2	+.2
6	2,000 Co	10	50	20.0	19.9	−.1
7	200 Pb	10	50	20.0	19.8	−.2
8	200 Mn	10	50	20.0	19.9	−.1
9	200 Hg	10	50	20.0	19.8	−.2
10	4,400 Ni	10	50	20.0	19.9	−.1
11	600 Pt	10	50	20.0	19.8	−.2
12	200 Re	10	50	20.0	19.8	−.2
13	200 Se	10	50	20.0	19.9	−.1
14	200 Ag	12	50	20.0	19.9	−.1
15	2,000 Sn	10	50	20.0	20.1	+.1
16	200 V	10	50	25.0	24.9	−.1

The reaction of some of these elements with dithiol may be of interest. The rhenium compound with dithiol is visually indistinguishable from that of molybdenum. Bismuth forms a brown precipitate, which is extracted by chloroform; tin behaves similarly except that the precipitate is red. Silver forms a black precipitate and, like copper, is removed by filtration. Selenium behaves similarly, forming a brown or pink precipitate. Platinum added as chloroplatinate divides, a part being removed by filtering the brown precipitate formed. The remainder reacts on the addition of stannous chloride during the development of the tungsten color to form a yellow complex, which is extracted by butyl acetate. An "off-colored" solution is obtained, but the extraneous color does not interfere when the absorbancy of the solution is measured at 635mμ as directed. Cobalt forms a blue complex on the addition of hydrochloric acid, but in the amount used in the test does not appear to interfere. The remaining elements did not give visible reactions in the concentrations tested.

6. References

[1] S. H. Allen and M. B. Hamilton, Anal. Chim. Acta **7,** 483 (1952).
[2] S. H. Allen and M. B. Hamilton, Anal. Chim. Acta. **7,** 487 (1952).
[3] B. Bagshaw and R. J. Truman, Analyst **72,** 189 (1947).
[4] C. F. Bickford, W. S. Jones and J. S. Keene, J. Am. Pharm. Assoc. **37,** 255 (1948).
[5] C. E. Crouthamel and C. E. Johnson, Anal. Chem. **26,** 1288 (1954).
[6] P. Greenberg, Anal. Chem. **29,** 896 (1957).
[7] J. H. Hamence, Analyst **65,** 152 (1940).
[8] W. H. Hillebrand, G. E. F. Lundell, H. A. Bright and J. I. Hoffman, Applied inorganic analysis, 2d ed., p. 686 (J. Wiley & Sons, Inc., New York, N. Y., 1953).
[9] L. Ikenberry, J. Leo Martin and W. J. Boyer, Anal. Chem. **25,** 1340 (1953).
[10] C. M. Johnson, Iron Age **157,** No. 14, 66–69 (1944)
[11] Methods of Analysis Committee, J. Iron Steel Inst. **172,** 413 (1952).
[12] Methods of Analysis Committee, J. Iron Steel Inst. **178,** 267 (1954).
[13] C. C. Miller and A. J. Lowe, J. Chem. Soc. **40,** 1262 (1940).
[14] C. C. Miller, Analyst **69,** 109 (1944).
[15] A. A. North, Analyst **81,** 660 (1956).
[16] R. Pemberton, Analyst **77,** 290 (1952).
[17] C. S. Piper and R. S. Beckwith, J. Soc. Chem. Ind. (London), **67,** 374 (1948).
[18] H. G. Short, Analyst **76,** 710 (1951).
[19] E. J. Vaughan and C. Whalley, J. Iron Steel Inst. **155,** 549 (1947).
[20] H. Yagoda and H. A. Fales, J. Am. Chem. Soc. **58,** 1495 (1936).

7. Appendix

7.1. Determination of Tungsten in Titanium

At the request of the Watertown Arsenal Task Force for the determination of tungsten in titanium metal, tungsten was determined by the dithiol procedure in their samples WA–22 and WA–8. Because titanium phosphate in quantity is not very soluble in sulfuric-phosphoric acid mixtures, the procedure was modified to provide a suitable solution for titanium-base alloys.

7.2. Modified Procedure

Transfer 0.2 g of the sample to a 125-ml Erlenmeyer flask, add 20 ml of diluted sulfuric acid (1+3) and 2 or 3 drops of hydrofluoric acid. Heat gently until the sample is dissolved and add, drop by drop (about 6 to 8 drops are required) hydrogen peroxide (30 percent) until the purple color of reduced titanium is discharged and a permanent yellow color of peroxidized titanium is formed. Evaporate the solution to fumes, and cool. Add 50 ml of diluted sulfuric acid (1+3) containing a gram of citric acid, and digest a few minutes to obtain a clear solution. Cool, transfer the solution to a 100-ml volumetric flask, and dilute to the mark with diluted sulfuric acid (1+3).

Transfer a suitable aliquot, as indicated in table 4, of the prepared sample solution to a 250-ml separatory funnel. Add 0.2 ml of ferric sulfate solution (10 mg of iron per ml of diluted sulfuric acid (1+9)), 7.5 ml of diluted sulfuric acid (1+1), and 5 ml of dilute sulfuric acid (1+3) saturated with sulfur dioxide, and complete the determination as described for steel. Because most titanium alloys contain little copper or other similarly reacting elements in sufficient amount to require a filtration, this step was omitted on these samples.

TABLE 4. *Results of determinations for tungsten in titanium-base materials*

Sample	Tungsten			Molybdenum added	Iron added	Titanium present
	Added	Found	Difference			
	μg	μg	μg	μg	mg	mg
1.	10.0	10.1	+0.1	------	2	20
2.	10.0	10.2	+.2	50	2	20
3.	10.0	10.0	.0	------	------	20
4.	50.0	49.7	−.3	------	2	10
5.	50.0	49.5	−.5	50	2	10
6.	50.0	48.2	−1.8	------	------	10
	%	%	%			
WA–8	------	0.372	------	------	2	10
	------	.368	------	------	2	10
	------	.374	------	------	2	10
	------	.371	------	------	2	10
WA–22	------	.057	------	------	2	20
	------	.056	------	------	2	20
	------	.056	------	------	2	20
	------	.056	------	------	2	20

The results obtained on a few synthetic mixtures, and on two samples, are given in table 4. Titanium was added to the six synthetic mixtures as portions of a titanium solution prepared from National Bureau of Standards Standard Sample 173, a 6-percent aluminum, 4-percent vanadium titanium-base alloy containing approximately 0.001 percent of tungsten. The values obtained by the Watertown Task Force, by a double α-benzoinoxime precipitation and hydroquinone photometric method, average about 0.40 percent of tungsten for sample WA–8 and approximately 0.05 to 0.06 percent for sample WA–22. Greenberg [6] has reported 0.38 and 0.055 percent of tungsten for the same samples by a dithiol procedure.

WASHINGTON, JUNE 12, 1957.

Journal of Research of the National Bureau of Standards Vol. 59, No. 6, December 1957 Research Paper 2813

On the Most General Form of the Compatibility Equations and the Conditions of Integrability of Strain Rate and Strain

Edmund H. Brown

The most general forms of the equations of compatibility are derived by a very simple analysis in terms of the material strain rate tensor and the rate of change of the Riemann-Christoffel curvature tensor during the deformations. It is shown that recent statements on the significance of the compatibility equations, essentially that their satisfaction is equivalent to the condition that the space be locally Euclidean, are misinterpretations based on restricted forms of the equations. In addition, a new form of the conditions of integrability of strain is derived in terms of the rate of change of the curvature tensor.

1. Definitions and Notations

Because of the great variety of usage of authors in the field, a few of the definitions and notations employed here will be discussed briefly. However, a general knowledge of tensor analysis and modern elasticity is assumed. For the most general, and at the same time most readable introduction to tensor analysis, including applications to elasticity, the reader is referred to Brillouin [1];[1] for an excellent and thorough review of modern elasticity through 1953, despite a frequently cumbersome notation, the paper of Truesdell [2] is highly recommended; for more recent general discussions, the treatise of Green and Zerna [3], or the article of Doyle and Ericksen [4] should be consulted.

To introduce the strain tensor, we imagine a complete n-dimensional material continuum G which, with an arbitrarily chosen coordinate system x^i, is defined by the form of the metric tensor $g_{ij}=g_{ij}(x^k)$. To show the covariant character of some of the quantities involved it will occasionally be necessary to transform from one coordinate system to another. Following Craig [5] we shall indicate quantities in one coordinate system by use of indices from the group i, j, k, h, l, and quantities in a second coordinate system by indices from the group p, q, r, s, t. Thus, such a transformation will be defined by an analytic relation of the form $x^r=x^r(x^k)$. Further, for convenience, the components of the transformation matrices $\partial x^k/\partial x^r$ or $\partial x^r/\partial x^k$ will be denoted by $X^k_r=\partial x^k/\partial x^r$ or $X^r_k=\partial x^r/\partial x^k$. Similarly, $\partial^2 x^k/\partial x^s\partial x^r$ will be denoted by X^k_{rs}. During such a coordinate transformation, then, in one physical state, the components of the metric tensor will transform according to the tensor law, $g_{rs}=g_{ij}X^i_rX^j_s$, the Christoffel symbols, or connections, will transform according to the Christoffel law, $\Gamma^i_{\cdot jk}=\Gamma^r_{\cdot st}X^s_jX^t_kX^i_r+X^s_{jk}X^i_s$, and the components of the Riemann-Christoffel curvature tensor by the tensor law, $R_{pq|rs}=R_{ij|kh}X^i_pX^j_qX^k_rX^h_s$. Note that we use a short vertical stroke between indices to emphasize various symmetry properties. In addition, following Green and Zerna, we use a full vertical stroke behind a quantity, as in the identity $g_{ij|k}\equiv 0$, to indicate the covariant derivative.

A material coordinate system is defined by assigning a value x^i to each particle of the material continuum, which it retains during any subsequent deformation. We shall assume that the deformation, itself, depends on a single scalar parameter μ, independent of the coordinates x^k, which in dynamic problems can be identified with the time t. Since the material coordinates of a particle do not change during a deformation, we must have $x^k(\mu_2)=x^k(\mu_1)$. However, during the progress of the deformation the intrinsic quantities associated with the space, such as the metric tensor g_{ij}, must change, assuming a continuous set of values $g_{ij}(\mu_1)$, $g_{ij}(\mu_2)$, ... When we wish to indicate several stages during a deformation, the appropriate values of μ_1, μ_2, . . . will be used, but more often only two stages, an "initial" state and a "final" state, are of interest, so that, for instance, we can write for the "initial" metric tensor, g_{ij}, and for the "final" metric tensor $\bar{g}_{ij}$. In such cases, we shall make a general practice of indicating a final state by placing bars over quantities which in the initial state are unbarred.

[1] Figures in brackets indicate the literature references at the end of this paper.

At this time, it is well to note that, parallel to the "material" representation of quantities, a "spatial" treatment can be used: A complete n-dimensional geometric, or spatial, continuum H can be specified, using an arbitrarily chosen fixed spatial coordinate system y^i, by the form of the spatial metric tensor, $h_{ij}=h_{ij}(y^k)$. We imagine that the deformation of G takes place in H, that is, that there is a one-to-one correspondence between the "particles" of G and the "points" of H which, however, varies in form with μ. Thus, there is a "mapping" of G on H by $y^i=y^i(x^k,\mu)$, whose variation with μ represents the deformation of the material continuum. Since during the deformation, that is, during the variation of μ, the particles of G move through the points of H, $y^i(x^k,\mu_2)\neq y^i(x^k\mu_1)$, but at each given point y^i, spatial quantities such as h_{ij} and the spatial Riemann-Christoffel curvature tensor $S_{ij|kh}$ remain constant. There is nothing of course to prevent one assuming that the space H may change with parameters other than μ, a device which could possibly be of some use in discussions of plasticity; but for simplicity we shall avoid this here. In any case, a necessary condition that G remain in H is

$$R_{ij|kh}=S_{pq|rs}\frac{\partial y^p}{\partial x^i}\frac{\partial y^q}{\partial x^j}\frac{\partial y^r}{\partial x^k}\frac{\partial y^s}{\partial x^h}$$

at each value of μ.

Quantities such as strain can be related to either the material or spatial systems, whereas the displacement u^i is essentially spatial. Since we intend to discuss strain only, for convenience we will use chiefly a material representation and make little further reference to the spatial treatment. We should remark, however, that one of the principal applications of the results for non-Euclidean continua is in cases where (unlike our definitions above) the dimension of G is m, the dimension of H is n, and $m<n$, since they are useful in reduced problems involving shells and curved rods. These problems, however, require the introduction of $n-m$ other mth-order quantities ("changes in curvature", "changes in torsion", etc.) in addition to the strain, so that we shall not consider such possibilities here.

2. Introduction of Strain and Derivation of Results

We shall take as a measure of finite strain the quantity

$$^{(12)}e_{ij}(x^k)=\tfrac{1}{2}[g_{ij}(x^k,\mu_2)-g_{ij}(x^k,\mu_1)], \tag{1}$$

or, if we wish to think only of some particular initial and final states,

$$e_{ij}(x^k)=\tfrac{1}{2}[\bar{g}_{ij}(x^k)-g_{ij}(x^k)], \tag{2}$$

since—even though it is less used in the modern theory of finite elasticity—it reduces to the familiar strain tensor of "classical" theory, such as is found in Love [6], in the infinitesimal case. According to the above definition, strain depends merely on the initial and final states, and is independent of the way in which the deformation took place. Such a definition is too general for strain to be uniquely related to stress in more complex cases involving permanent set or plastic behavior. Thus, we are led to the introduction of the rate of strain tensor $\dot{e}_{ij}$ defined by

$$\dot{e}_{ij}=\frac{\partial e_{ij}}{\partial\mu}=\frac{1}{2}\frac{\partial g_{ij}}{\partial\mu}. \tag{3}$$

We note that, since differentiation with respect to the scalar parameter μ does not affect the character of g_{ij}, $\dot{e}_{ij}$ like g_{ij} is a tensor in the x^k coordinate system for a given value of μ. Similarly, since both $\bar{g}_{ij}$ and g_{ij} are tensors, the finite strain $^{(12)}e_{ij}$ is a tensor. However, though $\bar{x}^k=x^k$ for all μ, the identities (based on the hypothesis of a Riemann space, that is, that a unique measure exists) $\bar{g}_{ij}|_{\bar{k}}\equiv 0$ and $g_{ij}|_k\equiv 0$ do not allow us to conclude either that $g_{ij}|_{\bar{k}}\equiv 0$, or $\bar{g}_{ij}|_k\equiv 0$, since g_{ij} is not the metric tensor of $\bar{G}$, nor $\bar{g}_{ij}$ the metric tensor of G. In G, $\bar{g}_{ij}$ is merely a tensor field and not the metric tensor; similar statements can be made about the character of g_{ij} in $\bar{G}$.

Now, considering $\dot{e}_{ij}$ to be a tensor field in G, in accord with the usual requirements for raising and lowering indices, we must have

$$\dot{e}^{ij}=g^{ik}g^{jh}\dot{e}_{kh}=-\frac{1}{2}\frac{\partial g^{ij}}{\partial \mu} \tag{4}$$

and

$$\dot{e}^{i}_{.j}=g^{ik}\dot{e}_{kj}=\frac{1}{4}\left(g^{ik}\frac{\partial g_{kj}}{\partial \mu}-g_{kj}\frac{\partial g^{ik}}{\partial \mu}\right). \tag{5}$$

Just as the metric tensor g_{ij} changes during the deformation, the Christoffel connection $\Gamma^{i}_{.jk}$ based on g_{ij} must change. We shall define the rate of change $\dot{E}^{i}_{.jk}$ of $\Gamma^{i}_{.jk}$ by

$$\dot{E}^{i}_{.jk}=\frac{\partial \Gamma^{i}_{.jk}}{\partial \mu}. \tag{6}$$

However, since $\Gamma^{i}_{.jk}$ transforms, when the coordinates are changed at one physical state, by the Christoffel law, and none of the quantities x^k, X^{k}_{r}, X^{k}_{rs} are functions of μ,

$$\dot{E}^{r}_{.st}=\frac{\partial \Gamma^{r}_{.st}}{\partial \mu}=\frac{\partial \Gamma^{i}_{.jk}}{\partial \mu}X^{j}_{s}X^{k}_{t}X^{r}_{i}=\dot{E}^{i}_{.jk}X^{j}_{s}X^{k}_{t}X^{r}_{i}, \tag{7}$$

which shows that—unlike $\Gamma^{i}_{.jk}$—the quantities $\dot{E}^{i}_{.jk}$, and thus $\dot{E}_{i|jk}=g_{ih}\dot{E}^{h}_{.jk}$, are tensors, a fact first pointed out by Bergmann [7].

Just as $\Gamma^{i}_{.jk}$ can be expressed, for a Riemann space, in terms of the metric tensor,

$$\Gamma^{i}_{.jk}=\frac{1}{2}g^{ih}\left[\frac{\partial g_{hj}}{\partial x^{k}}+\frac{\partial g_{hk}}{\partial x^{j}}-\frac{\partial g_{jk}}{\partial x^{h}}\right],$$

so the $\dot{E}^{i}_{.jk}$ can be written in terms of the strain rate $\dot{e}_{ij}$; for

$$\dot{E}^{i}_{.jk}=\frac{\partial \Gamma^{i}_{.jk}}{\partial \mu}=\frac{1}{2}\frac{\partial g^{ih}}{\partial \mu}\left[\frac{\partial g_{hj}}{\partial x^{k}}+\frac{\partial g_{hk}}{\partial x^{j}}-\frac{\partial g_{jk}}{\partial x^{h}}\right]+\frac{1}{2}g^{ih}\frac{\partial}{\partial \mu}\left[\frac{\partial g_{hj}}{\partial x^{k}}+\frac{\partial g_{hk}}{\partial x^{j}}-\frac{\partial g_{jk}}{\partial x^{h}}\right], \tag{8}$$

or, since g_{ij} is an analytic function of x^i and μ, and x^i and μ are independent,

$$\dot{E}^{i}_{.jk}=-2\dot{e}^{ih}\Gamma_{h|jk}+g^{ih}\left[\frac{\partial \dot{e}_{hj}}{\partial x^{k}}+\frac{\partial \dot{e}_{hk}}{\partial x^{j}}-\frac{\partial \dot{e}_{jk}}{\partial x^{h}}\right]. \tag{9}$$

Similarly, $\dot{E}_{i|jk}$ can be shown to be given by

$$\dot{E}_{i|jk}=g_{ih}\dot{E}^{h}_{.jk}=-2\dot{e}_{ih}\Gamma^{h}_{.jk}+\left[\frac{\partial \dot{e}_{ij}}{\partial x^{k}}+\frac{\partial \dot{e}_{ki}}{\partial x^{j}}-\frac{\partial \dot{e}_{jk}}{\partial x^{i}}\right], \tag{10}$$

or

$$\dot{E}_{i|jk}=\frac{\partial \Gamma_{i|jk}}{\partial \mu}-2\dot{e}_{ih}\Gamma^{h}_{.jk}. \tag{11}$$

Using the expression for the covariant derivative of the second order tensor $\dot{e}_{ij}$, the three partial derivatives of $\dot{e}_{ij}$ appearing above may be written

$$\begin{aligned}
\frac{\partial \dot{e}_{hj}}{\partial x^{k}}&=\dot{e}_{hj}|_{k}+\dot{e}_{lj}\Gamma^{l}_{.hk}+\dot{e}_{hl}\Gamma^{l}_{.kj}\\
\frac{\partial \dot{e}_{hk}}{\partial x^{j}}&=\dot{e}_{hk}|_{j}+\dot{e}_{lk}\Gamma^{l}_{.hj}+\dot{e}_{hl}\Gamma^{l}_{.kj}\\
-\frac{\partial \dot{e}_{jk}}{\partial x^{h}}&=-\dot{e}_{jk}|_{h}-\dot{e}_{lk}\Gamma^{l}_{.jh}-\dot{e}_{jl}\Gamma^{l}_{.kh}.
\end{aligned} \tag{12}$$

On adding these expressions, interchanging indices where symmetry permits, we obtain

$$\frac{\partial \dot{e}_{hj}}{\partial x^k}+\frac{\partial \dot{e}_{hk}}{\partial x^j}-\frac{\partial \dot{e}_{jk}}{\partial x^h}=\dot{e}_{hj}|_k+\dot{e}_{hk}|_j-\dot{e}_{jk}|_h+2\dot{e}_{hl}\Gamma^l_{\cdot kj}. \tag{13}$$

Introducing this in the expressions for $\dot{E}^i_{\cdot jk}$ and $\dot{E}_{i|jk}$ in terms of the strain rate, and making use of the fact that $g^{ih}|_k \equiv 0$ results in the more elegant forms,

$$\dot{E}_{i|jk}=\dot{e}_{ij}|_k+\dot{e}_{ki}|_j-\dot{e}_{jk}|_i \tag{14}$$

and

$$\dot{E}^i_{\cdot jk}=\dot{e}^i_{\cdot j}|_k+\dot{e}_k{}^i|_j-\dot{e}_{jk}|^i. \tag{15}$$

We must, finally, consider how the Riemann-Christoffel curvature tensor $R^i_{\cdot j|kh}$ based on g_{ij} varies during the deformation. Defining $\dot{\mathscr{E}}^i_{\cdot j|kh}=\partial R^i_{\cdot j|kh}/\partial\mu$, this rate of change of curvature is given by

$$\begin{aligned}\dot{\mathscr{E}}^i_{\cdot j|kh}&=\frac{\partial}{\partial x^k}\left(\frac{\partial \Gamma^i_{\cdot jh}}{\partial\mu}\right)-\frac{\partial}{\partial x^h}\left(\frac{\partial \Gamma^i_{\cdot jk}}{\partial\mu}\right)+\frac{\partial \Gamma^l_{\cdot jh}}{\partial\mu}\Gamma^i_{\cdot lk}+\Gamma^l_{\cdot jh}\frac{\partial \Gamma^i_{\cdot lk}}{\partial\mu}-\frac{\partial \Gamma^l_{\cdot jk}}{\partial\mu}\Gamma^i_{\cdot lh}-\Gamma^l_{\cdot jk}\frac{\partial \Gamma^i_{\cdot lh}}{\partial\mu}\\&=\frac{\partial \dot{E}^i_{\cdot jh}}{\partial x^k}+\dot{E}^l_{\cdot jh}\Gamma^i_{\cdot lk}-\dot{E}^i_{\cdot lh}\Gamma^l_{\cdot jk}-\dot{E}^i_{\cdot lk}\Gamma^l_{\cdot hk}-\left(\frac{\partial \dot{E}^i_{\cdot jk}}{\partial x^h}+\dot{E}^l_{\cdot jk}\Gamma^i_{\cdot lh}-\dot{E}^i_{\cdot lk}\Gamma^l_{\cdot jh}-\dot{E}^i_{\cdot jl}\Gamma^l_{\cdot kh}\right),\end{aligned} \tag{16}$$

or

$$\dot{\mathscr{E}}^i_{\cdot j|kh}=\dot{E}^i_{\cdot jh}|_k-\dot{E}^i_{\cdot jk}|_h, \tag{17}$$

and similarly,

$$\dot{\mathscr{E}}_{ij|kh}=g_{il}\dot{\mathscr{E}}^l_{\cdot j|kh}=\frac{\partial R_{ij|kh}}{\partial\mu}-2\dot{e}_{il}R^l_{\cdot j|kh}=\dot{E}_{i|jh}|_k-\dot{E}_{i|jk}|_h, \tag{18}$$

both of which are especially elegant forms for the rate of change of the curvature tensor.

Just as in the case of $\dot{E}_{i|jk}$, we can express $\dot{\mathscr{E}}_{ij|kh}$ in terms of the strain rate, and, in doing so, we obtain the equations of compatibility in their most general form. By substitution and simple algebra these identities may be written

$$\dot{\mathscr{E}}_{ij|kh}=(\dot{e}_{ij}|_{hk}-\dot{e}_{ij}|_{kh})+(\dot{e}_{ih}|_{jk}-\dot{e}_{ik}|_{jh})-(\dot{e}_{jh}|_{ik}-\dot{e}_{jk}|_{ih}). \tag{19}$$

It is well to examine the significance of these equations. There is no reason for us to assume that the strain rate is a tensor function (which would require that $\dot{e}_{ij}$ satisfy certain conditions of integrability), for in the most general case, the $\dot{e}_{ij}$ would be merely the components of a tensor field. However, the curvature tensor $R_{ij|kh}$ is an intrinsic property of the material continuum G and must be related, as stated previously, to the curvature tensor $S_{ij|kh}$ of the spatial continuum H, in order that G remain in H. Thus, $\dot{\mathscr{E}}_{ij|kh}$ must be related to $S_{ij|kh}$ by an equation of the form

$$\dot{\mathscr{E}}^i_{\cdot j|kh}=S^p_{\cdot q|rs}\frac{\partial}{\partial\mu}\left[\frac{\partial x^i}{\partial y^p}\frac{\partial y^q}{\partial x^j}\frac{\partial y^r}{\partial x^k}\frac{\partial y^s}{\partial x^h}\right]. \tag{20}$$

We have assumed that H does not vary, that is, that the value of $S_{ij|kh}$ at each point y^k is constant. In particular, if $S_{ij|kh}\equiv 0$, $R_{ij|kh}\equiv 0$, and thus, of course $\dot{\mathscr{E}}_{ij|kh}$ must also vanish. If, however, $S_{ij|kh}$ is not zero, $\dot{\mathscr{E}}_{ij|kh}$ will be constant, or more strongly, zero, only if other special conditions hold.

The conditions of integrability of the rate of strain tensor must now be investigated. Using the relation for $\dot{\mathscr{E}}_{ij|kh}$, and the fact that $R_{ij|kh}$ is skew-symmetric in the indices of both pairs, we can write

$$\dot{\mathscr{E}}_{ij|kh}+\dot{\mathscr{E}}_{ji|kh}=-2[\dot{e}_{il}R^l_{\cdot j|kh}+\dot{e}_{jl}R^l_{\cdot i|kh}]. \tag{21}$$

However, the equations

$$\dot{e}_{il}R^l_{\cdot j|kh}+\dot{e}_{jl}R^l_{\cdot i|kh}=\dot{e}_{ij}|_{kh}-\dot{e}_{ij}|_{hk} \tag{22}$$

are merely the conditions of integrability; the vanishing of either side of the above equation implies that if $\dot{e}_{ij}$ is subjected to parallel transport around a closed curve, it will return to its initial value at the starting point, and thus, may be considered a tensor function of the coordinates x^i rather than merely a tensor field.

Thus, the rate of strain is integrable if any one of the following equations holds identically:

$$\begin{gathered}\dot{e}_{ij}|_{kh}-\dot{e}_{ij}|_{hk}=0\\ \dot{e}_{il}R^l_{\cdot j|kh}+\dot{e}_{jl}R^l_{\cdot i|kh}=0\\ \dot{\mathscr{E}}_{ij|kh}+\dot{\mathscr{E}}_{ji|kh}=0,\end{gathered} \tag{23}$$

the last of the equations being equivalent to the requirement that $\dot{\mathscr{E}}_{ij|kh}$ be skew-symmetric in its first two indices (it is already skew-symmetric in the second pair as a consequence of its definition). It should be noticed that these integrability conditions are distinct from the compatibility equations, and in particular, it is not necessary for $\dot{\mathscr{E}}_{ij|kh}$ to vanish for $\dot{e}_{ij}$ to be integrable.

If, however, the strain rate is integrable, and we substitute the first of the above conditions in the compatibility equations, they take the simpler form

$$\dot{\mathscr{E}}_{ij|kh}=(\dot{e}_{ih}|_{jk}-\dot{e}_{ik}|_{jh})-(\dot{e}_{jh}|_{ik}-\dot{e}_{jk}|_{ih}). \tag{24}$$

In a great many practical cases, either the space is Euclidean, or some special relation may hold, such that $\dot{\mathscr{E}}_{ij|kh}=0$, which reduces the compatibility equations to the form

$$\dot{e}_{ih}|_{jk}-\dot{e}_{ik}|_{jh}=\dot{e}_{jh}|_{ik}-\dot{e}_{jk}|_{ih}. \tag{25}$$

It is of some interest to see the forms which the last equations take when $n\leq 3$. If $n=1$, all indices must be identical and we have, merely, $0=0$. If $n=2$, only two indices can be distinct, resulting in only one independent equation

$$\dot{e}_{ii}|_{kk}+\dot{e}_{kk}|_{ii}=2\dot{e}_{ik}|_{ik}, \qquad i\neq k, \tag{26}$$

indices not summed.

If $n=3$, three indices may be distinct, and two independent sets of, in all, six equations may be derived:

$$\dot{e}_{ii}|_{kk}+\dot{e}_{kk}|_{ii}=2\dot{e}_{ik}|_{ik} \qquad i\neq k, \tag{27}$$

indices not summed (3 equations), and

$$\dot{e}_{ii}|_{jk}+\dot{e}_{jk}|_{ii}=\dot{e}_{ij}|_{ik}+\dot{e}_{ik}|_{ij}, \qquad i\neq j\neq k, \tag{28}$$

indices not summed (3 equations).

The last two sets of equations, for $n=3$, are equivalent to those given by A. E. H. Love in Cartesian coordinates. Thus, our completely general form of the compatibility equations reduces to the more well-known form for the appropriate conditions.

We note that, since μ is a scalar parameter independent of x^i, derivatives of the infinitesimal strain tensor $de_{ij}=\dot{e}_{ij}d\mu$ may be written $de_{ij}|_k=\dot{e}_{ij}d\mu|_k=\dot{e}_{ij}|_k d\mu$. Similarly, derivatives of the finite strain $e_{ij}=\int\dot{e}_{ij}d\mu$ may be written $e_{ij}|_k=\int\dot{e}_{ij}d\mu|_k=\int\dot{e}_{ij}|_k d\mu$. Thus, all the relations and conditions derived above hold equally well for both the infinitesimal and finite strain tensors.

In conclusion, we can state the equations of integrability and the equations of compatibility are two independent sets of conditions. Satisfaction of the former implies that the

space to which the deforming medium is assigned is Euclidean. Satisfaction of the latter implies the medium remains in that assigned space. The fact that both must hold for the solution of actual problems in elasticity should not lead to considering them as identical, for each has its own physical significance.

3. References

[1] L. Brillouin, Les tenseurs en méchanique et en élasticité (Dover Publications, New York, N. Y., 1946).
[2] C. Truesdell, The mechanical foundations of elasticity and fluid dynamics, J. Rational Mech. and Anal. **1**, Nos. 1 and 2 (1952).
[3] A. E. Green and W. Zerna, Theoretical elasticity (Oxford Univ. Press, New York, N. Y., 1954).
[4] T. C. Doyle and J. L. Ericksen, Nonlinear elasticity, Advances in Appl. Mech. **4**, (1956).
[5] H. V. Craig, Vector and tensor analysis (McGraw Hill Book Co., Inc., New York, N. Y., 1943).
[6] A. E. H. Love, Theory of elasticity (Dover Publications, New York, N. Y., 1944).
[7] P. G. Bergmann, Theory of relativity (Prentice-Hall, Inc., New York, N. Y., 1946).
[8] A. S. Lodge, Compatibility equations for large strains, Quart. J. Mech. and Appl. Math. **4**, (1951).
[9] F. D. Murnaghan, Finite deformation of an elastic solid (John Wiley & Sons, Inc., New York, N. Y., 1951).

Boulder, Colo.

July 1, 1957.

Journal of Research of the National Bureau of Standards Vol. 59 No. 6, December 1957 Research Paper 2814

An Apparatus for Measuring the Piezoresistivity of Semiconductors[1]

R. F. Potter[2] and W. J. McKean

A detailed description is given of an apparatus and procedure designed to measure the piezoresistive effect in semiconductors over an extended temperature range. A tensile force up to 1 kilogram can be applied to the sample by means of a calibrated beam balance. The apparatus has been used for measurements on indium antimonide over the range 78° K to 300° K, and tensile stresses of the order of 5×10^7 dynes per square centimeter can be applied to samples that are cut in a special manner.

In modern solid-state physics, phenomena such as electrical conduction, Hall effect, and optical absorption have been studied extensively because of their direct connection with a well-developed theory of semiconductors. More recently several other effects have been receiving an increasing amount of attention by both the theorist and experimentalist; some of these are cyclotron resonance, photoelectromagnetic effect, magnetoresistivity, and piezoresistivity.

The latter parameter has been studied for some time in connection with metals, but it is only in comparatively recent years that large anisotropic changes in the resistivity with applied stress were measured for single crystals with cubic symmetry. Smith [1][3] measured large effects for both n- and p-type crystals of germanium and silicon at room and liquid-nitrogen temperatures, thus adding further to the evidence that the energy surfaces for electrons in these crystals are not spheres but ellipsoids. More recently, Morin, Geballe, and Herring [2] reported on measurements in which the piezoresistive effect was produced with compressive stress. Herring [3] has discussed the above phenomena in terms of a theory of "simple many-valley" semiconductors, which seems to describe the conduction bands for silicon and germanium, and possibly several III–V compound semiconductors.

The piezoresistivity coefficients are the elements of a fourth-rank tensor; the form has been given by Smith [1] for cubic crystals of the O_h and T_d classes, which apply to crystals of the diamond and zinc blende lattices, respectively, and is given by

$$\Pi=\begin{vmatrix} \Pi_{11} & \Pi_{12} & \Pi_{12} & 0 & 0 & 0 \\ \Pi_{12} & \Pi_{11} & \Pi_{12} & 0 & 0 & 0 \\ \Pi_{12} & \Pi_{12} & \Pi_{11} & 0 & 0 & 0 \\ 0 & 0 & 0 & \Pi_{44} & 0 & 0 \\ 0 & 0 & 0 & 0 & \Pi_{44} & 0 \\ 0 & 0 & 0 & 0 & 0 & \Pi_{44} \end{vmatrix}, \tag{1}$$

a form quite analogous to that for the elastic constants. The Π-constants are defined as follows:

$$\frac{\Delta\rho_{\alpha\beta}}{\rho_o X_{ij}}=\Pi_{\alpha\beta ij} \qquad \begin{aligned} \Pi_{11}&=\Pi_{11,\,11} \\ \Pi_{12}&=\Pi_{11,\,22} \\ \Pi_{44}&=\Pi_{12,\,12}. \end{aligned} \tag{2}$$

X_{ij} is the applied stress, and ρ is the resistivity, where the cubic axes are taken as the reference axes.

The change of resistance in a material is measured when a stress is applied in a given direction to a crystal while a constant current flows at a given angle to the stress direction. As in the case of elastic constants for a cubic material, three independent measurements must be made to determine the elements of the tensor of formula 1. Smith measured the longitudinal and the transverse effects in two samples of different orientations. The fourth determination served as a check on the other three. The longitudinal effect is defined as the relative change observed in the resistance per applied stress when both current and stress have the same direction. The transverse effect is measured when current and stress are perpendicular to each other.

In converting the resistance to resistivity it is necessary to consider the contraction due to strain. The piezoresistivity coefficients are given by the formulas

$$\Pi'_{11}=\frac{\Delta\rho'_{11}}{\rho_o X'_{11}}=\frac{\Delta R'_{11}}{R_o X'_{11}}-(S'_{11}-S'_{12}-S'_{13}) \qquad \text{(long.)}$$

$$\Pi'_{12}=\frac{\Delta\rho'_{22}}{\rho_o X'_{11}}=\frac{\Delta R'_{22}}{R_o X'_{11}}+(S'_{11}-S'_{12}+S'_{13}) \qquad \text{(trans.)}, \tag{3}$$

where S'_{ij} are the elastic compliances for the orientation used. Values for S_{ij} have been determined for silicon [4], germanium [4], and indium antimonide [5]. The Π'_{ij} are related to the elements of the tensor (1) by

$$\begin{aligned} \Pi'_{11}&=\Pi_{11}-2\Gamma\Pi' \\ \Pi'_{12}&=\Pi_{12}+\gamma\Pi', \end{aligned} \tag{4}$$

[1] This research was supported by the United States Air Force through the Air Force Office of Scientific Research of the Air Research and Development Command under Contract CSO 670-53-12.

[2] Present Address—U. S. Naval Ordnance Laboratory, Corona, Calif.

[3] Figures in brackets indicate the literature references at the end of this paper.

where $\Pi' = \Pi_{11} - \Pi_{12} - \Pi_{44}$, and Γ and γ are orientation factors related to the direction cosines of axes along the length and width of the sample as follows:

$$\Gamma = l_1^2 m_1^2 + n_1^2 m_1^2 + n_1^2 l_1^2,$$
$$\gamma = l_1^2 l_2^2 + m_1^2 m_2^2 + n_1^2 n_2^2. \quad (5)$$

A program was recently undertaken at the Bureau to study the piezoresistivity of the cubic semiconductor indium antimonide. (Concurrent studies were made of the magnetoresistivity of this material.)

Because of the nature and properties of the material, several considerations had to be taken in the design of an apparatus to measure piezoresistance. First was the matter of temperature. Reasonably pure indium antimonide is intrinsic at room temperature, whereas it is certainly extrinsic at 78° K; therefore, the temperature range down to that of liquid nitrogen had to be the minimum range studied. Indium antimonide is extremely brittle; a suitable method of clamping the sample had to be devised in order that known stresses could be applied along the axes of the sample. It is felt that the resultant design more than adequately solved the special problems posed by these properties.

A tensile-stress system was selected as being the simplest to apply and to measure in a closed system. As shown in figure 1, a balance beam (S) graduated in 100-g intervals up to 1 kg was devised and along which a weight (U) could be moved. Counterbalance weights (J and K) could be adjusted so that the beam balanced with zero load. The load was transmitted to the sample by means of a thin piano wire (N), which was coaxial with an inner stainless-steel tube (Q), which in turn was coaxial with the outer stainless-steel tube (P). As the load was applied or removed, the wire suffered a plastic strain, which could be compensated by moving the fulcrum (R) up or down by means of a nut (D). A given load could be applied or removed quickly by turning the handle (C), which activated the attached cam arrangement.

Figure 2 shows a schematic cross section of the sample holder. The problem of applying pure tensile stress to the sample was solved as follows. A magnetostrictive machine was used for cutting flat specimens into a suitable form for resistivity measurements by the standard four-probe method; a special die was made to produce samples of the shape shown in figure 3. Each end of the sample was placed in a clevis with a pin through the eye (see fig. 2). The upper clevis (L) was attached to the piano wire; and the bottom clevis (S) was the upper part of a screw. A spherical-shaped nut (V) on this screw seated in a mating socket allowed the sample to aline its axis in the direction of the applied tensile stress. This arrangement also permitted further adjustment in the vertical position of the sample. It was eventually

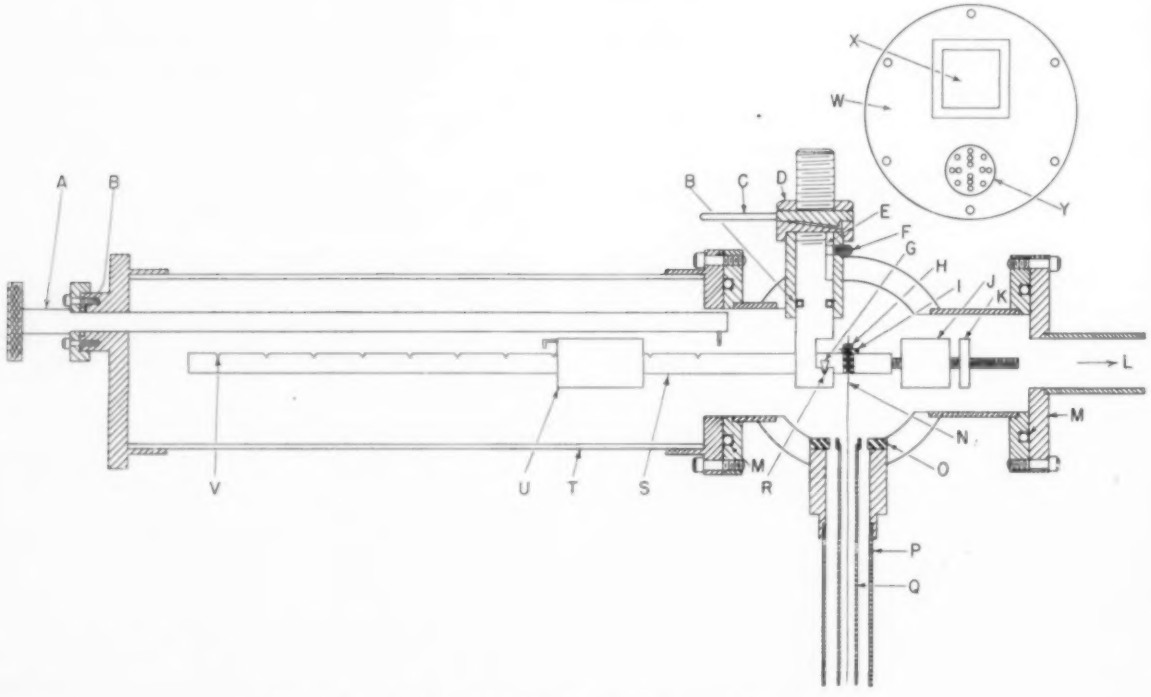

FIGURE 1. *Schematic drawing of the balance-beam mechanism.*

The entire system is enclosed with the sample. The balance-arm rider and the vertical position of the fulcrum can be adjusted by external manipulation. For dentification, the components are lettered as follows: A, Rider pickup arm; B, sliding O-ring vacuum seals (2); C, quick tension release; D, fulcrum height-adjusting screw; E, keyway; F, key; G, knife edge (hardened steel); H, tension wire bushing; I, Teflon insulator; J, zero-adjusting weight (coarse); K, zero-adjusting weight (fine); L, opening to vacuum line; M, static O-ring vacuum seals (2); N, tension wire (0.006-in.-diam. piano wire); O, upper guide (Teflon); P, outer stainless-steel tubing (½-in. o. d. by 0.020-in. wall); Q, inner stainless-steel tubing (3/16-in. o. d. by 0.004-in. wall); R, fulcrum (hardened steel); S, beam; T, Pyrex-glass tubing; U, rider; V, detents (11, 100 g apart); W, front cover for balance mechanism; X, glass inspection port; Y, 14-lead hermetic seal.

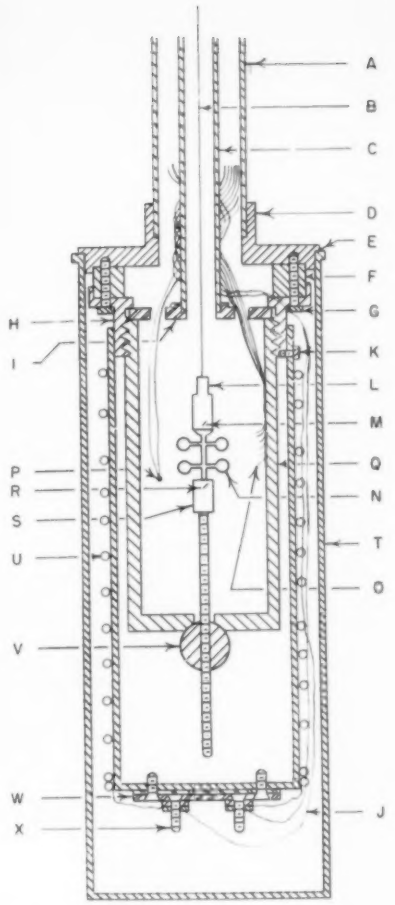

FIGURE 2. *Schematic drawing of the sample and holder.*

By means of the pins through the sample ends, the sample axis lines up with the applied stress. For identification the components are lettered as follows: A, Outer stainless-steel tubing (½-in. o. d. by 0.020-in. wall); B, tension wire (0.006-in.-diam. piano wire); C, inner stainless-steel tubing (3/16-in. o. d. by 0.004-in. wall); D, top; E, vacuum-tight removable solder joint (Wood's metal); F, lava thermal insulator; G, stainless-steel screws; H, frame holder; I, lower guide (Teflon); J, heater leads; K, heater retaining screw; L, upper clevis; M, clevis pin; N, sample; O, contact leads; P, thermocouple; Q, frame; R, clevis pin; S, lower clevis; T, outer can; U, heater; V, lower spherical adjusting nut; W, Teflon insulation; X, heater binding posts.

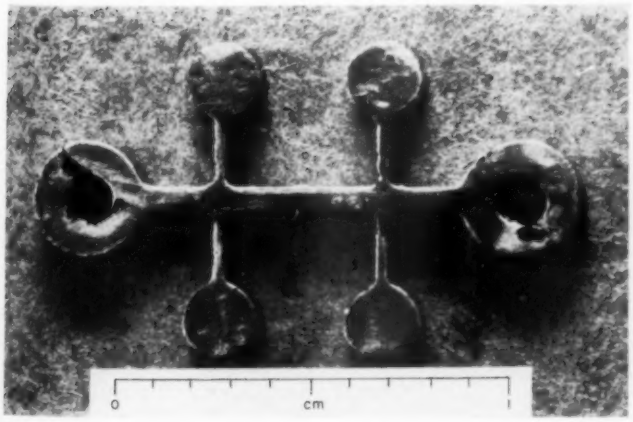

FIGURE 3. *Typical sample used with the apparatus.*

determined that a sample of this type and size (approximately 10^{-2} cm² cross section) can be safely recycled many times with loads up to 500 g.

An aluminum shield may be placed around the sample holder. On the outside of this shield is wound a Kanthal wire heater (U) for temperature control. A brass can (T) was soldered in place with Wood's metal; the entire interior could be evacuated or filled with a gas of suitable pressure. For use at temperatures between 78° and 300° K a Pyrex envelope was placed about the sample can and the stainless-steel tube (see fig. 4). This envelope was attached to a roughing pump, and the pressure of the gas inside varied from 1 atm to a few microns of mercury; this allowed the heat leak from the sample to be controlled when a suitable refrigerant bath was placed around the envelope. (For lower temperatures, e. g., 4° or 20° K, the envelope can be replaced by a Dewar designed for holding liquid helium or liquid hydrogen. Figure 4 shows the assembled apparatus with the Pyrex envelope.

Measurements on both *n*- and *p*-type indium antimonide have been made at temperatures between 78° and 300° K, and the results are reported elsewhere [6]. The resistances were measured by the potentiometric method, using a type K–2 potenti-

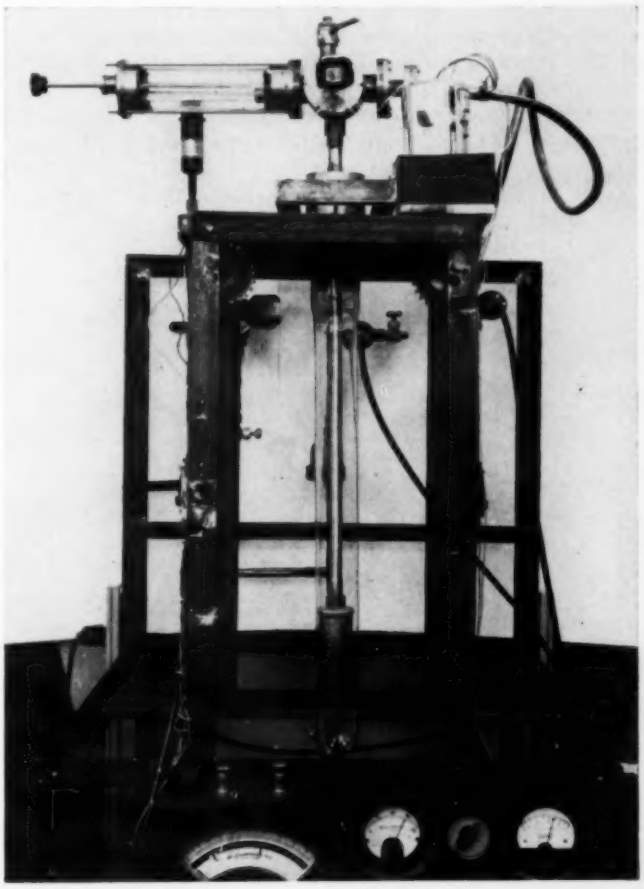

FIGURE 4. *Assembled apparatus with the Pyrex envelope.*

The frame supports associated vacuum lines, valves, meters, and pressure gages. It can also support a double Dewar for measurements in the liquid-helium range.

ometer a breaker-type d-c amplifier in place of the galvanometer. The output of the amplifier was fed to a driven chart recorder, so that as the load was changed the incremental change in resistance was recorded by the unbalanced potentiometer. Checks were made to insure that currents due to the unbalance has negligible effects. Effects due to changes in the ambient temperature were observed on the recorder and the necessary corrections made.

Samples were prepared in the following manner. Disks 2 mm thick and about 1 in. in diameter were sawed from single-crystal material with (001) axes normal to their flat surfaces. These were lapped to a thickness of 1.0 to 1.1 mm, taking care that both sides were parallel. The disks were then mounted on plate glass with glycol phthalate. An X-ray Laue back-reflection photograph was taken normal to the exposed side of each disk and analyzed. From the analysis the axes of the specimens were selected to lie along a particular orientation. A rotary milling table was used on the magnetostrictive machine so that the sample could be accurately oriented with respect to the tool. Indium electrodes were soldered to the four side arms and along the sides of the dumbbell-shaped ends. For the longitudinal effect, the end electrodes were used for the current leads, and two side arms were used for the potential leads. For the transverse measurements, the areas between a pair of arms on each side of the specimen were copper plated by applying a copper-sulfate solution momentarily and then rinsing, taking care that no short circuit across the sample occurred. The measurements were made by having one current lead and one potential lead opposite to another such pair while the stress was applied along the sample axis. As pointed out by Smith [1], the current lines are not straight across the sample. Hence, a correction must be made if the piezoresistive coefficients deduced from transverse and longitudinal measurements show appreciable differences.

It is felt that the apparatus has solved the special problems that are inherent in this type of measurement and a material like indium antimonide. Determination of the longitudinal effect by means of this apparatus if used in conjunction with hydrostatic-pressure measurements (cf. Long [7], Keyes [8], or Bridgman [9]) would eliminate the need for the transverse measurements. With a slight modification of the sample holder to insure a fixed orientation of the sample with respect to a magnetic field, one could also determine changes of the Hall coefficient and magnetoresistivity caused by applied stresses.

---

[1] C. S. Smith, Phys. Rev. **94,** 42 (1954).
[2] F. S. Morin, T. H. Geballe, and C. Herring, Phys. Rev. **105,** 525 (1957).
[3] C. Herring, Bell System Tech. J. **34,** 237 (1955).
[4] H. J. McSkimin, J. Appl. Phys. **24,** 988 (1953).
[5] R. F. Potter, Phys. Rev. **103,** 47 (1956).
[6] R. F. Potter, Bul. Am. Phys. Soc. [II] **2,** 121 (1957); Phys. Rev. **108** (1957).
[7] D. Long, Phys. Rev. **99,** 388 (1955).
[8] R. W. Keyes, Phys. Rev. **99,** 490 (1955).
[9] P. W. Bridgman, Proc. Am. Acad. Arts Sci. **60,** 305(1925)

WASHINGTON, May 6, 1957.

INDEX TO VOLUME 59

July to December 1957—Research Papers 2768 to 2814

A

Page

Acids, intercomparison of, RP2769 9
Algebraic number theory: Computation of cyclic cubic units, RP2783 155
Alkali-aggregate reaction in concrete, physical-chemical studies, RP2780 127
Allen, H. C., Jr., E. K. Plyler, L. R. Blaine, Some infrared bands of deuterium sulfide, RP2789 211
Alloy steels, slack-quenched impact properties, RP2799 273
Alloys, two-phase textural stresses in, RP2793 239
Antenna, insulated loop, immersed in a conducting medium, RP2781 133
Antenna, microwave, pattern of a flush mounted, RP2796 255
Apparatus for measurement of thermal conductivity of solids at low temperatures, RP2805 349
Apparatus for measuring the piezoresistivity of semiconductors, RP2814 427
Approximate expression for gamma-ray degradation spectra, RP2788 207
Arsenic sulfide glass, properties, RP2774 83
L-Ascorbic acid-C^{14}, synthesis of, RP2800 289
Attix, F. H., V. H. Ritz, A determination of the gamma-ray emission of radium, RP2801 293

B

Bates, R. G., E. Wichers, Precise intercomparison of acids by differential potentiometric titration with hydrogen electrodes, RP2769 9
—, *V. E. Power,* Standards for *p*H measurements from 60° to 95° C, RP2797 261
Beryllium oxide, thermal conductivity, from 40° to 750° C, RP2775 93
Bessel integral functions, expansions, RP2786 197
Black, M. H., F. W. Glaze, D. H. Blackburn, J. S. Osmalov, D. Hubbard, Properties of arsenic sulfide glass, RP2774 83
Blackburn, D. H., J. S. Osmalov, D. Hubbard, M. H. Black, F. W. Glaze, Properties of arsenic sulfide glass, RP2774 83
Blaine, L. R., E. K. Plyler, Infrared emission spectrum of methane at 3.3 microns, RP2803 317
—, *H. C. Allen, Jr., E. K. Plyler,* Some infrared bands of deuterium sulfide, RP2789 211
Blaine, R. L., L. A. Tomes, C. M. Hunt, Some factors affecting the surface area of hydrated portland cement as determined by water-vapor and nitrogen adsorption, RP2806 357
Bolometric power measurements, a self-balancing direct-current bridge for, RP2776 101
Power, V. E., R. G. Bates, Standards for *p*H measurements from 60° to 95° C, RP2797 261
Britton-Robinson universal buffers, increased chemical reactivity of the surface compared with that in the bulk volume of, RP2811 411
Brown, E. H., On the most general form of the compatibility equations and the conditions of integrability of strain rate and strain, RP2813 421
Buffer solutions, surface reactivity, RP2811 411
Buffers for *p*H standardization at 60° to 95° C, RP2797 261
Byers, F. C., E. E. Sager, Dissociation of 4-chloro-4′-aminodiphenylsulfone, RP2794 245

C

Calcium aluminate hydrate mono, observations on, RP2777 107
Calcium hydroxide, a thermochemical study of the reaction of, RP2785 187
Carbohydrate derivatives, infrared spectra, RP2772 41
Carbohydrates, carbon-14-labeled, RP2800 289
Carlson, E. T., Some observations on hydrated monocalcium aluminate and monostrontium aluminate, RP2777 107
Carwile, N. L., G. W. Geil, Some effects of low temperatures and notch depth on the mechanical behavior of an annealed commercially pure titanium, RP2790 215
Catalán, M. A., R. Velasco, W. F. Meggers, P. F. A. Klinkenberg, Term analysis of the first spectrum of rhenium (Re I), RP2804 319
Cationic detergents in water, turbidity and viscosity measurements on, RP2778 113
Cement, portland, hydrated, some factors affecting the surface area, RP2806 357
Chemical reactivity at the surface compared with that in the bulk volume of buffer solutions, RP2811 411
4-Chloro-4′-aminodiphenylsulfone, dissociation of, RP2794 245
Cleek, G. W., S. Spinner, E. H. Hamilton, Determination and use of the sag point as a reference point in the heating of glasses, RP2791 227
Coffin, D. O., W. M. Rogers, R. L. Powell, An apparatus for measurement of thermal conductivity of solids at low temperatures, RP2805 349
Cohn, H., A numerical study of Dedekind's cubic class number formula, RP2798 265
—, *S. Gorn,* A computation of cyclic cubic units, RP2783 155
Compatibility equations, of strain rate and strain, RP2813 421
Complex plane, formulas for inverse osculatory interpolation in the complex plane, RP2792 233
Computation of cyclic cubic units, RP2783 155
Concrete, alkali-aggregate reaction in, physical-chemical studies, RP2780 127
Conda, A. M., J. F. Wait, Radiation from slots on dielectric-clad and corrugated cylinders, RP2802 307
Conductivity, thermal, of solids at low temperatures, RP2805 349
Cooter, I. L., R. E. Mundy, Cunife wire magnets of small size, RP2808 379
Copper, coalesced, thermal conductivity, RP2805 349
Creitz, E. C., H. S. Isbell, F. A. Smith, H. L. Frush, J. D. Moyer, J. E. Stewart, Infrared spectra of sugar acetates in solution, RP2772 41
Cunife wire magnets of small size, RP2808 379
Cyclic cubic units, a computation of, RP2783 155

D

Page

Dedekind's cubic class number formula, a numerical study of, RP2798 265
Determination and use of the sag point as a reference point in the heating of glasses, RP2791 227
Determination of the gamma-ray emission of radium, RP2801 293
Deuterium sulfide, some infrared bands of, RP2789 211
Direct-current bridge for accurate bolometric power measurements, RP2776 101
Dissociation of 4-chloro-4′-aminodiphenylsulfone, RP2794 245
Ditmars, D. A., D. C. Ginnings, Thermal conductivity of beryllium oxide from 40° to 750° C, RP2775 93

E

Effects of low temperatures and notch depth on the mechanical behavior of an annealed commercially pure titanium, RP2790 215
Eigenvalues of a free plate, RP2784 169
Electrodes, hydrogen, titration of acids with, RP2769 9
Engen, G. F., A self-balancing direct-current bridge for accurate bolometric power measurements, RP2776 101
Estimation of the frequencies of thin elastic plates with free edges, RP2784 169
Excitation of surface waves on conducting, stratified, dielectric-clad, and corrugated surfaces, RP2807 365
Extreme-value distribution: Table of the first moment of ranked extremes, RP2787 203

F

Fano, U., A. T. Nelms, An approximate expression for gamma-ray degradation spectra, RP2788 207
Formulas for inverse osculatory interpolation in the complex plane, RP2792 233
Frush, H. L., H. S. Isbell, F. A. Smith, E. C. Creitz, J. D. Moyer, J. E. Stewart, Infrared spectra of sugar acetates in solution, RP2772 41
—, —, Syntheses of C^{14}-labeled L-sorbose and L-ascorbic acid, RP2800 289
Fujita, H., T. Kato, Y. Nakata, M. Newman, Estimation of the frequencies of thin elastic plates with free edges, RP2784 169

G

Gamma-ray degradation spectra, an approximate expression for, RP2788 207
Gamma-ray emission of radium, determination of, RP2801 293
Geil, G. W., N. L. Carwile, Some effects of low temperatures and notch depth on the mechanical behavior of an annealed commercially pure titanium, RP2790 215
Genensky, S. M., A problem in self-heating of a spherical body, RP2773 79
Ginnings, D. C., D. A. Ditmars, Thermal conductivity of beryllium oxide from 40° to 750° C, RP2775 93
Glass, arsenic sulfide, properties, RP2774 83
Glass, silica, noncrystal ionic model for, RP2782 139
Glasses, optical, relative stress-optical coefficients, RP2779 121
Glasses, sag point as a reference point in heating of, RP2791 227
Glaze, F. W., D. H. Blackburn, J. S. Osmalov, D. Hubbard, M. H. Black, Properties of arsenic sulfide glass, RP2774 83
Gorden, R., Jr., E. R. Weaver, E. E. Hughes, S. M. Gunther, S. Schuhmann, N. T. Redfearn, Interpretation of mass spectra of condensates from urban atmospheres, RP 2809 383
Gorn, S., H. Cohn, A computation of cyclic cubic units, RP2783 155
Greenspan, M., C. E. Tschiegg, Speed of sound in water by a direct method, RP2795 249
Ground-wave propagation, RP2770 19
Gunther, S. M., E. R. Weaver, E. E. Hughes, S. Schuhmann, N. T. Redfearn, R. Gorden, Jr., Interpretation of mass spectra of condensates from urban atmospheres, RP2809 383

H

Hague, J. L., L. A. Machlan, Photometric determination of tungsten in steel and titanium alloys with dithiol, RP2812 415
Hamilton, E. H., G. W. Cleek, S. Spinner, Determination and use of the sag point as a reference point in the heating of glasses, RP2791 227
Heating elements, silicon carbide, spectral emittance of, RP2810 405
Heating of glasses, sag point as a reference point in, RP2791 227
Householder, J., J. R. Wait, Mixed-path ground-wave propagation: 2. Larger distances, RP2770 19
Hubbard, D., M. H. Black, F. W. Glaze, D. H. Blackburn, J. S. Osmalov, Properties of arsenic sulfide glass, RP2774 83
—, *R. G. Pike,* Increased chemical reactivity of the surface compared with that in the bulk volume of Britton-Robinson universal buffers, RP2811 411
—, —, Physical-chemical studies of the destructive alkali-aggregate reaction in concrete, RP2780 127
Hubbard, W. D., R. A. Parker, L. M. Kushner, Turbidity and viscosity measurements on some cationic detergents in water and in sodium chloride solutions, RP2778 113
Hughes, E. E., E. R. Weaver, S. M. Gunther, S. Schuhmann, N. T. Redfearn, R. Gorden, Jr., Interpretation of mass spectra of condensates from urban atmospheres, RP2809 383
Hunt, C. M., L. A. Tomes, R. L. Blaine, Some factors affecting the surface area of hydrated portland cement as determined by water-vapor and nitrogen adsorption, RP2806 357
Hydrogen electrodes, titration of acids with, RP2769 9

I

Page

Impact properties of slack-quenched alloy steels, RP2799 ... 273
Infrared bands of deuterium sulfide, RP2789 ... 211
Infrared emission spectrum of methane at 3.3 microns, RP2803 ... 317
Infrared emission spectrum of silicon carbide heating elements, RP2810 ... 405
Infrared spectra of sugar acetates in solution, RP2772 ... 41
Insulated loop antenna immersed in a conducting medium, RP2781 ... 133
Integrability of strain rate and strain, conditions of, RP2813 ... 421
Interpretation of mass spectra of condensates from urban atmospheres, RP 2809 ... 383
Ionic model, noncrystal, for silica glass, RP2782 ... 139
Isbell, H. S., F. A. Smith, E. C. Creitz, H. L. Frush, J. D. Moyer, J. E. Stewart, Infrared spectra of sugar acetates in solution, RP2772 ... 41
—, *H. L. Frush*, Synthesis of C^{14}-labeled L-sorbose and L-ascorbic acid, RP2800 ... 289

K

Kato, T., H. Fujita, Y. Nakata, M. Newman, Estimation of the frequencies of thin elastic plates with free edges, RP2784 ... 169
Klinkenberg, P. F. A., W. F. Meggers, R. Velasco, M. A. Catalán, Term analysis of the first spectrum of rhenium (Re I), RP2804 ... 319
Kushner, L. M., W. D. Hubbard, R. A. Parker, Turbidity and viscosity measurements on some cationic detergents in water and in sodium chloride solutions, RP2778 ... 113

L

Length changes, thermal, of refractory castables, RP2768 ... 1
Lieblein, J., H. E. Salzer, Table of the first moment of ranked extremes, RP2787 ... 203
Linnig, F. J., J. E. Stewart, A spectroscopic study of oils used in oil-extended rubber, RP2771 ... 27
Low temperatures and notch depth, effects of, on the mechanical behavior of an annealed commercially pure titanium, RP2790 ... 215

M

Machlan, L. A., J. L. Hague, Photometric determination of tungsten in steel and titanium alloys with dithiol, RP2812 ... 415
Magnets, Cunife wire, RP2808 ... 379
Mass spectra of condensates from urban atmospheres, interpretation of, RP2809 ... 383
McKean, W. J., R. F. Potter, An apparatus for measuring the peizoresistivity of semiconductors, RP2814 ... 427
Meggers, W. F., P. F. A. Klinkenberg, R. Velasco, M. A. Catalán, Term analysis of the first spectrum of rhenium (Re I), RP2804 ... 319
Methane, infrared emission spectrum, at 3.3 microns, RP2803 ... 317
Meyerson, M. R., S. J. Rosenberg, Impact properties of slack-quenched alloy steels, RP2799 ... 273
Microwave antenna, pattern of a flush-mounted, RP2796 ... 255
Mixed-path ground-wave propagation: 2. Larger distances, RP2770 ... 19
Mong, L. E., S. J. Schneider, Thermal length changes of some refractory castables, RP2768 ... 1
Moyer, J. D., H. S. Isbell, F. A. Smith, E. G. Creitz, H. L. Frush, J. E. Stewart, Infrared spectra of sugar acetates in solution, RP2772 ... 41
Mundy, R. E., I. L. Cooter, Cunife wire magnets of small size, RP2808 ... 379

N

Nakata, Y., T. Kato, H. Fujita, M. Newman, Estimation of the frequencies of thin elastic plates with free edges, RP2784 ... 169
Napolitano, A., R. M. Waxler, Relative stress-optical coefficients of some National Bureau of Standards optical glasses, RP2779 ... 121
Nelms, A. T., U. Fano, An approximate expression for gamma-ray degradation spectra, RP2788 ... 207
Newman, E. S., A thermochemical study of the reaction of calcium hydroxide, silica gel, and water, RP2785 ... 187
Newman, M., T. Kato, H. Fujita, Y. Nakata, Estimation of the frequencies of thin elastic plates with free edges, RP2784 ... 169
Newton, C. J., H. C. Vacher, An X-ray study of textural stresses in two-phase alloys, RP2793 ... 239
Noncrystal ionic model for silica glass, RP2782 ... 139
Notch depth and low temperatures, effects of, on the mechanical behavior of an annealed commercially pure titanium, RP2790 ... 215
Numerical analysis:
RP2783 ... 155
RP2798 ... 265
Numerical study of Dedekind's cubic class number formula, RP2798 ... 265

O

Oberhettinger, F., On some expansions for Bessel integral functions, RP2786 ... 197
Oils used in oil-extended rubber, RP2771 ... 27
Optical glasses, relative stress-optical coefficients of, RP2779 ... 121
Osculatory interpolation in the complex plane, formulas for, RP2792 ... 233
Osmalov, J. S., D. Hubbard, M. H. Black, F. W. Glaze, D. H. Blackburn, Properties of arsenic sulfide glass, RP2774 ... 83

P

Parker, R. A., L. M. Kushner, W. D. Hubbard, Turbidity and viscosity measurements on some cationic detergents in water and in sodium chloride solutions, RP2778 ... 113
Pattern of a flush-mounted microwave antenna, RP2796 ... 255
Photoelastic constants of some optical glasses, RP2779 ... 121
Photometric determination of tungsten in steel and titanium alloys with dithiol, RP2812 ... 415
pH standards at 60° to 95° C, RP2797 ... 261
Physical-chemical studies of the destructive alkali-aggregate reaction in concrete, RP2780 ... 127
Piezoresistivity of semiconductors, apparatus for measuring, RP2814 ... 427
Pike, R. G., D. Hubbard, Increased chemical reactivity of the surface compared with that in the bulk volume of Britton-Robinson universal buffers, RP2811 ... 411
—, —, Physical-chemical studies of the destructive alkali-aggregate reaction in concrete, RP2780 ... 127
Plyler, E. K., H. C. Allen, Jr., L. R. Blaine, Some infrared bands of deuterium sulfide, RP2789 ... 211
—, *L. R. Blaine*, Infrared emission spectrum of methane at 3.3 microns, RP2803 ... 317
Polytetrafluoroethylene, thermal conductivity, RP2805 ... 349
Portland cement, hydrated, some factors affecting the surface area, RP2806 ... 357
Potter, R. F., W. J. McKean, An apparatus for measuring the piezoresistivity of semiconductors, RP2814 ... 427
Powell, R. L., W. M. Rogers, D. O. Coffin, An apparatus for measurement of thermal conductivity of solids at low temperatures, RP2805 ... 349
Precise intercomparison of acids by differential potentiometric titration with hydrogen electrodes, RP2769 ... 9
Problem in self-heating of a spherical body, RP2773 ... 79
Propagation of radio ground waves, RP2770 ... 19
Properties of arsenic sulfide glass, RP2774 ... 83

R

Radiation from slots on dielectric-clad and corrugated cylinders, RP2802 ... 367
Radio propagation, excitation of surface waves on conducting, stratified, dielectric-clad, and corrugated surfaces, RP2807 ... 393
Radio propagation:
Fields of an insulated loop immersed in a conducting medium, RP2781 ... 133
Mixed-path ground-wave propagation, RP2770 ... 19
Pattern of a flush-mounted microwave antenna, RP2796 ... 255
Radium, determination of the gamma-ray emission of, RP2801 ... 293
Redfearn, N. T., E. R. Weaver, E. E. Hughes, S. M. Gunther, S. Schuhmann, R. Gorden, Jr., Interpretation of mass spectra of condensates from urban atmospheres, RP2809 ... 383
Refractory castables, thermal length changes of, RP2768 ... 1
Relative stress-optical coefficients of some National Bureau of Standards optical glasses, RP2779 ... 121
Rhenium, term analysis of the first spectrum of, RP2804 ... 319
Richmond, J. C., J. E. Stewart, Infrared emission spectrum of silicon carbide heating elements, RP2810 ... 405
Ring conformation of sugar acetates, RP2772 ... 41
Ritz, V. H., F. H. Attix, A determination of the gamma-ray emission or radium, RP2801 ... 293
Rogers, W. M., R. L. Powell, D. O. Coffin, An apparatus for measurement of thermal conductivity of solids at low temperatures, RP2805 ... 349
Rosenberg, S. J., M. R. Meyerson, Impact properties of slack-quenched alloy steels, RP2799 ... 273
Rubber, oil-extended, oils used in, RP2771 ... 27

S

Sag point as a reference point in the heating of glasses, RP2791 ... 227
Sager, E. E., F. C. Byers, Dissociation o :4-chloro-4'-aminodiphenylsulfone, RP2794 ... 245
Salzer, H. E., Formulas for inverse osculatory interpolation in the complex plane, RP2792 ... 233
—, *J. Lieblein*, Table of the first moment of ranked extremes, RP2787 ... 203
Schneider, S. J., L. E. Mong, Thermal length changes of some refractory castables, RP2768 ... 1
Schuhmann, S., E. R. Weaver, E. E. Hughes, S. M. Gunther, N. T. Redfearn, R. Gorden, Jr., Interpretation of mass spectra of condensates from urban atmospheres, RP2809 ... 383
Self-balancing direct-current bridge for accurate bolometric power measurements, RP2776 ... 101
Self-heating of a spherical body, RP2773 ... 79
Semiconductors, apparatus for measuring the piezoresistivity of, RP2814 ... 427
Silica gel, a thermochemical study of the reaction of, RP2785 ... 187
Silica glass, noncrystal ionic model for, RP2782 ... 139
Silicon carbide heating elements, infrared emission spectrum of, RP2810 ... 405
Slack-quenched alloy steels, impact properties, RP2799 ... 273
Smith, F. A., H. S. Isbell, E. C. Creitz, H. L. Frush, J. D. Moyer, J. E. Stewart, Infrared spectra of sugar acetates in solution, RP2772 ... 41
Sodium chloride solutions, turbidity and viscosity measurements in, RP2778 ... 113
Some observations on hydrated monocalcium aluminate and monostrontium aluminate, RP2777 ... 107
L-Sorbose-C^{14}, synthesis of, RP2800 ... 289
Sound, speed of in water, RP2795 ... 249
Spectra, gamma-ray degradation, an approximate expression for, RP2788 ... 207
Spectra, infrared, of sugar acetates in solution, RP2772 ... 41
Spectral absorbency of 4-chloro-4'-aminodiphenylsulfone, RP2794 ... 245
Spectral emittance of a silicon carbide heating element, RP2810 ... 405
Spectroscopic study of oils used in oil-extended rubber, RP2771 ... 27
Spectrum, infrared emission, of methane at 3.3 microns, RP2803 ... 317
Spectrum of rhenium, first, term analysis of, RP2804 ... 319
Speed of sound in water by a direct method, RP2795 ... 249
Spherical body, a problem in self-heating, RP2773 ... 79
Spinner, S., G. W. Cleek, E. H. Hamilton, Determination and use of the sag point as a reference point in the heating of glasses, RP2791 ... 227
Standards for pH measurements from 60° to 95° C, RP2797 ... 261
Steel, photometric determination of tungsten in, RP2812 ... 415
Steels, slack-quenched alloy, impact properties, RP2799 ... 273
Stewart, J. E., F. J. Linnig, A spectroscopic study of oils used in oil-extended rubber, RP2771 ... 27
—, *H. S. Isbell, F. A. Smith, E. C. Creitz, H. L. Frush, J. D. Moyer*, Infrared spectra of sugar acetates in solution, RP2772 ... 41
—, *J. C. Richmond*, Infrared emission spectrum of silicon carbide heating elements, RP2810 ... 405

Page

Strain rate and strain, compatibility equations and conditions of integrability, RP2813 421
Stresses (residual) in two-phase alloys, RP2793 239
Strontium aluminate hydrate mono, observations on, RP2777 107
Sugar acetates, infrared spectra, RP2772 41
Surface area of hydrated portland cement, determination by water-vapor and nitrogen adsorption, RP2806 357
Surface reactivity of buffer solutions, RP2811 411
Surface waves, excitation, on conducting, stratified, dielectric-clad, and corrugated surfaces, RP2807 365
Synthesis of C^{14}-labeled L-sorbose and L-ascorbic acid, RP2800 289

T

Table of the first moment of ranked extremes, RP2787 203
Term analysis of the first spectrum of rhenium (Re I), RP2804 319
Textural stresses in two-phase alloys, RP2793 239
Thermal conductivity of beryllium oxide from 40° to 750° C, RP2775 93
Thermal conductivity of solids at low temperatures, RP2805 349
Thermal length changes of some refractory castables, RP2768 1
Thermochemical study of the reaction of calcium hydroxide, silica gel, and water, RP2785 187
Tilton, L. W., Nonerystal ionic model for silica glass, RP2782 139
Titanium alloys with dithiol, RP2812 415
Titanium, some effects of low temperatures and notch depth on the mechanical behavior of, RP2790 215
Titration of acids, differential, RP2769 9
Tomes, L. A., C. M. Hunt, R. L. Blaine, Some factors affecting the surface area of hydrated portland cement as determined by water-vapor and nitrogen adsorption, RP2806 357
Tschiegg, C. E., M. Greenspan, Speed of sound in water by a direct method, RP2795 249
Tungsten in steels, photometric determination, RP2812 415
Turbidity and viscosity measurements on some cationic detergents in water and in sodium chloride solutions, RP2778 113

U

Urban atmospheres, interpretation of condensates from, RP2809 383

V

Page

Vacher, H. C., C. J. Newton, An X-ray study of textural stresses in two-phase alloys, RP2793 239
Velasco, R., W. F. Meggers, P. F. A. Klinkenberg, M. A. Catalán, Term analysis of the first spectrum of rhenium (Re I), RP2804 319
Vibration of thin elastic plates with free edges, RP2784 169
Viscosity and turbidity measurements of some cationic detergents in water and sodium chloride solutions, RP2778 113
Vitron, noncrystal ionic model for silica glass, RP2782 139

W

Wait, J R., A. M. Conda, Radiation from slots on dielectric clad and corrugated cylinders, RP2802 307
—, Excitation of surface waves on conducting, stratified, dielectric-clad and corrugated surfaces, RP2807 365
—, Insulated loop antenna immersed in a conducting medium, RP2781 133
—, *J. Householder*, Mixed-path ground-wave propagation: 2. Larger distances, RP2770 19
—, Pattern of a flush-mounted microwave antenna, RP2796 255
Water, a thermochemical study of the reaction of, RP2785 187
Water-vapor and nitrogen adsorption, determination of surface area of hydrated portland cement by, RP2806 357
Waxler, R. M., A. Napolitano, Relative stress-optical coefficients of some National Bureau of Standards optical glasses, RP2779 121
Weaver, E. R., E. E. Hughes, S. M. Gunther, S. Schuhmann, N. T. Redfearn, R. Gorden, Jr., Interpretation of mass spectra of condensates from urban atmospheres, RP2809 383
Wichers, E., R. G. Bates, Precise intercomparison of acids by differential potentiometric titration with hydrogen electrodes, RP2769 9
Wire magnets, Cunife, RP2808 379

X

X-ray study of textural stresses in two-phase alloys, RP2793 239

THE NATIONAL BUREAU OF STANDARDS

The scope of activities of the National Bureau of Standards at its headquarters in Washington, D. C., and its major field laboratories in Boulder, Colorado, is suggested in the following listing of the divisions and sections engaged in technical work. In general, each section carries out specialized research, development, and engineering in the field indicated by its title. A brief description of the activities, and of the resultant publications, appears on the inside of the front cover.

WASHINGTON, D. C.

Electricity and Electronics. Resistance and Reactance. Electron Devices. Electrical Instruments. Magnetic Measurements. Dielectrics. Engineering Electronics. Electronic Instrumentation. Electrochemistry.

Optics and Metrology. Photometry and Colorimetry. Optical Instruments. Photographic Technology. Length. Engineering Metrology.

Heat. Temperature Physics. Thermodynamics. Cryogenic Physics. Rheology. Engine Fuels. Free Radicals Research.

Atomic and Radiation Physics. Spectroscopy. Radiometry. Mass Spectrometry. Solid State Physics. Electron Physics. Atomic Physics. Neutron Physics. Nuclear Physics. Radioactivity. X-rays. Betatron. Nucleonic Instrumentation. Radiological Equipment. AEC Radiation Instruments.

Chemistry. Organic Coatings. Surface Chemistry. Organic Chemistry. Analytical Chemistry. Inorganic Chemistry. Electrodeposition. Molecular Structure and Properties of Gases. Physical Chemistry. Thermochemistry. Spectrochemistry. Pure Substances.

Mechanics. Sound. Mechanical Instruments. Fluid Mechanics. Engineering Mechanics. Mass and Scale. Capacity, Density, and Fluid Meters. Combustion Controls.

Organic and Fibrous Materials. Rubber. Textiles. Paper. Leather. Testing and Specifications. Polymer Structure. Plastics. Dental Research.

Metallurgy. Thermal Metallurgy. Chemical Metallurgy. Mechanical Metallurgy. Corrosion. Metal Physics.

Mineral Products. Engineering Ceramics. Glass. Refractories. Enameled Metals. Concreting Materials. Constitution and Microstructure.

Building Technology. Structural Engineering. Fire Protection. Air Conditioning, Heating, and Refrigeration. Floor, Roof, and Wall Coverings. Codes and Specifications. Heat Transfer.

Applied Mathematics. Numerical Analysis. Computation. Statistical Engineering. Mathematical Physics.

Data Processing Systems. SEAC Engineering Group. Components and Techniques. Digital Circuitry. Digital Systems. Analog Systems. Application Engineering.

• Office of Basic Instrumentation.

• Office of Weights and Measures.

BOULDER, COLORADO

Cryogenic Engineering. Cryogenic Equipment. Cryogenic Processes. Properties of Materials. Gas Liquefaction.

Radio Propagation Physics. Upper Atmosphere Research. Ionospheric Research. Regular Propagation Services. Sun-Earth Relationships.

Radio Propagation Engineering. Data Reduction Instrumentation. Modulation Systems. Navigation Systems. Radio Noise. Tropospheric Measurements. Tropospheric Analysis. Radio Systems Application Engineering.

Radio Standards. High Frequency Electrical Standards. Radio Broadcast Service. High Frequency Impedance Standards. Calibration Center. Microwave Physics. Microwave Circuit Standards.

Recent Publications of the National Bureau of Standards

Journal of Research of the National Bureau of Standards, Volume 59, No. 6, October 1957 (RP2792 to RP2800 incl.). 60 cents. Annual subscription $4.00.

Technical News Bulletin, Volume 41, No. 10, October 1957. 10 cents. Annual subscription $1.00.

Basic Radio Propagation Predictions for January 1958. Three months in advance. CRPL-D 158. Issued October 1957. 10 cents. Annual subscription $1.00.

Circulars

C584. Simulator for use in development of jet engine controls. 20 cents.

C586. Electric hygrometers. 20 cents.

Miscellaneous Publications

M221. Hydraulic research in the United States, 1957. $1.50. *Available from the Superintendent of Documents, U. S. Government Printing Office, Washington 25, D. C. (foreign postage, one-fourth additional).*

UNITED STATES
GOVERNMENT PRINTING OFFICE
DIVISION OF PUBLIC DOCUMENTS
WASHINGTON 25, D. C.

OFFICIAL BUSINESS

PENALTY FOR PRIVATE USE TO AVOID PAYMENT OF POSTAGE, $300 (GPO)

Journal of Research of the National Bureau of Standards Vol. 59, No. 6 December 19

Contents

		Page
Some factors affecting the surface area of hydrated portland cement as determined by water-vapor and nitrogen adsorption. L. A. Tomes, C. M. Hunt, and R. L. Blaine.	RP2806	357
Excitation of surface waves on conducting, stratified, dielectric-clad, and corrugated surfaces. James R. Wait.	RP2807	365
Cunife wire magnets of small size. Irvin L. Cooter and Robert E. Mundy.	RP2808	379
Interpretation of mass spectra of condensates from urban atmospheres. E. R. Weaver, E. E. Hughes, Shirley M. Gunther, Schuford Schuhmann, Nancy T. Redfearn, and Ralph Gorden, Jr.	RP2809	383
Infrared emission spectrum of silicon carbide heating elements. James E. Stewart and Joseph C. Richmond.	RP2810	405
Increased chemical reactivity of the surface compared with that in the bulk volume of Britton-Robinson universal buffers. Robert G. Pike and Donald Hubbard.	RP2811	411
Photometric determination of tungsten in steel and titanium alloys with dithiol. Lawrence A. Machlan and John L. Hague.	RP2812	415
On the most general form of the compatibility equations and the conditions of integrability of strain rate and strain. Edmund H. Brown.	RP2813	421
An apparatus for measuring the piezoresistivity of semiconductors. R. F. Potter and W. J. McKean.	RP2814	427
Index to volume 59 (July to December 1957, Research Papers RP2768 to RP2814).		431

[A list of recent NBS publications is given on page 3 of the cover.]

6158

For sale by the Superintendent of Documents, U. S. Government Printing Office, Washington 25, D. C. Price 60 cents (single copy). Subscription price: $4.00 a year; $1.25 additional for foreign mailing.

UNITED STATES GOVERNMENT PRINTING OFFICE, WASHINGTON : 1957